Diss. ETH No. 12709

Improved techniques to calculate two-loop anomalous dimensions in QCD

A dissertation submitted to the
SWISS FEDERAL INSTITUTE OF TECHNOLOGY ZURICH
(ETH Zürich)

for the degree of
Doctor of Natural Sciences

presented by
Gudrun Heinrich
Dipl. Phys. Univ. Freiburg im Breisgau
born January 15, 1968
German citizen

accepted on the recommendation of
Prof. Dr. Zoltan Kunszt, examiner
Prof. Dr. Christoph Schmid, co-examiner

1998

Contents

Abstract

In this thesis, the calculation of the full flavour non-singlet Altarelli-Parisi splitting functions as well as the N_c^2 part of the gluon-gluon splitting functions in next-to-leading order is presented. The calculation has been performed by employing the method of Curci, Furmanski and Petronzio (CFP), which is based on the light-cone gauge.
In previous calculations relying on the CFP method, the spurious poles of the gluon propagator in light-cone gauge always had been regularized by using the "principal value" (PV) prescription. As the PV prescription is formally unsatisfactory in several respects, it entails the application of some "phenomenological rules", whose working principles are not really understood, to obtain the correct result.

The calculation presented here has been done by applying the Mandelstam-Leibbrandt (ML) prescription, which has a solid field-theoretical foundation, to regulate the gauge induced poles. As a consequence, the phenomenological rules needed in the PV case became obsolete. On the other hand, the use of the ML prescription increased the complexity of the calculation, mainly due to the fact that unitarity requires the inclusion of so-called "axial ghost" degrees of freedom.
The calculation can be organized by studying gauge invariant subparts defined by a certain colour structure. The part proportional to C_F^2, being of Abelian nature, constitutes an opportunity to study the effects of the ML prescription in isolation from other complications. The non-Abelian part proportional to $C_F N_c$ turned out to be much more involved, revealing new features concerning the cancellation mechanism of the spurious poles and entailing the application of techniques which have not been used before in this context in order to overcome the technical difficulties.
For colour structure $C_F T_f$, the calculation of the two-loop quark selfenergy has been included, thus being able to extract the full endpoint contribution at $x = 1$. In this way it was possible to check the consistency with the sum rules expressing fermion number conservation, which constitutes a new test not only of the ML prescription, but also of the CFP method itself.
In order to investigate the viability of the ML prescription in all possible one-loop structures of QCD, the N_c^2 part of the gluon-gluon splitting function, which contains the highly nontrivial one-loop three-gluon vertex, also has been calculated. Using the methods developed for the $C_F N_c$ part, the usefulness and reliability of the ML

prescription in this context again could be confirmed.

Having in mind an extension of the calculation to the three-loop splitting functions, one has to be aware of the fact that the technical complexity of the calculation with ML prescription might constitute an unsurmountable problem in three loops. Therefore, it is a challenge to further exploit the insights gained from the calculation with ML prescription. One aspect consists in explaining why the "phenomenological rules" related to the use of PV prescription gave the correct result, thus being able to judge whether they will still work in three loops. As I also did the full calculation with PV prescription, some interesting relations between the two prescriptions could be worked out.
Another appealing perspective, which may be also useful for a better understanding of the PV procedure, could consist in reducing the complexity of the ML calculation, for example by exploiting – even in the context of the *non-physical* anomalous dimensions – the fact that the axial ghost degrees of freedom decouple from *physical* quantities.
In summary, having established the CFP method with ML prescription as a method without conceptual loopholes, this work might serve as a powerful tool to extend the calculation to three loops.

Zusammenfassung

In dieser Dissertation wird die Berechnung der gesamten flavour non-singlet Altarelli-Parisi Splitting Funktionen sowie des Beitrags proportional zu N_c^2 der Gluon-Gluon Splitting Funktionen in nächstführender Ordnung vorgestellt. Die Rechnung wurde unter Anwendung der Methode von Curci, Furmanski und Petronzio (CFP), welche auf der lichtartigen axialen Eichung beruht, durchgeführt.
In früheren Rechnungen innerhalb der CFP Methode wurden die künstlichen Pole des Gluon–Propagators in lichtartiger axialer Eichung immer mit Hilfe der "Principal Value" (PV) Vorschrift regularisiert. Da die PV Vorschrift jedoch in verschiedener Hinsicht formal unbefriedigend ist, zog dies die Zuhilfenahme von gewissen "phänomenologischen Regeln" – deren Funktionsweise nicht wirklich verstanden ist – nach sich, um das richtige Resultat zu erhalten.

Die Rechnung, welche hier präsentiert wird, beruht auf der Anwendung der Mandelstam–Leibbrandt (ML) Vorschrift zur Regularisierung der durch die Eichung induzierten Pole. Es konnte gezeigt werden, dass die phänomenologischen Regeln, die im Fall der PV Vorschrift gebraucht wurden, dann nicht mehr notwendig sind. Andererseits erhöhte die Anwendung der ML Vorschrift die Komplexität der Rechnung, hauptsächlich durch das Auftreten der sogenannten "axialen Geist"–Freiheitsgrade, welche aus Unitaritätsgründen mit einbezogen werden müssen.
Die Rechnung kann in Untereinheiten organisiert werden, welche durch eine bestimmte colour–Struktur gegeben sind. Der Teil proportional zu C_F^2 ist Abelscher Natur und bietet sich deshalb an, die Auswirkungen der ML Vorschrift isoliert von anderen Schwierigkeiten zu studieren. Der nicht–Abelsche Teil proportional zu $C_F N_c$ stellte sich als wesentlich komplizierter heraus. Es zeigten sich andersartige Kürzungsmechanismen für die künstlichen Pole, und es mussten Techniken angewandt werden, die in diesem Zusammenhang noch nie gebraucht worden sind, um die rechentechnischen Schwierigkeiten zu überwinden.
Für die colour–Struktur $C_F T_f$ wurde zusätzlich die Quark–Selbstenergie in Zwei–Schleifen–Näherung berechnet, was die Berechnung des gesamten Endpunkt–Beitrages bei $x = 1$ ermöglichte. Dies stellt einen weiteren Test nicht nur der ML Vorschrift, sondern auch der CFP Methode selbst dar, denn die Endpunkt–Beiträge sind noch nie zuvor direkt berechnet worden.
Um die Anwendbarkeit der ML Vorschrift in allen Ein–Schleifen–Strukturen der Quan-

tenchromodynamik, welche überhaupt möglich sind, zu testen, wurde auch der Teil proportional zu N_c^2 der Gluon–Gluon Splitting Funktion, welcher den äusserst nicht–trivialen Drei–Gluon–Vertex enthält, berechnet. Unter Anwendung der Methoden, die für den $C_F N_c$–Teil entwickelt wurden, konnten der Nutzen und die Verlässlichkeit der ML Vorschrift in diesem Zusammenhang erneut gezeigt werden.

Im Hinblick auf die Berechnung der Splitting Funktionen in Drei–Schleifen–Näherung muss man sich darüber im Klaren sein, dass die rechentechnische Komplexität der Methode mit ML Vorschrift in dieser Ordnung ein unüberwindliches Problem darstellen könnte. Deshalb stellt es eine Herausforderung dar, aus den den Einblicken, welche bei der Rechnung mit ML Vorschrift gewonnen wurden, weitere Nutzen zu ziehen. Ein Aspekt besteht darin, zu erklären, warum die "phänomenologischen Regeln" im Zusammenhang mit der PV Vorschrift zum korrekten Ergebnis führten, so dass man beurteilen kann, ob sie in Drei–Schleifen–Näherung immer noch verlässlich sind. Da ich die gesamte Rechnung auch mit PV Vorschrift ausgeführt habe, konnten einige interessante Beziehungen zwischen den beiden Vorschriften ausgearbeitet werden.
Ein anderer Aspekt der Weiterentwicklung, der auch zum besseren Verständnis der PV Methode beitragen könnte, besteht darin, zu versuchen, die Komplexität der Rechnung mit ML Vorschrift zu reduzieren. Dies könnte zum Beispiel erreicht werden, indem man – selbst im Fall der *unphysikalischen* anomalen Dimensionen – ausnutzt, dass die "axialen Geist"–Freiheitsgrade von *physikalischen* Grössen entkoppeln.
Insgesamt könnte diese Arbeit einen wichtigen Baustein liefern für die Entwicklung einer Methode, welche sowohl in formaler Hinsicht vertrauenswürdig als auch effizient genug ist, um die Drei–Schleifen–Rechnung in Angriff zu nehmen.

Chapter 1

Introduction

Quantum chromodynamics (QCD) is the theory of the strong interactions between quarks and gluons, which bind together to form hadrons like the proton or the neutron. The description of the strong interactions by a non-Abelian gauge theory based on the $SU(3)$ colour group [1, 2] nowadays is a main building block of the "Standard Model" of elementary particle physics. Just like the photon which is an Abelian gauge field mediating electromagnetic interactions between charged particles in quantum electrodynamics (QED), the non-Abelian gauge field in QCD, the gluon, mediates colour interactions between quarks. While photons have no electric charge, gluons carry colour charges and hence interact which each other. These self-interactions are the main reason for the fact that the coupling constant α_s of the strong interactions *decreases* at small distances, a phenomenon which is called *asymptotic freedom* [3, 4]. At *long distances*, QCD is characterized by the property of *confinement*: Quark and gluon degrees of freedom never have been observed as states which propagate over macroscopic distances; it is always the colourless hadrons that are observed.

Only after the discovery of asymptotic freedom it became justified to calculate short-distance cross-sections in QCD as a perturbative series in the coupling constant α_s, supported by *factorization* properties which permit cross sections to be written as products of a hard scattering piece and a factor which contains the long-distance physics.

One of the earliest tests of QCD, respectively of its predecessor, the "naive parton model" [5], was provided by deep inelastic electron-nucleon scattering. The outcome of these experiments could be successfully described by applying the method of operator product expansion (OPE) initiated by Wilson [6]. Factorization, which guarantees the safe application of perturbation theory to the description of deep inelastic scattering, has been proven within the context of OPE by Zimmermann [7, 8]. The OPE techniques together with the use of the renormalization group equations [9, 10, 11, 12] allowed for a description of deep inelastic scattering which was able to explain the logarithmic scaling violations found experimentally, thus improving considerably the naive parton model. An elegant reformulation of the factorization properties proven

within OPE was given by Altarelli and Parisi [13]. They worked out a form of the QCD improved parton model based on parton densities in configuration space, which is closer to physical intuition. These parton densities obey evolution equations known as Altarelli-Parisi equations, also denoted by DGLAP equations since they were independently also considered by Gribov, Lipatov and Dokshitzer [14]. The kernels of these equations are the so-called *splitting functions*, whose Mellin transforms coincide with the anomalous dimensions present in the OPE formulation.

In the following years, QCD became continuously better established as the theory of the strong interactions [15, 16]. In particular, a systematic separation of the dynamics associated with short and long distance scales could be achieved also beyond the scope of deep inelastic scattering, showing that the concept of factorization is quite universal, although it breaks down in special cases [17]. The insights gained into the infrared singularity structure of QCD are expressed in terms of fundamental cancellation [18] and factorization theorems [19, 20]. Hence the success of perturbative QCD could be extended from deep inelastic scattering to a considerable number of different processes studied at high energy colliders, like for example photoproduction, multi-jet production or vector boson production [16].

As cross sections involving hadrons can be measured at present and future high energy colliders with increasingly high accuracy, the theoretical description of these precision data requires the evaluation of next-to-leading order or even higher order corrections in perturbative QCD. These QCD corrections will be of particular interest for the near future since the machines after LEP with the highest center-of-mass energies, that is, LHC and the Tevatron, will both be hadron colliders.
A considerable number of next-to-leading order corrections are by now available in the literature (see e.g. [16] and references therein). Next-to-next-to-leading order (NNLO) corrections, however, could be calculated only in few cases [21, 22, 23, 24, 25]. Considering for example the structure functions F_2 and F_L of deep inelastic electron-nucleon scattering, their knowledge in NNLO is of considerable interest for an accurate comparison of perturbative QCD with experiment. To obtain the NNLO expression for these structure functions, the anomalous dimensions of the corresponding operators are needed in three-loop order. For the non-singlet moments $N = 2, 4, 6, 8, 10$ and the singlet moments $N = 2, 4, 6, 8$ these three-loop anomalous dimensions have been calculated by Larin, van Ritbergen, Vermaseren and Nogueira [24]. A NNLO analysis based on these moments is possible only as long as one limits oneself to large x and small Q^2, and has been done in [26]. But if one wants to study the behaviour of the structure functions at small x and large Q^2 in NNLO, the knowledge of the full three-loop anomalous dimensions is indispensable.
Similarly, in the case of hard processes with two initial hadrons, no complete NNLO result is available. Although the NNLO coefficient functions of the Drell-Yan process have been obtained in [23], the phenomenological application of this result requires the calculation of the NNLO Altarelli-Parisi splitting functions (three-loop anomalous

dimensions) as well.
But as long as there is no highly efficient and formally transparent method to calculate the two-loop anomalous dimensions, it is pointless to go on to the full three-loop calculation. Therefore significant technical and formal development concerning the two-loop calculation has to be achieved.

Two rather different methods [27], [28, 29, 30] have been used for the evaluation of the spin independent two-loop anomalous dimensions. Both methods recently have been applied successfully to the calculation of the NLO corrections of the spin dependent Altarelli-Parisi splitting functions [31, 32]. The first method is based on operator product expansion (OPE) and requires the evaluation of the overall ultraviolet divergences of twist-two local operator insertions. The results are obtained in moment space and the calculation can be carried out in Feynman gauge. Unfortunately, the number of the operator insertions increases very rapidly in higher orders and the treatment of operator mixing in the singlet sector has been unclear for a long time. Due to this conceptual difficulty there was an error in the original OPE calculation of the *singlet* anomalous dimensions which could be fixed only recently [33, 34]. The work of [33, 34] thus finally established the OPE technique to calculate higher order anomalous dimensions as a method which is conceptually impeccable, but of enormous algebraic complexity. Nevertheless a considerable number of programs already exists, such that recently even the *finite* terms of the two-loop operator matrix elements could be calculated [35].
The second method, developed by Curci, Furmanski and Petronzio (CFP) [28, 29, 30], is based on the factorization properties of mass singularities in axial gauges, so it is built on the *infrared* properties of the underlying processes. It leads to the two-loop splitting functions in configuration space and admits a physical interpretation which is very close to the intuitive parton picture. The $x-$space representation also is more useful from an experimental point of view.
The most important technical ingredient of the CFP method is the use of light-like axial gauge ($n_\mu A^\mu = 0$, $n^2 = 0$), also called light-cone gauge. It enormously reduces the complexity of the calculation as compared to the $n^2 \neq 0$ case and provides a direct link with the OPE method in deep inelastic scattering. On the other hand, the $1/nq-$factor in the gluon propagator in light-like axial gauge gives rise to so-called "spurious poles", gauge induced singular terms in both, the real and the virtual contributions. Although these singularities have to cancel in gauge invariant quantities, one has to apply some regularization prescription in order to be able to evaluate the individual diagrams. There are basically two prescriptions to regulate these spurious poles, the *principal value* (PV) prescription and the *Mandelstam-Leibbrandt* (ML) prescription [36, 37]. The PV prescription has been applied by Curci, Furmanski and Petronzio on the basis of rather phenomenological rules. Using the PV prescription, Wick rotation produces extra pole terms such that power counting theorems break down. This entails spurious poles and momentum dependent terms in the UV renormalization constants, whose treatment is not a priori clear. Another reason to

question the validity of the phenomenological rules of CFP is the fact that after the work of CFP it was pointed out that the principal value prescription is not consistent with canonical quantization in light-like axial gauge [38, 39]. Correctly performed canonical quantization leads to the ML prescription.
Nevertheless, the "recipe" of CFP to subtract the dubious terms together with the usual UV poles produced the correct result. (Although the result obtained by Furmanski and Petronzio [30] for the *singlet* anomalous dimensions could be confirmed from the OPE side only more than ten years later.)
CFP were aware of the fact that there remains some work to be done in order to build the treatment of the spurious poles on solid theoretical grounds. Literally, they say [29]: "Hopefully, it will be a challenge for field theory experts to provide a more formal support for our 'phenomenological' rules. "
In order to clarify this issue, it is of particular interest to study the CFP method with the ML prescription. A first attempt already appeared in the literature: The one-loop Altarelli-Parisi splitting functions have been calculated by Bassetto [40]. The calculation of the two-loop splitting functions with ML prescription never has been tried before and will be presented here. It will turn out that with ML prescription, the phenomenological rules needed in the PV case become obsolete. On the other hand, the complexity of the calculation increases, mainly due to the so-called "axial ghosts" which appear as a consequence of the ML prescription.
Hence the CFP method with ML prescription due to the present work has reached a comparable status of conceptual clarity as the OPE method, but the price to pay for this gain in formal solidity is an increase in technical complexity.

The organization of the thesis is as follows: A general introduction, elucidating the role of anomalous dimensions in QCD, is given in Chapter two. First the parton model approach to anomalous dimensions will be treated: After the definition of parton distributions, the important concept of factorization will be described. Then the Altarelli-Parisi equation will be introduced, leading immediately to the splitting functions which are the Mellin transforms of certain anomalous dimensions.
Then the approach to anomalous dimensions via operator product expansion will be presented, with emphasis on the operator product expansion in deep inelastic scattering, the latter being the most important application of operator product expansion in perturbative QCD.
In Chapter three, first an overview on the existing methods to calculate anomalous dimensions in two loops will be given. The method of CFP, which will be extended later, is described in some detail in Section 3.2. The features of the light-cone gauge and the different aspects of PV and ML regularization are treated in Section 3.3. As an example, some basic differences arising from PV respectively ML regularization already in leading order will be exhibited. As the different ultraviolet behaviour of PV respectively ML regularized integrals is of crucial importance for the whole calculation, the next subsection will be dedicated to UV renormalization.
In the following two sections, the calculation of certain two-loop anomalous dimensions

with ML prescription will be presented in detail. In Section 3.4, the contribution to the non-singlet splitting function with colour structure C_F^2 will be given. This colour structure has several special features, partly due to the fact that it is of "Abelian" nature, containing no three-gluon-vertices. "Non-Abelian" contributions to the splitting functions will be studied in Section 3.5. There, completely new features compared to the C_F^2 part will arise, which entailed the development of alternative techniques to be able to calculate some of the diagrams. The colour structure $C_F T_f$ is treated in some detail as a pedagogical example. For this colour structure, the full endpoint contributions at $x = 1$ also have been calculated. In this way the sum rules derived from fermion number conservation could be used as an important test for both, the ML prescription as well as the CFP method itself. This fundamental consistency check never had been provided in previous calculations. The next subsection treats the calculation of the colour structure $C_F N_c$ of the non-singlet two-loop splitting functions, which is by far more complicated than the C_F^2 and $C_F T_f$ parts. Having accomplished this task provides a test of all possible one-loop insertions of QCD except for the non-Abelian one-loop three-gluon-vertex. Therefore finally the contributions proportional to N_c^2 of the gluon-gluon splitting function, which contain this remaining structure, have been calculated. This means that altogether, an exhaustive test of the ML prescription within a highly nontrivial application has been provided.
As I also did the full calculation of the non-singlet and singlet splitting functions with PV prescription, some insight could be gained into the relations between PV and ML prescriptions, which is discussed in Section 3.6, especially in view of a possible extension of one of these schemes to three loops. This view will be broadened in the conclusions in Chapter four.

Chapter 2

Anomalous dimensions in QCD

In a general field theory, anomalous dimensions appear as a consequence of ultraviolet renormalization and the renormalization group. As soon as an operator (a quantum field or a product of quantum fields) or a parameter requires to be renormalized, its scale dimension d can differ from its naive mass dimension d_0 by a quantity γ. Therefore γ is called *anomalous dimension.*
There are basically two different approaches to the calculation of the anomalous dimensions which are relevant for QCD. One is based on operator product expansion (OPE), the other one on the QCD improved parton model. The OPE approach is quite general and relies on the scaling properties of certain operators, extracted by using the renormalization group equations. The parton model approach is special to QCD and is closer to an intuitive physical picture of perturbative QCD. Therefore we will start with the parton model to enter into the subject.

2.1 QCD and the parton model

It is well-known that the "naive" parton model [5] gets corrections in perturbative QCD. Nevertheless much of the structure of the parton model remains valid because of the property of *factorization.* Factorization permits scattering amplitudes with incoming high energy hadrons to be written as a product of a hard scattering piece and a remainder which contains the physics of low energies and momenta. The former contains only high energy and momentum components and, because of asymptotic freedom, is calculable in perturbation theory. The latter piece describes non-perturbative physics, but can be described by a single, process independent function for each type of parton, called the *parton distribution function.* Without these properties of asymptotic freedom and factorization it would be impossible to make reasonable predictions for processes involving hadrons by using perturbation theory.

2.1.1 Deep inelastic scattering

One of the most powerful tests of perturbative QCD is the breaking of Bjorken scaling in deep inelastic lepton-hadron scattering (DIS). Moreover, the analysis of deep inelastic structure functions serves to determine the momentum distributions of partons in hadrons, needed as an input in predicting cross sections in high-energy hadron collisions.

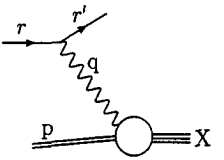

Figure 2.1: Deep inelastic scattering

We consider for definiteness the scattering of a high-energy charged lepton off a proton target (see Fig. 2.1). The standard deep inelastic scattering variables are defined by

$$\begin{aligned} Q^2 &= -q^2 \quad ; \quad M^2 = p^2 \\ \nu &= p\cdot q = M(E'-E) \\ x &= \frac{Q^2}{2\nu} \quad ; \quad y = \frac{q\cdot p}{r\cdot p} = 1 - \frac{E'}{E} \end{aligned}$$

where the energy variables refer to the target rest frame and M is the proton mass. The structure functions $F_i(x,Q^2)$ which parametrize the structure of the proton as "seen" by the virtual photon can be defined in terms of the lepton scattering cross section[1]:

$$\begin{aligned} \frac{d^2\sigma^{em}}{dxdy} &= \frac{8\pi\alpha^2 ME}{Q^4}\Big\{[1+(1-y)^2]\,x\,F_1^{em}(x,Q^2) \\ &\quad +(1-y)(F_2^{em}(x,Q^2) - 2xF_1^{em}(x,Q^2)) - \frac{M}{2E}\,xy\,F_2^{em}(x,Q^2)\Big\} \quad (2.1) \end{aligned}$$

The Bjorken limit is defined as $Q^2,\nu \to \infty$ with x fixed. In this limit the structure functions are observed to obey an approximate scaling law:

$$F_i(x,Q^2) \to F_i(x)\,.$$

[1]This expression is strictly valid only for $Q^2 \ll M_Z^2$.

Bjorken scaling implies that the virtual photon scatters off *point-like constituents*, since otherwise the dimensionless structure functions would depend on the ratio Q/Q_0 with $1/Q_0$ some length scale characterizing the size of the constituents.
The parton model picture becomes obvious in the *infinite momentum frame* in which the proton is moving very fast, $p^\mu \simeq (P, 0, 0, P)\,;\, P \gg M$. In this frame, we can consider a simple model where the photon scatters off a point-like quark constituent which is moving parallel with the proton, carrying a fraction ξ of its momentum, and the proton mass can be neglected. Then Eq. (2.1) can be rewritten as

$$\frac{d^2\sigma^{em}}{dxdQ^2} = \frac{4\pi\alpha^2}{Q^4}\Big\{[1+(1-y)^2]\,F_1(x,Q^2) + \frac{(1-y)}{x}(F_2(x,Q^2) - 2xF_1(x,Q^2))\Big\} \quad (2.2)$$

The terms proportional to F_1 and $F_2 - 2xF_1$ correspond to the absorption of transversely respectively longitudinally polarized virtual photons. Therefore, the combination $F_L = F_2 - 2xF_1$ is called the *longitudinal structure function.*

The basic assumption of the parton model thus is that the interactions of hadrons are due to the interactions of constituent partons. A necessary condition for such a picture to make sense is that changes in the number and momenta of the partons should be negligible during the time in which they are probed. In QCD, Bjorken scaling is broken by logarithms of Q^2. The reason is that the transverse momentum of the partons is *not* restricted to be small. A quark can emit a gluon and acquire large transverse momentum $k_\perp$ with probability $\sim \alpha_s\, dk_\perp^2/k_\perp^2$ at large $k_\perp$. The $k_\perp$–integral, extending up to the kinematic limit Q^2, then gives rise to contributions $\sim \alpha_s \log Q^2$ which break scaling. These logarithmic scaling violations are a particular property of renormalizable gauge theories with point-like fermion–vector boson interactions.

2.1.2 Parton distributions

The amplitude for the process depicted in Fig. 2.1 is given by

$$\mathcal{A} = e\bar{u}(r')\gamma^\alpha u(r)\frac{1}{q^2}\langle X|j_\alpha(0)|P\rangle$$

where j_α is the electromagnetic current. The cross section can be factored into a leptonic and a hadronic piece:

$$\frac{d^2\sigma}{dxdy} \sim L_{\alpha\beta}W^{\alpha\beta} \quad (2.3)$$

The structure of the leptonic tensor $L_{\alpha\beta}$, assuming photon exchange only, is completely determined by QED. The hadronic tensor[2] contains all the information about the

[2]We omit spin labels and sums here, so $\langle P|\hat{O}|P\rangle$ implicitly means $\frac{1}{2}\sum_\lambda \langle \lambda P|\hat{O}|P\lambda\rangle$.

interaction of the current j_α with the hadron P:

$$\begin{aligned} W_{\alpha\beta}(p,q) &= \frac{1}{4\pi}\sum_X \langle P|j_\alpha(0)|X\rangle\langle X|j_\beta(0)|P\rangle (2\pi)^4\,\delta^4(q+p-p_X) \\ &= \frac{1}{4\pi}\int d^4z e^{iqz}\langle P|[j_\alpha(z),j_\beta(0)]|P\rangle \end{aligned} \tag{2.4}$$

It is easy to show that the amplitude $W_{\alpha\beta}$ is related to the absorptive part (discontinuity) of the forward virtual Compton amplitude $T_{\alpha\beta}$:

$$W_{\alpha\beta} = \frac{1}{2\pi}\,\mathrm{Disc}\,T_{\alpha\beta} \tag{2.5}$$

$$T_{\alpha\beta} = i\int d^4z e^{iqz}\langle P|T\,[j_\alpha(z)j_\beta(0)]|P\rangle \tag{2.6}$$

$$\mathrm{Disc}\,T_{\alpha\beta} = \lim_{\epsilon\to 0^+}\frac{1}{2i}\left[T_{\alpha\beta}(q_0+i\epsilon)-T_{\alpha\beta}(q_0-i\epsilon)\right]$$

Since the electromagnetic current is conserved, we have $q^\alpha W_{\alpha\beta}=0$. Therefore the most general form of $W_{\alpha\beta}$ for charged lepton-hadron interaction can be written as

$$W_{\alpha\beta}(p,q) = \left(g_{\alpha\beta}-\frac{q_\alpha q_\beta}{q^2}\right)W_1(x,Q^2)+\left(p_\alpha+\frac{q_\alpha}{2x}\right)\left(p_\beta+\frac{q_\beta}{2x}\right)W_2(x,Q^2) \tag{2.7}$$

Comparing Eqs. (2.7) and (2.1) finally leads to the relations

$$\begin{aligned} F_1(x,Q^2) &= W_1(x,Q^2) \\ F_2(x,Q^2) &= \nu\, W_2(x,Q^2) \end{aligned}$$

To analyze the hadronic tensor $W_{\alpha\beta}$ it is convenient to introduce two light-like vectors p and n with $n\cdot p=1$. Any four-vector k can then be written in terms of p, n and a space-like two-dimensional transverse vector $k_\perp$:

$$\begin{aligned} k^\mu &= ap^\mu + bn^\mu + k_\perp^\mu \\ p^2 &= n^2 = n\cdot k_\perp = p\cdot k_\perp = 0\,. \end{aligned} \tag{2.8}$$

In a frame where the struck proton is moving very fast along the positive $z-$axis, an explicit representation of the vectors p and n is

$$\begin{aligned} p^\mu &= (P,0,0,P) \\ n^\mu &= (\frac{1}{2P},0,0,-\frac{1}{2P}) \end{aligned} \tag{2.9}$$

In the following we will ignore the target mass M such that the proton momentum can be identified with p^μ.

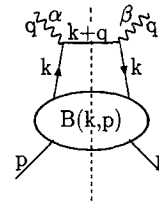

Figure 2.2: 'Handbag' diagram

Making the assumption that the photon scatters incoherently off the individual partons, the hadronic tensor $W_{\alpha\beta}$ is obtained from the diagram shown in Fig. 2.2.

$$W_{\alpha\beta}(p,q) = \sum_{q,\bar{q}} e_q^2 \int \frac{d^4k}{(2\pi)^4} [\gamma_\alpha(\not{k} + \not{q})\gamma_\beta]_{ij} B_{ji}(k,p)\, \delta((k+q)^2) \tag{2.10}$$

The quark four-momentum k, carrying the longitudinal momentum fraction ξ of the incoming momentum p, can be written as

$$k^\mu = \xi\, p^\mu + \frac{k^2 + k_\perp^2}{2\xi}\, n^\mu + k_\perp^\mu \tag{2.11}$$

The assumption of the parton model is that the structure of the amplitude $B(k,p)$ is such that it is strongly damped when the transverse momentum $k_\perp^2$ and the virtuality k^2 are large. Thus the integral (2.10) is dominated by small values of these variables and the delta function may be approximated by

$$\delta((k+q)^2) = \delta(k^2 + 2\xi\nu - 2q_\perp k_\perp + q^2) \approx \delta(2\xi\nu - Q^2) = \frac{1}{2\nu}\delta(\xi - x)$$

This gives, using $q^\mu = \nu\, n^\mu + q_\perp^\mu$

$$\begin{aligned} \nu W_2 = F_2 &= \sum_{q,\bar{q}} \frac{e_q^2}{2} \int \frac{d^4k}{(2\pi)^4} [\not{n}(\not{k} + \not{q})\ \not{n}]_{ij} B_{ji}(k,p)\delta(\xi - x) \\ &= \sum_{q,\bar{q}} e_q^2 x \int \frac{d^4k}{(2\pi)^4} [\not{n}]_{ij} B_{ji}(k,p)\delta(\xi - x) \\ &= \sum_{q,\bar{q}} e_q^2\, x\, q(x) \end{aligned} \tag{2.12}$$

where $q(x)$ is the *quark distribution*

$$q(x) = \int \frac{d^4k}{(2\pi)^4} Tr[\not{n} B(k,p)]\, \delta(nk - x) \tag{2.13}$$

So we can see that the structure function *scales*, that is, it depends only on the dimensionless variable x.

It is also possible to give an operator representation [43, 20, 44] for the quark distribution $q(x)$. In this representation, the distribution functions are matrix elements in a hadron state of certain operators that act to count the number of quarks or gluons carrying a fraction ξ of the hadron's momentum. The definition may be motivated by looking at the theory quantized on the plane $x^+ = 0$ in the light-cone gauge $A^+ = 0$, since in this picture field theory has its closest connection with the parton model. We work in a frame where the hadron's momentum is $P = (P^+, P^-, \vec{0}) = (P^+, M^2/2P^+, \vec{0})$, where the plus and minus components are defined as $r^\pm = \frac{1}{\sqrt{2}}(r^0 \pm r^3)$ for an arbitrary four-vector r. In this approach the quark field has two components that represent the independent degrees of freedom. $\gamma^+\psi(x)$ contains only these components. One can expand the two independent components in terms of quark destruction operators $b(k^+, k_\perp, s)$ and antiquark creation operators $d(k^+, k_\perp, s)^\dagger$ as follows:

$$\begin{aligned}\gamma^+\psi(0, x^-, x_\perp) &= (2\pi)^{-3} \sum_s \int_0^\infty \frac{dk^+}{2k^+} \int dk_\perp \\ &\quad \cdot\{\gamma^+ U(k,s) e^{-ikx} b(k^+, k_\perp, s) + \gamma^+ V(k,s) e^{ikx} d(k^+, k_\perp, s)^\dagger\} .\end{aligned}$$

The quark distribution function is just the hadron matrix element of the operator that counts the number of quarks:

$$f_{q/A}(\xi) d\xi = (2\pi)^{-3} \sum_s \int_0^\infty \frac{d(\xi P^+)}{2\xi P^+} \int dk_\perp \langle P| b(\xi P^+, k_\perp, s)^\dagger b(\xi P^+, k_\perp, s)|P\rangle .$$

In terms of $\psi(x)$, this is

$$f_{q/A}(\xi) = \frac{1}{4\pi} \int dx^- \, e^{-i\xi P^+ x^-} \langle P|\bar{\psi}(0, x^-, 0_\perp)\gamma^+ \psi(0,0,0_\perp)|P\rangle . \tag{2.14}$$

The above definition is gauge dependent: What is defined to be a quark in one gauge is a quark plus gluons in another gauge. In order to arrive at a gauge invariant definition, we have to insert the path ordered exponential of the gluon field

$$\mathcal{G} = \mathcal{P} \exp\left\{ig \int_0^{x^-} dy^- \, A_c^+(0, y^-, 0_\perp) t^c\right\} . \tag{2.15}$$

In the light-cone gauge $A^+ = 0$ we obviously have $\mathcal{G} = 1$. So the gauge invariant definition of the parton densities is given by

$$f_{q/A}(\xi) = \frac{1}{4\pi} \int dx^- \, e^{-i\xi P^+ x^-} \langle P|\bar{\psi}(0, x^-, 0_\perp)\gamma^+ \mathcal{G}\psi(0,0,0_\perp)|P\rangle . \tag{2.16}$$

For gluons, the definition based on the same reasoning is

$$f_{g/A}(\xi) = \frac{1}{2\pi\xi P^+}\int dx^- e^{-i\xi P^+x^-}\langle P|F_a^{+\nu}(0,x^-,0_\perp)\mathcal{G}^{ab}F_{b,+\nu}(0,0,0_\perp)|P\rangle\,. \qquad (2.17)$$

where $F_a^{\mu\nu}$ is the gluon field strength operator and in $\mathcal{G}$ we now use the adjoint representation of the colour group generators.

As we already mentioned, the parton model result (2.12) gets higher order corrections in α_s in perturbation theory. In our example of a quark being the interacting parton, the $\mathcal{O}(\alpha_s)$ correction is due to one-gluon emission of the parton before the interaction with the photon takes place.
So consider the parton process shown in Fig. 2.3 in which the quark emits a gluon:

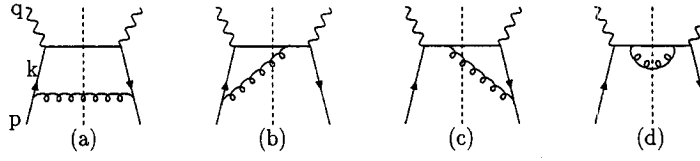

Figure 2.3: Real gluon emission diagrams

$$\gamma^*(q) + q(p) \to g(r) + q(l) \qquad (2.18)$$

Calculating these diagrams and including also the diagrams for virtual gluon radiation, we obtain

$$\hat{F}_2(x,Q^2) = e_q^2\, x\Big\{\delta(1-x) + \frac{\alpha_s}{2\pi}\,[P_{q/q}(x)\ln\frac{Q^2}{\kappa^2} + C(x)]\Big\} \qquad (2.19)$$

where the "hat" in $\hat{F}_2$ indicates that this structure function refers to a quark instead of a proton target as we deal with the process (2.18). $C(x)$ is a calculable and finite function. The logarithm $\ln\frac{Q^2}{\kappa^2}$ is stemming from the integral over the quark virtuality $|k^2|$:

$$\hat{F}_2|_{\rm div} = e_q^2\frac{\alpha_s}{2\pi}\,x\,P_{q/q}(x)\int_{\kappa^2}^{Q^2/x}\frac{d|k^2|}{|k^2|} \qquad (2.20)$$

We introduced the cutoff κ^2 to regulate the divergence at small $|k^2|$. The origin and treatment of this singularity will be discussed below.
The coefficient $P_{q/q}(x)$ of the $\ln\frac{Q^2}{\kappa^2}$–term is called the *quark-quark splitting function.* It is of the form

$$P_{q/q}(x) = C_F\left\{\frac{1+x^2}{(1-x)_+} + \frac{3}{2}\,\delta(1-x)\right\} \qquad (2.21)$$

where the "plus" distribution is defined by

$$\int_0^1 dx \frac{f(x)}{(1-x)_+} = \int_0^1 dx \frac{[f(x)-f(1)]}{1-x} \tag{2.22}$$

for any sufficiently smooth function $f(x)$.
Note that due to fermion number conservation in the splitting of quarks we have the sum rule

$$\int_0^1 dx\, P_{q/q}(x) = 0\,,$$

whose validity can immediately be checked in this order in α_s if the "plus" distribution is used.

From Eq. (2.19) we can see that beyond leading order the structure function becomes Q^2−dependent. The quark distribution function to this order in perturbation theory is given by

$$q(x,Q^2) = \delta(1-x) + \frac{\alpha_s}{2\pi}\left[P_{q/q}(x)\ln\frac{Q^2}{\kappa^2} + C(x)\right].$$

2.1.3 Factorization

The singularity at $|k^2| = 0$ in Eq. (2.20) arises when the gluon is emitted parallel to the quark ($k_\perp^2 = |k^2|(1-\xi) = 0$). For this reason it is called a *collinear divergence*. The limit $k_\perp^2 \to 0$ corresponds to a long-range part of the strong interaction which is not calculable in perturbation theory. Nevertheless, reliable predictions for processes with large momentum transfer can be obtained by exploiting the property of *factorization*: The aim is to absorb the infrared singularities due to collinear long-distance effects into the parton distribution functions, such that the full cross section factorizes into an infrared safe hard scattering cross section and the parton distribution functions which have to be measured at a certain scale, but whose evolution with Q^2 can be calculated. The parton distribution functions are *universal* in the sense that they do not depend on the particular hard process, but only on the type of the incoming parton. For outgoing partons, the procedure is analogous, dealing with parton *fragmentation functions* instead of the parton distribution functions.
In our example, factorization is achieved in the following way: In order to obtain the proton structure function F_2, we must convolute the quark structure function $\hat{F}_2$ of Eq. (2.19) with a "bare" distribution q_0 of a quark in a proton and sum over quark flavours, leading to

$$F_2(x,Q^2) = x\sum_{q,\bar{q}} e_q^2 \left\{ q_0(x) + \frac{\alpha_s}{2\pi}\int_x^1 \frac{d\xi}{\xi}\, q_0(\xi)[P_{q/q}(\frac{x}{\xi})\ln\frac{Q^2}{\kappa^2} + C(\frac{x}{\xi})] + \mathcal{O}(\alpha_s{}^2)\right\} \tag{2.23}$$

Exactly as for the renormalization of the coupling constant, we can regard $q_0(x)$ as an unmeasurable, *bare* distribution. The collinear singularities are absorbed into this bare

distribution at a factorization scale μ, which plays a similar role as the renormalization scale. So we define a "renormalized" distribution $q(x,\mu^2)$ by

$$q(x,\mu^2) = q_0(x) + \frac{\alpha_s}{2\pi}\int_x^1 \frac{d\xi}{\xi}\, q_0(\xi)[P_{q/q}(\frac{x}{\xi})\ln\frac{\mu^2}{\kappa^2} + C(\frac{x}{\xi})] + \mathcal{O}({\alpha_s}^2) \tag{2.24}$$

such that

$$F_2(x,Q^2) = x\sum_{q,\bar{q}} e_q^2 \int_x^1 \frac{d\xi}{\xi}\, q(\xi,\mu^2)\Big\{\delta(1-\frac{x}{\xi}) + \frac{\alpha_s}{2\pi}\, P_{q/q}(\frac{x}{\xi})\ln\frac{Q^2}{\mu^2} + \mathcal{O}({\alpha_s}^2)\Big\} \tag{2.25}$$

The distribution $q(\xi,\mu^2)$ cannot be calculated from first principles in perturbation theory, since it receives contributions from the long-distance (non-perturbative) part of the strong interaction. It has to be determined from structure function data.
The *factorization scale* μ is an arbitrary parameter. From its origin in the above discussion, it can be thought of as the scale which separates long– and short–distance physics. On the other hand, exploiting its arbitrariness, it is often set approximately equal to the scale Q^2 in order to keep the logarithm $\ln\frac{Q^2}{\mu^2}$, i.e. the higher order corrections, small. Thus μ^2 can vary from about 2 GeV to very large scales. The hard-scattering (short-distance) cross section is obtained from the parton-scattering cross section by removing long-distance pieces and factoring them into the parton distribution functions. Hence a parton emitted with a transverse momentum less than the scale μ is considered as a part of the hadron structure and is absorbed into the parton distribution. A parton emitted at a transverse momentum larger than μ is part of the short-distance cross section. The more terms included in the perturbative expansion, the weaker the dependence on μ will be, analogous to the case of the renormalization scale. In fact, renormalization and factorization scales are often set equal.

Note that while factorization provides a prescription for dealing with the logarithmic singularities, there is an arbitrariness in how the finite contributions are treated. How much of the finite contribution is factored out defines what is called the *factorization scheme*. In the $\overline{\rm MS}$ scheme, only the divergent part and the terms $\ln(4\pi) - \gamma_E$ are absorbed into the parton distribution.

In order to obtain a complete description of the deep inelastic structure functions in terms of parton distributions, we also have to include the $\mathcal{O}(\alpha_s)$ contribution from the process $\gamma^* g \to q\bar{q}$. The result is

$$\hat{F}_2^g(x,Q^2) = x\sum_{q,\bar{q}} e_q^2 \frac{\alpha_s}{2\pi}[P_{q/g}(x)\ln\frac{Q^2}{\kappa^2} + C_g(x)] \tag{2.26}$$

where the splitting function is now

$$P_{q/g}(x) = T_R\,[x^2 + (1-x)^2]\,.$$

To obtain the physical structure function, the contribution (2.26) must be folded with a bare gluon distribution $g_0(x)$ and added to the result obtained in Eq. (2.23), leading to

$$\begin{aligned} q(x,\mu^2) &= q_0(x) + \frac{\alpha_s}{2\pi}\int_x^1 \frac{d\xi}{\xi}\, q_0(\xi)[P_{q/q}(\frac{x}{\xi})\ln\frac{\mu^2}{\kappa^2} + C_q(\frac{x}{\xi})] \\ &\quad + \frac{\alpha_s}{2\pi}\int_x^1 \frac{d\xi}{\xi}\, g_0(\xi)[P_{q/g}(\frac{x}{\xi})\ln\frac{\mu^2}{\kappa^2} + C_g(\frac{x}{\xi})] + \mathcal{O}({\alpha_s}^2) \end{aligned} \tag{2.27}$$

such that in the $\overline{\rm MS}$ scheme

$$\begin{aligned} F_2(x,Q^2) &= x\sum_{q,\bar{q}} e_q^2 \int_x^1 \frac{d\xi}{\xi}\, q(\xi,Q^2)\Big\{\delta(1-\frac{x}{\xi}) + \frac{\alpha_s}{2\pi} C_q^{\overline{MS}}(\frac{x}{\xi}) + \mathcal{O}({\alpha_s}^2)\Big\} \\ &\quad + x\sum_{q,\bar{q}} e_q^2 \int_x^1 \frac{d\xi}{\xi}\, g(\xi,Q^2)\Big\{\frac{\alpha_s}{2\pi} C_g^{\overline{MS}}(\frac{x}{\xi}) + \mathcal{O}({\alpha_s}^2)\Big\} \end{aligned} \tag{2.28}$$

The functions $C_q(x)$ and $C_g(x)$ are called *coefficient functions*. They depend on the factorization and renormalization schemes and also on the structure function under consideration.

Including also higher order corrections, factorization for the DIS structure functions is of the following structure:

$$\begin{aligned} F_1(x,Q^2) &= \sum_a \int_x^1 \frac{d\xi}{\xi}\, f_{a/A}(\xi,\mu^2)\, C_{1a}(\frac{x}{\xi}, \frac{Q^2}{\mu^2}, \alpha_s(\mu^2)) + \text{ remainder} \\ \frac{1}{x}F_2(x,Q^2) &= \sum_a \int_x^1 \frac{d\xi}{\xi}\, f_{a/A}(\xi,\mu^2)\, C_{2a}(\frac{x}{\xi}, \frac{Q^2}{\mu^2}, \alpha_s(\mu^2)) + \text{ remainder} \end{aligned} \tag{2.29}$$

Here $f_{a/A}(\xi,\mu^2)$ are the parton distribution functions (defined with charges included). The quantity $f_{a/A}(\xi,\mu^2)d\xi$ can be interpreted as the probability of finding a parton of type a (a = gluon,$u,\bar{u},d,\bar{d},\ldots$) in a hadron A carrying a longitudinal momentum fraction ξ to $\xi + d\xi$ of the hadron's momentum. The parton densities are *universal*: They depend only on whether the evolving parton has space-like momentum (like in DIS) or time-like momentum (like in e^+e^- annihilation).
The hard scattering coefficients C_{ia} are infrared safe functions that depend on the parton type a (and on the factorization scheme, as stated above), but *not* on the external hadron A. Being free from long-distance effects, they are calculable in perturbation theory due to asymptotic freedom.
The independence of the C_{ia} from the external hadron A allows to calculate these functions with the simplest choice of the external hadron: $A = b, b$ being a parton.
The remainders in Eq. (2.29) are suppressed by powers of $1/Q^2$. Inspired by the terminology of operator product expansion (see Section 2.2), they are called the *higher twist contributions*.

Summing up, the fundamental content of the factorization theorem is that all the short-distance dependence resides in the coefficient functions C_{ia}, while all long-distance dependence has been absorbed into universal parton distributions. Corrections to factorization are suppressed by powers of Q^2.

A rigorous proof of factorization to all orders could be provided for deep inelastic scattering in the context of operator product expansion [7, 8]. The proof for other hadronic cross sections is highly nontrivial [19, 20, 46, 28] and formally has not reached the status of the treatment by OPE. While the OPE proof could exploit the properties of Green functions in Euclidean space, the proofs beyond OPE require a detailed examination of all the dangerous momentum regions of massless particles in Minkowski space.

The plausibility of factorization properties for processes with one incoming hadron can be seen from the following argument: Considering electron-hadron scattering by virtual photon exchange at high momentum transfer in the center-of-mass frame, two important things happen to the hadron: It is Lorentz contracted in the direction of the collision, and its internal interactions are time dilated. Hence as the center-of-mass energy increases, the lifetime of any virtual partonic state is lengthened, while the time it takes the electron to traverse the hadron is shortened. When the latter is much shorter than the former, the hadron will be in a single virtual state characterized by a definite number of partons during the entire time the electron takes to cross it. Since the partons do not interact during this time, each one may be thought of as carrying a definite fraction x of the hadron's momentum. It now makes sense to talk about the electron interacting with partons of definite momentum, rather than with the hadron as a whole. In addition, if the momentum transfer is very high, the virtual photon which mediates the electron-parton scattering cannot travel far. Therefore, if the density of the partons is not too high, the electron will be able to interact with only one single parton. So roughly one can say that the initial state interactions, which give rise to soft and collinear singularities, are too early, the final state interactions are too late relative to the short time scale of the hard scattering. Therefore it is appropriate that these singularities are included in the wave functions of the incoming hadrons and not in the short-distance cross section. The proofs of factorization establish that this simple picture is in fact valid in perturbation theory for a large class of processes.

In hadron-hadron collisions, the analysis is more complicated since the question arises whether the partons in hadron H_1, through the influence of their colour fields, change the distribution of partons in hadron H_2, thus spoiling the simple parton picture. Soft gluons which are emitted long before the collision are potentially troublesome in this respect. But it can be argued that soft gluons do in general *not* spoil this picture, using a simple model from classical electrodynamics [16]: Consider a particle with charge e travelling in the positive z direction with constant velocity β. At an observation point described by the coordinates x, y, z, (the position of hadron H_2), the vector potential A_μ at a time t due to the passage of the fast moving charge can

be calculated to be

$$\begin{aligned} A^t(t,\vec{x}) &= \frac{e\gamma}{\sqrt{x^2+y^2+\gamma^2(\beta t-z)^2}} \\ A^x(t,\vec{x}) &= A^y(t,\vec{x})=0 \\ A^z(t,\vec{x}) &= \frac{e\gamma\beta}{\sqrt{x^2+y^2+\gamma^2(\beta t-z)^2}} \end{aligned} \tag{2.30}$$

where $\gamma^2 = 1/(1-\beta^2)$. Now it can be shown that the vector potential (2.30) leads to field strengths which vanish at high energy. For example, the electric field along the z direction is

$$E^z(t,\vec{x}) = \frac{\partial A^z}{\partial t} + \frac{\partial A^t}{\partial z} = \frac{e\gamma(\beta t-z)}{[x^2+y^2+\gamma^2(\beta t-z)^2]^{\frac{3}{2}}} . \tag{2.31}$$

Hence at high energy, the field strengths are of order $1/\gamma^2 \approx M^4/s^2$. Thus the force experienced by a colour charge in the hadron H_2 at any fixed time before the arrival of the quark decreases as M^4/s^2. There are residual interactions which distort the distribution of partons in hadron H_2, but their effects vanish at high energies. A breakdown of factorization at order $1/s^2$ is therefore to be expected in perturbation theory, and has been demonstrated explicitly in ref. [17]. Note that these effects are due to the long-range nature of the massless vector field. In the realistic case of an incoming colour neutral hadron, there are no long-range colour fields. It is therefore possible that power corrections to factorization, i.e. terms of order $(M^2/s)^n$, will occur in general only at a higher power of n than suggested by the above argument.

2.1.4 The Altarelli-Parisi equation

We have seen in the last section that the parton distributions cannot be calculated in perturbation theory. However, what *can* be calculated perturbatively is their dependence on the factorization scale μ^2. The structure functions of course have to be independent of μ^2, so taking the derivative $\partial/\partial \ln \mu^2$ on both sides of Eq. (2.25) will give us a differential equation for the μ^2−dependence of $q(x,\mu^2)$ and hence for the Q^2−dependence of the structure functions. Defining $t = \mu^2$, we obtain

$$t\frac{\partial}{\partial t} q(x,t) = \frac{\alpha_s}{2\pi}\int_x^1 \frac{d\xi}{\xi} P_{q/q}(\frac{x}{\xi}) q(\xi,t) \tag{2.32}$$

This equation, known as the (Dokshitzer-)Gribov-Lipatov-Altarelli-Parisi (GLAP) equation [13, 14], is the analogue of the equation for the β function describing the variation of $\alpha_s(t)$ with t and is one of the most important equations in perturbative QCD.

A more rigorous treatment based on operator product expansion and the renormalization group equations [11, 12] extends the above result to higher orders in perturbation

theory, leading to

$$t\frac{\partial}{\partial t}\,q(x,t) = \int_x^1 \frac{d\xi}{\xi}\,P_{q/q}\Big(\frac{x}{\xi},\alpha_s(t)\Big)\,q(\xi,t) \tag{2.33}$$

where $P_{q/q}(z,\alpha_s)$ can be calculated as a power series in α_s:

$$P_{q/q}(z,\alpha_s) = \frac{\alpha_s}{2\pi}\,P^{(0)}_{q/q}(z) + \Big(\frac{\alpha_s}{2\pi}\Big)^2 P^{(1)}_{q/q}(z) + \mathcal{O}({\alpha_s}^3)\,. \tag{2.34}$$

The above equation holds for distributions which are *non-singlets* under the flavour group: $q_{\rm ns} = q_i - q_j$ with q_i, q_j being a quark or antiquark of any flavour. More generally, the GLAP equation is a $(2n_f+1)-$dimensional matrix equation in the space of quarks, antiquarks and gluons,

$$t\frac{\partial}{\partial t}\begin{pmatrix} q_i(x,t) \\ g(x,t)\end{pmatrix} = \sum_{q_j,\bar{q}_j}\int_x^1 \frac{d\xi}{\xi}\begin{pmatrix} P_{q_i/q_j}(\frac{x}{\xi},\alpha_s(t)) & P_{q_i/g}(\frac{x}{\xi},\alpha_s(t)) \\ P_{g/q_j}(\frac{x}{\xi},\alpha_s(t)) & P_{g/g}(\frac{x}{\xi},\alpha_s(t))\end{pmatrix}\begin{pmatrix} q_j(\xi,t) \\ g(\xi,t)\end{pmatrix} \tag{2.35}$$

where each splitting function is calculable as a power series in α_s.
Beyond leading order, the flavour structure of the function P_{q_i/q_j} is nontrivial. Using $SU(n_f)$ flavour symmetry, we can define the following flavour singlet (S) and non-singlet (V) quantities:

$$\begin{aligned} P_{q_i/q_j} &= \delta_{ij}P^{(V)}_{q/q} + P^{(S)}_{q/q} \\ P_{q_i/\bar{q}_j} &= \delta_{ij}P^{(V)}_{q/\bar{q}} + P^{(S)}_{q/\bar{q}} \\ P^{\pm} &= P^{(V)}_{q/q} \pm P^{(V)}_{q/\bar{q}} \end{aligned} \tag{2.36}$$

At next-to-leading order, the functions $P^{(S)}_{q/q}$ and $P^{(S)}_{q/\bar{q}}$ are nonzero, but we have the additional relation

$$P^{(S)}_{q/q} = P^{(S)}_{q/\bar{q}}\,.$$

Now we define for each flavour the sum respectively difference of the quark and anti-quark distributions as

$$q_i^{\pm} = q_i \pm \bar{q}_i \tag{2.37}$$

It is then straightforward to show that at NLO, the combinations

$$\begin{aligned} V_i &= q_i^- \\ T_l &= \sum_{i=1}^{k} q_i^+ - k q_k^+\;;\; i,k = 1,\ldots,n_f\;; l = (k+1)^2 - 1 \end{aligned}$$

are *non-singlets*, i.e., evolve according to Eq. (2.33) with the kernels P^- and P^+, respectively.
The one remaining combination of quark distributions is the *singlet distribution*

$$\Sigma(x,t) = \sum_{i=1}^{n_f}\left[\,q_i(x,t) + \bar{q}_i(x,t)\,\right] \tag{2.38}$$

Note that because of charge conjugation invariance and $SU(n_f)$ flavour symmetry the splitting functions $P_{q/g}$ and $P_{g/q}$ are independent of the quark flavour and the same for quarks and antiquarks. Hence taking into account the considerations above, Eq. (2.35) simplifies to

$$t\frac{\partial}{\partial t}\begin{pmatrix}\Sigma(x,t)\\ g(x,t)\end{pmatrix}=\int_x^1\frac{d\xi}{\xi}\begin{pmatrix}P_{q/q}(\frac{x}{\xi},\alpha_s(t)) & 2n_fP_{q/g}(\frac{x}{\xi},\alpha_s(t))\\ P_{g/q}(\frac{x}{\xi},\alpha_s(t)) & P_{g/g}(\frac{x}{\xi},\alpha_s(t))\end{pmatrix}\begin{pmatrix}\Sigma(\xi,t)\\ g(\xi,t)\end{pmatrix}. \quad (2.39)$$

where now

$$P_{q/q}=P^+ + n_f\,[P^{(S)}_{q/q}+P^{(S)}_{q/\bar{q}}]=P^+ + 2n_f\,P^{(S)}_{q/\bar{q}} \quad (2.40)$$

The leading order splitting functions $P^{(0)}_{a/b}(x)$ can be interpreted as the probabilities of finding a parton of type a in a parton of type b with a fraction x of the longitudinal momentum of the parent parton and a transverse momentum squared much less than μ^2. The interpretation as probabilities implies that the splitting functions are positive definite for $x<1$, and satisfy the following sum rules which correspond to quark number conservation and momentum conservation in the splittings of quarks respectively gluons:

$$\begin{aligned}\int_0^1 dx P^{(0)}_{q/q}(x) &= 0\\ \int_0^1 dx\,x\,[P^{(0)}_{q/q}(x)+P^{(0)}_{g/q}(x)] &= 0\\ \int_0^1 dx\,x\,[2n_fP^{(0)}_{q/g}(x)+P^{(0)}_{g/g}(x)] &= 0\end{aligned}$$

The leading order splitting functions are given by [13]

$$P^{(0)}_{q/q}(x) = C_F\Big\{\frac{1+x^2}{(1-x)_+}+\frac{3}{2}\delta(1-x)\Big\} \quad (2.41)$$

$$P^{(0)}_{q/g}(x) = T_R\Big\{x^2+(1-x)^2\Big\}\quad T_R=\frac{1}{2} \quad (2.42)$$

$$P^{(0)}_{g/q}(x) = C_F\Big\{\frac{1+(1-x)^2}{x}\Big\} \quad (2.43)$$

$$\begin{aligned}P^{(0)}_{g/g}(x) &= 2N_c\Big\{\frac{x}{(1-x)_+}+\frac{1-x}{x}+x(1-x)\Big\}\\ &\quad +\delta(1-x)[\frac{11}{6}N_c-\frac{2}{3}n_fT_R]\end{aligned} \quad (2.44)$$

The calculation of the next-to-leading order splitting functions $P^{(1)}_{a/b}(x)$ will be the subject of Chapter 3.

2.1.5 Anomalous dimensions in the parton model

The GLAP equation, which is an integro-differential equation in $x-$space, can be written in a factorized form by taking moments (Mellin transforms) with respect to the variable x, defined for any function $f(x)$ by

$$f(N) = \int_0^1 dx\, x^{N-1} f(x)\,.$$

Convolutions reduce to products under these moments. Therefore, the $t-$dependence of a non-singlet quark distribution function is given in terms of moments by

$$t\frac{\partial}{\partial t}\, q_{\rm ns}(N,t) = \gamma_{q/q}(N,\alpha_s(t))\, q_{\rm ns}(N,t)\,, \tag{2.45}$$

where the *anomalous dimension* $\gamma_{q/q}(N,\alpha_s(t))$ is given by the Mellin transform of the splitting function:

$$\gamma_{q/q}(N,\alpha_s(t)) = \int_0^1 dx\, x^{N-1} P_{q/q}(x,\alpha_s(t))\,. \tag{2.46}$$

The equation analogous to Eq. (2.45) for the moments $\Sigma(N,t)$ and $g(N,t)$ of the singlet quark and gluon distributions correspondingly is given by

$$t\frac{\partial}{\partial t}\begin{pmatrix}\Sigma(N,t)\\ g(N,t)\end{pmatrix} = \begin{pmatrix}\gamma_{q/q}(N,\alpha_s(t)) & 2n_f\,\gamma_{q/g}(N,\alpha_s(t))\\ \gamma_{g/q}(N,\alpha_s(t)) & \gamma_{g/g}(N,\alpha_s(t))\end{pmatrix}\begin{pmatrix}\Sigma(N,t)\\ g(N,t)\end{pmatrix}. \tag{2.47}$$

The solution of the non-singlet GLAP equation (2.45) is, in terms of moments, given by

$$q_{\rm ns}(N,t) = q_{\rm ns}(N,t_0)\left(\frac{\alpha_s(t_0)}{\alpha_s(t)}\right)^{d_{qq}(N)} \quad ; \quad d_{qq}(N) = \frac{\gamma^{(0)}_{q/q}(N)}{2\pi b} \tag{2.48}$$

where the lowest order form $\alpha_s(Q^2) = 1/(b\ln\frac{Q^2}{\Lambda^2})$; $b = (33-2n_f)/12\pi$ for the running coupling has been used.
At this point not only the conceptual, but also the practical importance of anomalous dimensions becomes obvious: Their knowledge allows for a prediction of the parton densities at a scale $t = \mu^2$ once they have been measured at a scale μ_0^2.

2.2 Operator product expansion

As we already explained in Section 2.1.2, the parton distributions $q_{\rm ns}(x,t)$ or, more general, $f_{a/b}(x,t)$, can be calculated as matrix elements of certain operators. In moment space, the analogous structure is obtained by using operator product expansion (OPE). It allows to relate the moments of the parton distributions to the matrix elements between hadron states of local operators. The predictive power of the operator

product expansion will come from the fact that the coefficient functions C_i have an increasing power law suppression as the dimensions of the corresponding operators O_i get larger. Therefore, only a small number of terms is relevant, and the renormalization group plus finite order perturbation theory may be used to compute the coefficient functions to a useful approximation. Furthermore, the Q^2-dependence of the moments of the parton densities can be worked out by summing the leading logarithmic corrections to the matrix elements of twist two operators.

2.2.1 Composite operators

Products of fields at the same space-time point are called *composite operators*. When computed naively, composite operators are not well-defined since they have ultraviolet divergences. The aim of operator product expansion is to construct finite, renormalized composite operators. The operator product expansion has been introduced by Wilson [6] and is based on the idea that the products of operators $\hat{A}(x), \hat{B}(y)$ can be expanded in a series of well-defined local operators $\hat{O}_i(z)$ with singular $c-$number coefficients C_i:

$$\hat{A}(x)\hat{B}(y) = \sum_{i=0}^{\infty} C_i(x-y)\,\hat{O}_i(\frac{x+y}{2}) \tag{2.49}$$

The local operator $\hat{O}_i(z)$ is regular in the sense that the singularity of the product $\hat{A}(x)\hat{B}(y)$ for $y = x$ is fully contained in the coefficient functions $C_i(x-y)$. The series in Eq. (2.49) is arranged in the order of decreasing singularity, so $C_0(x-y)$ is the most singular coefficient as $y \to x$.
Operator product expansion was proven by Zimmermann [7, 8] within the framework of perturbation theory using the BHPZ method [56].

Renormalization of composite operators

Now we will consider Green functions which are extended to include the insertions of composite operators and discuss the renormalization of such Green functions.
To be specific, we look at the insertion of the product of two currents in a scalar field theory, which can be expanded in the following way:

$$\langle 0|T[j(x)j(0)\phi(x_1)\dots\phi(x_n)]|0\rangle = \sum_k C_k(x)\langle 0|T[O_k(0)\phi(x_1)\dots\phi(x_n)]|0\rangle \tag{2.50}$$

In momentum space, Eq. (2.50) can be written as

$$F(q,p_1,\dots,p_n) = \sum_k \tilde{C}_k(q)E_k(p_1,\dots,p_n) \tag{2.51}$$

where $F(q,p_1,\dots,p_n)$ is the truncated $n-$point Green function with insertion of the current product. The Green function $F(q,p_1,\dots,p_n)$ satisfies the standard renorma-

lization group equation[3]

$$[\mathcal{D} - n\gamma(g)]\, F = 0 \tag{2.52}$$

$$\begin{aligned} \text{where} \quad \mathcal{D} &= \mu\frac{\partial}{\partial\mu} + \beta(g)\frac{\partial}{\partial g} - \gamma_m(g) m\frac{\partial}{\partial m} \\ \gamma_m(g) &= -\mu\frac{\partial \ln m}{\partial\mu}\Big|_{g_B, m_B \text{ fixed}} \\ \gamma(g) &= \frac{1}{2}\mu\frac{\partial \ln Z_3}{\partial\mu}\Big|_{g_B, m_B \text{ fixed}} \end{aligned}$$

Z_3 is the renormalization constant of the fields $\phi(x)$.
On the other hand, the Green function $E_k(p_1, \ldots, p_n)$ can be shown to obey the renormalization group equation

$$[\mathcal{D} + \gamma_{O_k}(g) - n\gamma(g)]\, E_k = 0 \tag{2.53}$$

where $\gamma_{O_k}(g)$ is the anomalous dimension of the composite operator $O_k(x)$:

$$\gamma_{O_k}(g) = \mu\frac{\partial \ln Z_{O_k}}{\partial\mu}\Big|_{g_B, m_B \text{ fixed}} \quad ; \quad O_k = Z_{O_k}^{-1} \cdot O_k^B \tag{2.54}$$

Hence applying $\mathcal{D}$ to both sides of Eq. (2.51) and using (2.52) and (2.53) leads to

$$[\mathcal{D} - \gamma_{O_k}(g)]\, \tilde{C}_k(q) = 0\,. \tag{2.55}$$

This is the renormalization group equation which serves to determine the behavior of the coefficient function $C_k(q)$ for large momenta $-q^2 \to \infty$.

If there exist several composite operators O_i which have the same quantum numbers and canonical dimension, those operators mix with each other in the renormalization procedure, such that the renormalized operators are defined by

$$O_{Ri} = \sum_j Z_{ij}^{-1} O_j^B \tag{2.56}$$

This phenomenon is called *operator mixing* and plays a crucial role in the calculation of the flavour *singlet* anomalous dimensions in next-to-leading order via OPE.

[3] We assume that the current $j(x)$ is conserved. If this is not the case, $j(x)$ will be renormalized by a constant Z_j and the corresponding anomalous dimension $\gamma_j(g) = \mu\,\partial \ln Z_j/\partial\mu$ has to be included in Eq. (2.52).

2.2.2 Operator product expansion in deep inelastic scattering

The aim of this section is to derive an operator product expansion for the hadronic tensor $W_{\mu\nu}$ introduced in Eq. (2.5) in the context of the parton model. In this case, our composite operator is the time ordered product of two electromagnetic currents, $T[j_\mu(x)j_\nu(x')]$. Its general form can be determined by the requirements of Lorentz invariance and current conservation,

$$\begin{aligned} T[j_\mu(x)j_\nu(x')] &= (\partial_\mu\partial'_\nu - g_{\mu\nu}\partial^\rho\partial'_\rho)\, O_L(x,x') \\ &\quad +(g_{\mu\lambda}\partial_\rho\partial'_\nu + g_{\rho\nu}\partial_\mu\partial'_\lambda - g_{\mu\nu}\partial_\lambda\partial'_\rho - g_{\mu\lambda}g_{\rho\nu}\partial^\alpha\partial'_\alpha)\, O_2^{\lambda\rho}(x,x') \\ &\quad +\text{antisymmetric part} \end{aligned} \tag{2.57}$$

where $\partial_\mu = \partial/\partial x_\mu$ and the antisymmetric part does not contribute to the spin-averaged structure functions such that we will not consider it further.
In order to express the bilocal operators $O(x,x')$ in terms of local operators, we make use of the so-called *light-cone dominance*[4]:
For deep inelastic scattering with $-q^2 \to \infty$ and $-q^2/\nu$ fixed, the dominant contribution to $W_{\mu\nu}$ comes from the region $0 \le x^2 \le \text{const.}/(-q^2)$.
Therefore we can expand the Green functions near the light-cone, leading to

$$\begin{aligned} O_L(x,x') &= \sum_{i,n} C_{L,n}^{(i)}(y^2) y^{\mu_1}\ldots y^{\mu_n}\, O^{(i)}_{L\mu_1\ldots\mu_n}\left(\frac{x+x'}{2}\right) \\ O_2^{\lambda\rho}(x,x') &= \sum_{i,n} C_{2,n}^{(i)}(y^2) y^{\mu_1}\ldots y^{\mu_n}\, O^{(i)\lambda\rho}_{2\mu_1\ldots\mu_n}\left(\frac{x+x'}{2}\right) \end{aligned} \tag{2.58}$$

where $y = x - x'$.
For the spin averaged matrix element between proton states we therefore obtain from Eqs. (2.6),(2.57) and (2.58) after Fourier transformation:

$$\begin{aligned} -i\,T_{\mu\nu} &= \int d^4x\, e^{iqx}\langle P|T\,[j_\mu(x)j_\nu(0)]|P\rangle \\ &= (q_\mu q_\nu - q^2 g_{\mu\nu}) \sum_{i,n}\langle P|O^{(i)}_{L\mu_1\ldots\mu_n}(0)|P\rangle \int d^4x\, x^{\mu_1}\ldots x^{\mu_n} C_{L,n}^{(i)}(x^2)\, e^{iqx} \\ &\quad +(g_{\mu\lambda}q_\rho q_\nu + g_{\rho\nu}q_\mu q_\lambda - g_{\mu\nu}q_\rho q_\lambda - q^2 g_{\mu\lambda}g_{\rho\nu}) \\ &\quad \cdot\sum_{i,n}\langle P|O^{(i)\lambda\rho}_{2\mu_1\ldots\mu_n}(0)|P\rangle \int d^4x\, x^{\mu_1}\ldots x^{\mu_n} C_{2,n}^{(i)}(x^2)\, e^{iqx} \end{aligned} \tag{2.59}$$

The matrix elements of the composite operators appearing in Eq. (2.59) have the following tensor structures:

$$\begin{aligned} \langle P|O^{(i)}_{L\mu_1\ldots\mu_n}(0)|P\rangle &= A^{(i)}_{L,n} p_{\mu_1}\ldots p_{\mu_n} + \text{ terms containing } g_{\mu_i\nu_j} \\ \langle P|O^{(i)\lambda\rho}_{2\mu_1\ldots\mu_n}(0)|P\rangle &= A^{(i)}_{2,n+2} p^\lambda p^\rho p_{\mu_1}\ldots p_{\mu_n} + \text{ terms containing } g_{\mu_i\nu_j} \end{aligned} \tag{2.60}$$

[4]The proof is straightforward, see for example [57].

From expressions (2.59) and (2.60), sum rules for the DIS structure functions can be derived by using dispersion integrals, since the forward virtual Compton amplitude $T_{\mu\nu}$ is related to the hadronic tensor $W_{\mu\nu}$, as already stated in Eq. (2.5).

$$\int_0^1 dx\, x^{n-2} F_L(x,Q^2) = \sum_i A_{L,n}^{(i)}\, \tilde{C}_{L,n}^{(i)}(Q^2)$$
$$\int_0^1 dx\, x^{n-2} F_2(x,Q^2) = \sum_i A_{2,n}^{(i)}\, \tilde{C}_{2,n}^{(i)}(Q^2) \tag{2.61}$$

Equations (2.61) are called the *moment sum rules* for the structure functions. They exhibit the property of factorization already discussed in the context of the parton model: The coefficient functions $\tilde{C}_n^{(i)}(Q^2)$ are of short-distance nature and thus calculable within the framework of perturbative QCD. The long-distance effects are fully contained in the $A_n^{(i)}$, which correspond to the moments of the parton densities, as can be checked by comparing Eq. (2.61) to Eq. (2.29) derived in the context of the parton model. If the expressions $A_n^{(i)}$ were really constants, Bjorken scaling would be satisfied exactly. However, as we already know from the discussion of the parton model, these quantities actually depend on Q^2, i.e. on the renormalization point of the operators. Since this dependence comes only through operator rescaling, it involves only logarithms of Q^2, and so contributes only to a slow violation of Bjorken scaling. The Q^2 dependence can be worked out quantitatively by summing the leading logarithmic corrections to the matrix elements of twist two operators, finally arriving at the solution of the Altarelli-Parisi equation in terms of moments, which for the non-singlet case already has been given in Eq. (2.48).

Now it also becomes clear why the remainders in Eq. (2.29) have been called *higher twist* contributions: For dimensional reasons, following from Eq. (2.59), the light-cone singularity of the coefficient functions $C_n^{(i)}$ has to be of the form

$$C_n^{(i)}(x^2) \sim (x^2)^{-d_j + (d_O^i(n) - n)/2} \tag{2.62}$$

where d_j and $d_O^i(n)$ are the scale dimensions of the current and the composite operator $O_{\mu_1 \ldots \mu_n}^{(i)}$ respectively, and n corresponds to the maximum spin (i.e., number of vector indices) of the operator. The quantity

$$\tau_n^i = d_O^i(n) - n$$

is called the *twist* of the composite operator $O_{\mu_1 \ldots \mu_n}^{(i)}$. It is a measure for the strength of the light-cone singularity of $C_n^{(i)}(x^2)$: The smaller the value of τ_n^i, the stronger the singularity of $C_n^{(i)}(x^2)$. Since twist controls the singularities on the light-cone, it controls the high Q^2 behaviour of the Fourier transforms of the products of the currents, which are directly related to the DIS structure functions as has been shown above.

Therefore, the leading behaviour of the DIS structure functions can be determined by retaining only the operators of the lowest twist $\tau_n^i = 2$; the higher twist contributions are suppressed by powers of $1/Q^2$.
The quark operators of lowest twist are of the form

$$O^F_{\mu_1\ldots\mu_n} = i^{n-1} S\bar{\psi}\gamma_{\mu_1} D_{\mu_2}\ldots D_{\mu_n}\psi - g_{\mu_i\nu_j} \text{ terms} \tag{2.63}$$

where $D_\mu = \partial_\mu + ig\lambda^a A^a_\mu$ is the covariant derivative with λ^a being the colour group generators. $\bar{\psi}$ and ψ are quark fields and S denotes the symmetrization of Lorentz indices, whose number is always even for a non-vanishing operator. The symmetrization is necessary since we are dealing with unpolarized scattering. The subtraction of the $g_{\mu_i\nu_j}$ terms (the so-called trace terms) makes the operator have definite spin. That the operator in (2.63) is of lowest twist can be seen as follows: Consider a composite operator consisting only of quark fields whose canonical dimension is 3/2. Since an increase in the number of quark fields in the composite operator results in an increase in its canonical dimension, the number of quark fields involved must be minimal, that is, two, in order to keep the twist as small as possible. Hence the expected form of the minimum twist operator is

$$\bar{\psi}\Lambda_{\mu_1\ldots\mu_n}\psi$$

where $\Lambda_{\mu_1\ldots\mu_n}$ can be composed of γ_μ, ∂_μ and A^a_μ. By gauge invariance, ∂_μ and A^a_μ can appear only in the combination specified by D_μ. A γ_μ can appear only once because any multiple of γ_μ always reduces to a single or no γ_μ due to the symmetrization S. Thus we are left with an operator of the form (2.63) which has dimension $n+2$ and spin n and thus is of twist two, while the operators containing $g_{\mu_i\nu_j}$ terms have higher twist.
In order to classify all twist two composite operators relevant for DIS, one has to consider their transformation properties with respect to the flavour group. As we are interested in deep inelastic scattering, the quark masses may be safely neglected and so the flavour symmetry $SU(n_f)$ can be considered as exact. Since the quark fields ψ and the gluon field A^a_μ belong to the fundamental and singlet representation of $SU(n_f)$ respectively, the twist two composite operators containing two quark fields belong to the singlet or adjoint representation. Explicitly, the twist two *non-singlet* operator is given by

$$O^a_{\mu_1\ldots\mu_n} =: O^a_n = i^{n-1} S\bar{\psi}\gamma_{\mu_1} D_{\mu_2}\ldots D_{\mu_n} t^a\psi - \text{ trace terms} \tag{2.64}$$

where t^a $(a = 1, \ldots, n_f^2 - 1)$ are the generators of flavour $SU(n_f)$.
The twist-two composite operators which transform as *singlets* under the flavour group are of the form

$$O^F_{\mu_1\ldots\mu_n} = i^{n-1} S\bar{\psi}\gamma_{\mu_1} D_{\mu_2}\ldots D_{\mu_n}\psi - \text{ trace terms} \tag{2.65}$$

$$O^V_{\mu_1\ldots\mu_n} = 2i^{n-2} S F^{a_1}_{\mu_1\lambda} D^{a_1 a_2}_{\mu_2}\ldots D^{a_{n-1}a_{n-2}}_{\mu_{n-1}} F^{a_{n-1}\lambda}_{\mu_n} - \text{ trace terms} \tag{2.66}$$

where $O^V_{\mu_1\ldots\mu_n}$ is built from gluon fields, $F^a_{\mu\nu}$ being the gluon field strength tensor. Since there are two twist-two singlet operators, *operator mixing* will occur in the renormalization process, which complicates the calculation of the two-loop anomalous dimensions in the singlet sector.

2.2.3 Renormalization-group-improved perturbation theory

The renormalization group equation for the Fourier transforms $\tilde{C}_n^{(i)}(Q^2)$ of the coefficient functions[5] defined in Eq. (2.59) is given analogous to Eq. (2.55) by

$$[\mathcal{D} - \gamma_n(g)]\,\tilde{C}_n(\frac{q^2}{\mu^2}, g) = 0 \tag{2.67}$$

$$\text{where} \quad \gamma_n(g) = \frac{\partial}{\partial\mu}\ln Z_n\Big|_{g_B, m_B \text{ fixed}} \tag{2.68}$$

is the anomalous dimension of the operators $O_{\mu_1\ldots\mu_n}$ defined in Eq. (2.59). The solution of Eq. (2.67) is given by

$$\tilde{C}_n(\frac{q^2}{\mu^2}, g) = \tilde{C}_n(1, \bar{g}(t,g))\,\exp\{-\int_g^{\bar{g}(t)} d\lambda\,\frac{\gamma_n(\lambda)}{\beta(\lambda)}\} \tag{2.69}$$

$$\text{where} \quad t = \ln(\frac{-q^2}{\mu^2})$$

and the running coupling constant $\bar{g}(t)$ is the solution of the differential equation

$$\frac{d}{dt}\bar{g}(t,g) = \beta(\bar{g}) \quad ; \quad \bar{g}(0,g) = g\,. \tag{2.70}$$

Expanding $\gamma_n(\bar{g})$ and $\beta(\bar{g})$ perturbatively

$$\begin{aligned}\gamma_n(\bar{g}) &= \gamma_n^{(0)}\bar{g}^2 + \gamma_n^{(1)}\bar{g}^4 + \ldots \\ \beta(\bar{g}) &= -\beta_0\bar{g}^3 - \beta_1\bar{g}^5 + \ldots\end{aligned} \tag{2.71}$$

we obtain from Eq. (2.69), keeping the first two terms in the expansions above

$$\tilde{C}_n(\frac{q^2}{\mu^2}, g) \sim \tilde{C}_n(1, \bar{g}_0)\left(\frac{\bar{g}_0^2}{g^2}\right)^{\frac{\gamma_n^{(0)}}{2\beta_0}}\left(\frac{\beta_0 + \beta_1\bar{g}_0^2}{\beta_0 + \beta_1 g^2}\right)^{\frac{\gamma_n^{(0)}}{2\beta_0} - \frac{\gamma_n^{(1)}}{2\beta_1}} \tag{2.72}$$

where $\bar{g}_0^2 = 1/(2\beta_0 t)$ is the solution of Eq. (2.70) with only the first term in the expansion of β kept. The values of $\gamma_n^{(0)}, \beta_0$ and β_1 are well-known; the calculation of $\gamma_n^{(1)}$ is the main issue of Chapter 3.

[5] The subscripts L and 2 will be omitted here since the reasoning for both is the same.

Eq. (2.72) fully exhibits the virtues of the renormalization group equations in order to obtain predictions at different scales. Note that the coefficient functions are scheme dependent, the scheme dependence cancelling out when being combined with the parton densities (see Eqs. (2.29),(2.48),(2.61)) to the full cross section.

Using a perturbative expansion also for $\tilde{C}_n(1,\bar{g})$:

$$\tilde{C}_n(1,\bar{g}) = c_{0n} + c_{1n}\bar{g}^2 + \dots$$

and expanding Eq. (2.72) we obtain

$$\begin{aligned}\tilde{C}_n(Q^2) &= N_n \left(\ln\frac{Q^2}{\Lambda^2}\right)^{-\frac{\gamma_n^{(0)}}{2\beta_0}} \left[c_{0n} + \left(\beta_0 \ln\frac{Q^2}{\Lambda^2}\right)^{-1}\right. \\ &\quad \left.\cdot\left\{c_{1n} + c_{0n}\left(\frac{\gamma_n^{(1)}}{2\beta_0} - \frac{\beta_1\gamma_n^{(0)}}{2\beta_0^2}\right) - c_{0n}\frac{\beta_1\gamma_n^{(0)}}{2\beta_0^2}\ln\ln\frac{Q^2}{\Lambda^2}\right\} + \dots\right] \quad (2.73)\end{aligned}$$

where N_n is the constant

$$N_n = \left(\frac{1+\beta_1 g^2/\beta_0}{\beta_0 g^2}\right)^{\frac{\gamma_n^{(0)}}{2\beta_0}} (1+\beta_1 g^2/\beta_0)^{\frac{\gamma_n^{(1)}}{2\beta_1}}$$

and Λ is the QCD *scale parameter*, defined in this order by

$$\Lambda = \mu\, e^{-1/(2\beta_0 g^2)} \left(\frac{1+\beta_1 g^2/\beta_0}{\beta_0 g^2}\right)^{\beta_1/(2\beta_0^2)} .$$

Equation (2.73) is a basic formula for practical applications of perturbative QCD in deep inelastic scattering. So in order to know the coefficient functions to order g^2, it is necessary to calculate the anomalous dimensions $\gamma_n(g)$ to order g^4.

Note that the values $\gamma_n^{(1)}$ depend on the renormalization scheme that is used, whereas physical quantities clearly do not. It has been shown [27] that the prescription dependence of $\gamma_n^{(1)}$ is cancelled by that of the coefficient of $\bar{g}^2$ in the expansion of $\tilde{C}_n(1,\bar{g})$.

The *gauge independence* of the anomalous dimensions $\gamma_n(g)$ in the MS or $\overline{\text{MS}}$ scheme follows by Eq. (2.68) from the gauge independence of the renormalization constant Z_n in the MS or $\overline{\text{MS}}$ scheme, which in turn can be shown using the gauge invariance of the unrenormalized composite operator.

Chapter 3

Calculation of anomalous dimensions in two loops

3.1 OPE method

The method based on operator product expansion to calculate the two-loop anomalous dimensions relevant for deep inelastic scattering was developed by Floratos, Ross and Sachrajda [27]. It is based on the scaling properties of the lowest twist ($\tau_n = 2$) operators that control the short-distance behaviour of the deep inelastic structure functions. These operators already have been worked out in Section 2.2.2 and are given by Eqs. (2.64) to (2.66). In order to outline the method, we will concentrate on the non-singlet part which is not plagued by operator mixing.

If we insert the operator $O^a_{\mu_1\ldots\mu_n}$ of Eq. (2.64) in all possible ways as a vertex into the internal lines of a 1PI m-point Green function $\Gamma^{(m)}(p_1\ldots p_m)$, then the resulting Green function $\Gamma^{(m)}_{O_n}$ will have an overall degree of UV divergence $D^{(m)} = d_0 - m$, where $d_0 = n+2$ is the naive dimension of the operator O^a_n. Because we need only the twist-two part of the functions $\Gamma^{(m)}_{O_n}$ we have to consider only the terms proportional to the external momenta $p^{\mu_1}_{i_1},\ldots,p^{\mu_n}_{i_n}$; $i_k = 1,\ldots,m$. So the twist-two part of $\Gamma^{(m)}_{O_n}$ has a degree of UV divergence $D^{(m)}_{\tau=2} = d_0 - m - n = \tau - m$. Therefore we see that only the two-point Green functions give counterterms and their divergence is logarithmic. Since only the quark carries flavour, we need to calculate for the non-singlet part only the Green function $\Gamma^{(2)}_{O_n}(p,-p)$ with two external quark lines.
Defining the bare operators

$$\begin{aligned} O^a_{n,B} &= \bar\psi_B Q^a_{n,B}\psi_B = Z_O\, O^a_{n,R} \\ Q^a_{n,B} &= = Z_Q\, Q^a_{n,R} \end{aligned}$$

we find that $Z_O = Z_F Z_Q^{-1}$ where Z_F is the quark wave function renormalization

constant. Thus the bare and the renormalized Green functions are related by

$$\Gamma^{(2)}_{O_n,R}(g_R,\mu) = Z_O^{-1} Z_F \Gamma^{(2)}_{O_n,B}(g_B,\epsilon) = Z_Q \Gamma^{(2)}_{O_n,B}(g_B,\epsilon) \tag{3.1}$$

such that the counterterms we obtain from the calculation of $\Gamma^{(2)}_{O_n}$ determine Z_Q and not directly Z_O.
The anomalous dimensions for O_n^a, ψ and the $\beta-$function are defined by

$$\gamma_{O_n} = \mu\frac{\partial}{\partial\mu}\ln Z_{O_n}\Big|_{g_B,\epsilon\,\text{fixed}} \tag{3.2}$$

$$\gamma_F = \frac{1}{2}\mu\frac{\partial}{\partial\mu}\ln Z_F\Big|_{g_B,\epsilon\,\text{fixed}} \tag{3.3}$$

$$\beta = \mu\frac{\partial}{\partial\mu}g_R\Big|_{g_B,\epsilon\,\text{fixed}} \tag{3.4}$$

From these definitions and the μ independence of $\Gamma^{(2)}_{O_n,B}$ we obtain the renormalization group equation for $\Gamma^{(2)}_{O_n,R}$:

$$\left(\mu\frac{\partial}{\partial\mu} + \beta(g_R)\frac{\partial}{\partial g_R} + \gamma_{O_n} - 2\gamma_F\right)\Gamma^{(2)}_{O_n,R} = 0 \tag{3.5}$$

For the anomalous dimension of the operator Q_n^a we derive, using (3.1)

$$\gamma_{Q_n} = \mu\frac{\partial}{\partial\mu}\ln Z_{Q_n}\Big|_{g_B,\epsilon\,\text{fixed}} = 2\gamma_F - \gamma_{O_n} \tag{3.6}$$

Thus we see that the two-loop calculation of γ_{O_n} contains the two-loop calculation of γ_F and of the 1PI Green functions $\Gamma^{(2)}_{O_n}$.
In dimensional regularization, the anomalous dimension γ_{Q_n} can be calculated [27] from the single pole part of the renormalization constant of the operator Q_n: Z_{Q_n} has the expansion

$$Z_{Q_n} = 1 + \sum_{k=0}^{\infty}\frac{Z_k(g_R)}{\epsilon^k}\,.$$

Using the form of the $\beta-$function in $4-2\epsilon$ dimensions

$$\beta(g_R,\epsilon) = -g\,\epsilon + \beta(g_R) \tag{3.7}$$

and Eq. (3.6) leads to

$$\gamma_{Q_n} = -g_R^2\frac{\partial Z_1}{\partial g_R^2}\,. \tag{3.8}$$

So we see that the anomalous dimension γ_{Q_n} is simply minus twice the coefficient of the $1/\epsilon-$part in Z_{Q_n}.
To perform the actual calculation, the symmetrization and removal of the traces is

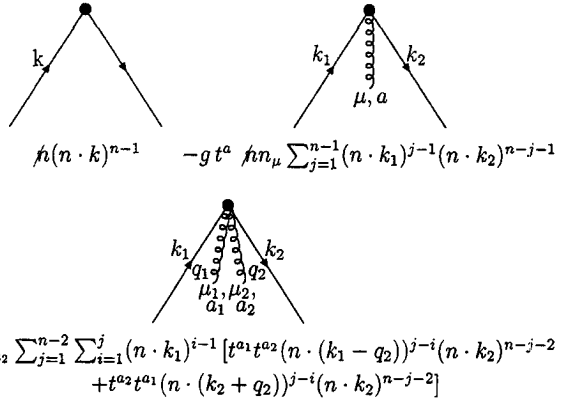

Figure 3.1: Feynman rules for the effective vertices with zero, one and two outgoing gluons.

most easily achieved by multiplying the operator in Eq. (2.63) by the tensor $n^{\mu_1}\ldots n^{\mu_n}$ where n is an arbitrary light-like vector. This operator gives rise to effective vertices consisting of an incoming and an outgoing fermion line and and 0,1,2 to $n-1$ gluons. In next-to-leading order, the cases zero, one and two gluon vertices are required. The Feynman rules for these vertices are given in Fig. 3.1. The anomalous dimension γ_{Q_n} is obtained by considering the matrix elements of the operator between off-shell quark states of momentum p ($-p^2 \gg$ quark mass squared). The diagrams which contribute to this 1PI two-point Green function in two loops are shown in Fig. 3.2.

According to Eq. (3.6), we also have to calculate the fermion wave function renormalization in order to obtain γ_{O_n}. Fig. 3.3 gives the diagrams needed for the wave function renormalization of the fermion field.

The calculation has been done in Feynman gauge in order to have the simplest form of the gluon propagators. The result is rather lengthy and given in [27]. The method is quite tedious since full two-loop diagrams have to be calculated. Furthermore, one has the complication of operator mixing in the calculation of the singlet part. Therefore, another method, based on axial gauge and cut diagrams, will be presented in the next section.

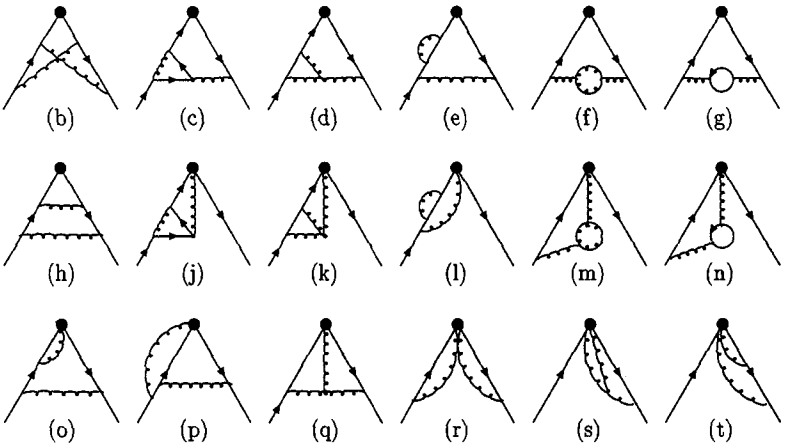

Figure 3.2: Diagrams which contribute to the 1PI two-point Green function in two loops. For diagrams which are not symmetric crossed diagrams have to be included. In diagrams (f) and (m), the contributions from Faddeev-Popov ghosts and tadpoles have to be added.

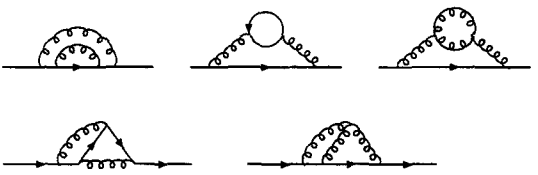

Figure 3.3: Diagrams contributing to the fermion selfenergy in two loops. In the diagram containing the gluon selfenergy, the Faddeev-Popov ghost– and tadpole terms have to be added.

3.2 The method of Curci, Furmanski and Petronzio

The method developed by Curci, Furmanski and Petronzio (CFP) [29] to calculate the two-loop anomalous dimensions is very close to the parton picture. In contrast to the OPE method, which leads to the moments of the splitting functions $P_{a/b}(x, \alpha_s)$ defined in Eqs. (2.33) and (2.39), the CFP method directly leads to these functions in $x-$space. Apart from the fact that the $x-$representation of $P_{a/b}(x, \alpha_s)$ is simpler than the expressions for the moments, it admits the physical interpretation to be the generalization to all orders in α_s of the Altarelli-Parisi probabilities and is in addition more useful for experimental analysis.
The most important technical ingredient of the CFP method is the use of light-like axial gauge, $n_\mu A^\mu = 0$, $n^2 = 0$. This gauge gives rise to spurious singularities which may be regularized by essentially two different prescriptions. A precise analysis of the validity and practical usefulness of these prescriptions is crucial for all attempts to calculate the anomalous dimensions beyond next-to-leading order with the CFP method. Therefore we will devote the main part of chapter 3.3 to the discussion of the light-cone gauge.

The CFP method will be outlined now briefly, for further details the reader is referred to [28, 29].
As already explained in Section 2.1.3, the matrix element squared for a specific hard process can be written in $x-$space in form of a convolution of some universal parton density $\Gamma(x, Q^2)$ with the "short-distance" cross section $C(x, Q^2)$ which is characteristic for a given process and contains by construction no mass singularities. The density $\Gamma(x, Q^2)$ depends only on whether the evolving parton has space-like momentum (like in deep inelastic scattering) or time-like momentum (like in e^+e^- annihilation). The Q^2-evolution of the densities Γ is governed by the probabilities $P_{a/b}(x, \alpha_s)$ which can be calculated perturbatively in the falling coupling constant.
To be specific, consider the matrix element squared M for virtual (space-like) photon-quark interaction. M can be expanded into a generalized ladder of two-particle-irreducible (2PI) kernels C_0 and K_0 as shown in Fig. 3.4. As will be explained in more detail below, it has been proven [28] that the 2PI amplitudes *in the axial gauge* with no unphysical degrees of freedom propagating are finite as long as the external legs are kept unintegrated. Hence all collinear singularities originate from the integration over the momenta flowing in the lines connecting various kernels. (By definition, the kernels K_0 contain full propagators of upper lines, and do not contain lower lines.) For simplicity of notation, all spinor (or vector) indices and momentum dependences will be suppressed, so we write C_0 for $C^{\beta\beta'}_{0\alpha\alpha'}(q, p)$. The product $C = A \cdot B$ of two kernels is a shorthand notation for

$$C^{\alpha\alpha'}_{\beta\beta'}(k_1, k_2) = \sum_{\gamma,\gamma'} \int \frac{d^m l}{(2\pi)^m} A^{\alpha\alpha'}_{\gamma\gamma'}(k_1, l) B^{\gamma\gamma'}_{\beta\beta'}(l, k_2)$$

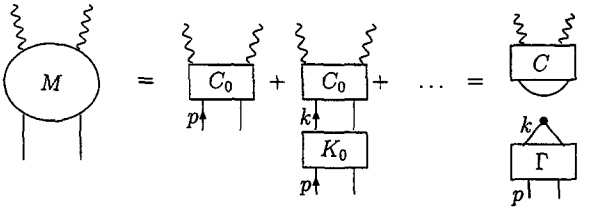

Figure 3.4: The generalized ladder expansion in terms of 2PI kernels C_0 and K_0 and the final factorized form. M is the matrix element squared for virtual photon-quark interaction.

The contraction of spinor indices will be written shortly as

$$\begin{aligned} [\ \not{k} A \quad &\text{denotes} \quad \sum_{\gamma,\gamma'} (\not{k})_{\gamma\gamma'} A^{\gamma\gamma'}_{\alpha\alpha'} \\ A\ \not{k}] \quad &\text{denotes} \quad \sum_{\gamma,\gamma'} A^{\gamma\gamma'}_{\alpha\alpha'} (\not{k})_{\gamma\gamma'} \end{aligned}$$

The generalized ladder expansion in Fig. 3.4 can then be written as

$$M = C_0 (1 + K_0 + K_0^2 + \ldots) = \frac{C_0}{1 - K_0} \equiv C_0 \Gamma_0$$

where C_0 as a 2PI kernel is finite and Γ_0 contains all mass singularities. As C_0 and Γ_0 are still coupled by momentum integrations and spinor indices, we introduce a projector $\mathcal{P}$ which serves to achieve full factorization: We define $\mathcal{P} = \mathcal{P}_\epsilon + \mathcal{P}_n$ where $\mathcal{P}_n$ acts in spinor space, decoupling C_0 and Γ_0 in spinor indices, and $\mathcal{P}_\epsilon$ extracts the singular parts (i.e. poles in ϵ) of the $d^m k-$integrals, thus decoupling C_0 and Γ_0 in momentum space. Using the parametrization $k^\mu = xp^\mu + bn^\mu + k_\perp^\mu = k_\parallel^\mu + bn^\mu + k_\perp^\mu$ already introduced in Eq. (2.8) and the fact that only $k_\parallel^\mu$ can give rise to collinear poles, it can be easily shown [29] that $\mathcal{P}_n$ can be defined as

$$A \mathcal{P}_n B = A\ \not{k}] [\frac{\not{n}}{4kn} B .$$

The operator $\mathcal{P}_\epsilon$ sets $k^2 = 0$ in the $A\ \not{k}]$ part and extracts the pole in the dk^2/k^2 integral from the $[\frac{\not{n}}{4kn} B$ part.
The factorization of the infrared singularity in the $C_0 K_0$ term then looks as follows: Think of M being one of the partonic structure functions $\hat{F}^{(i)}$ in deep inelastic scattering. Then we have

$$\hat{F}^{(i)} = \frac{1}{2} \left[C_0^{(i)} K_0\ \not{p} \right] = \frac{1}{2} \left[C_0^{(i)} \mathcal{P} K_0\ \not{p} \right] + \frac{1}{2} \left[C_0^{(i)} (1 - \mathcal{P}) K_0\ \not{p} \right] \qquad (3.9)$$

where the second term is finite and

$$\begin{aligned}\frac{1}{2}\left[C_0^{(i)}\mathcal{P}K_0\ \not{p}\right] &= \frac{1}{2}\left[C_0^{(i)}\mathcal{P}_\epsilon\otimes\mathcal{P}_n K_0\ \not{p}\right]\\ &= \frac{1}{2}\left[C_0^{(i)}\ \not{k}\right]\mathcal{P}_\epsilon\left[\frac{\not{n}}{4kn}K_0\ \not{p}\right]\\ &= \int_0^1\frac{dx}{x}\frac{1}{2}\left[C_0^{(i)}\ \not{k}\right]_{k^2=0}\cdot\tilde{\Gamma}(\frac{Q^2}{\mu^2},x,\frac{1}{\epsilon})\ ,\\ \tilde{\Gamma}(\frac{Q^2}{\mu^2},x,\frac{1}{\epsilon}) &= x\,PP\int\frac{d^mk}{(2\pi)^m}\,\delta(x-\frac{kn}{pn})\left[\frac{\not{n}}{4kn}K_0\ \not{p}\right]\ .\end{aligned}$$

The symbol PP denotes the pole part of the d^mk integral. From kinematics one has $k_\perp^2=0$ for $k^2=0$ so that $[C_0^{(i)}\ \not{k}]_{k^2=0}$ can be taken out from the $d^{m-2}\vec{k}_\perp$ integral. Therefore, after the action of the projector $\mathcal{P}$, both kernels are coupled only by the x integral, which can be written in form of a convolution

$$\begin{aligned}\frac{1}{2}\left[C_0^{(i)}\mathcal{P}K_0\ \not{p}\right] &= \int_0^1 dy\,\tilde{C}_0^{(i)}(\frac{Q^2}{\mu^2},y)\int_0^1 dz\,\tilde{\Gamma}(\frac{Q^2}{\mu^2},z,\frac{1}{\epsilon})\,\delta(x_B-yz)\\ &\text{where}\\ \tilde{C}_0^{(i)}(\frac{Q^2}{\mu^2},y) &= [C_0^{(i)}\ \not{k}]_{k^2=0}\quad;\quad y=\frac{Q^2}{2kq}\end{aligned}$$

and $x_B=Q^2/(2pq)$ is the Bjorken variable.

The procedure to carry out the factorization of mass singularities in all orders in the generalized ladder expansion is iterative. First the singular part of the last kernel K_0 is factorized:

$$M=C_0\left[1+\sum_{i=1}^{\infty}K_0^{i-1}\mathcal{P}K_0+\sum_{i=1}^{\infty}K_0^{i-1}(1-\mathcal{P})K_0\right] \tag{3.10}$$

which can be rewritten as

$$M(1-\mathcal{P}K_0)=C_0\left[1+\sum_{i=1}^{\infty}K_0^{i-1}(1-\mathcal{P})K_0\right]\ . \tag{3.11}$$

In the next step one factorizes the singular part of $K_0(1-\mathcal{P})K_0$ on the right hand side of Eq. (3.11). Carrying on in this way, one finally ends up with a series which can be written in compact form

$$M=\left(\frac{C_0}{1-(1-\mathcal{P})K_0}\right)\left(\frac{1}{1-\mathcal{P}K}\right) \tag{3.12}$$

where

$$K=K_0/(1-(1-\mathcal{P})K_0)=K_0\,(1+(1-\mathcal{P})K_0+(1-\mathcal{P})(K_0(1-\mathcal{P})K_0+\ldots) \tag{3.13}$$

and the kernel $1/(1-\mathcal{P}K)$ is defined by the series expansion in which $\mathcal{P}$ acts only on the adjacent K on the right:

$$\frac{1}{1-\mathcal{P}K} \equiv 1 + \mathcal{P}K + (\mathcal{P}K)(\mathcal{P}K) + \ldots \tag{3.14}$$

The final step in constructing the deep inelastic scattering *partonic* structure functions consists in performing the necessary contractions and multiplying M by Z_F, the residue of the pole of the full quark propagator, leading finally to

$$\hat{F}^{(i)}\left(\frac{Q^2}{\mu^2}, x_B, \alpha_s, \frac{1}{\epsilon}\right) = \int_0^1 dy\, C^{(i)}\left(\frac{Q^2}{\mu^2}, y, \alpha_s\right) \int_0^1 dz\, \Gamma\left(z, \alpha_s, \frac{1}{\epsilon}\right) \delta(x_B - yz) \tag{3.15}$$

$$C^{(i)} = \frac{1}{2}\left[C_0^{(i)} \frac{1}{1-(1-\mathcal{P})K_0}\, \not{k}\right]_{k^2=0} \quad ; \quad y = \frac{Q^2}{2kq} \tag{3.16}$$

$$\Gamma\left(z, \alpha_s, \frac{1}{\epsilon}\right) = Z_F\Big\{\delta(1-z) + PP\int \frac{d^m k}{(2\pi)^m}\delta(z - \frac{kn}{pn}) \cdot z\left[\frac{\not{n}}{4kn} K \frac{1}{1-\mathcal{P}K}\, \not{p}\right]\Big\} \tag{3.17}$$

In terms of x_B moments, Eq. (3.15) simply reads

$$\hat{F}^{(i)}\left(\frac{Q^2}{\mu^2}, N, \alpha_s, \frac{1}{\epsilon}\right) = C^{(i)}\left(\frac{Q^2}{\mu^2}, N, \alpha_s\right) \Gamma\left(N, \alpha_s, \frac{1}{\epsilon}\right) \tag{3.18}$$

In general, Γ is a matrix in flavor space. In the non-singlet case, we need only the diagonal quark-quark part $\Gamma_{q/q}$.

Factorization and finiteness of the kernels K_0 in axial gauges

For the whole factorization procedure outlined above, the generalized ladder structure, that is, the finiteness of the kernels K_0, is crucial. To show in general that factorization is correct, it is necessary to demonstrate (i) that the singularities of all Feynman diagrams contributing to a given process can be cast into a factorizable form and (ii) that the singular pieces depend only on the type of the incoming parton leg and *not* on the particular hard process.

In QCD, the graphs which contain singularities depend on the gauge chosen for the exchanged gluon. The clearest singularity structure is obtained in an axial gauge, in which the graphs responsible for collinear singularities are the generalized ladder graphs shown in Fig 3.4. It is obviously a great advantage in demonstrating property (i) to have to consider only ladder graphs in which there is already a separation between the hard process and the parton dressing coming from the rungs of the ladder.

In leading order in light-like axial gauge, the only graph which contains a singularity is the ladder graph with one rung, given by graph (a) in Fig 2.3. This property can be demonstrated by a power counting argument based on helicity conservation and the scaling properties of the quark-gluon vertex:
Consider an incoming quark which emits a spin one gluon. Since the quark-gluon vertex is proportional to γ^α the helicity of the quark line must be conserved. Consequently the amplitude for gluon emission must vanish in the forward direction when the transverse momentum $k_\perp$ of the emitted gluon tends to zero because of angular momentum conservation. In fact the amplitude vanishes as one power of $k_\perp$. This factor in the numerator is sufficient to make all graphs finite except for the ladder graph, which contains two singular denominators: The divergence in the matrix element squared for the ladder graph is of the form $k_\perp^2/k^4 \sim 1/k_\perp^2$.

Note the importance of the spin of the gluon for this argument. In covariant gauges, such as the Feynman gauge, longitudinal gluons propagate in individual graphs and invalidate the above arguments. It is only after summing all graphs, including those where the gluon is attached to the struck quark line, that the light-cone gauge result is recovered. Thus in covariant gauges we lose the physical picture of the singularities being due to collinear gluon emission from incoming legs.
The proof to all orders [28] that the kernels K_0 are finite, such that the collinear singularities come only from the integrations over the momenta connecting the various kernels, in principle is based on analogous helicity conservation and power counting arguments as in leading order. First the diagrams involving only gluons and quartic gluon couplings are considered. This has the structure of ϕ^4 theory, where power counting arguments can safely establish the finiteness of the 2PI diagrams. The crucial step now consists in extending the result to include also trilinear vertices. To demonstrate the required scaling behaviour of trilinear vertices, a judicious definition of effective vertices and propagators is worked out. This is where axial gauge is crucial: The extra suppression which leads to the right scaling behaviour is provided by the structures of effective vertices and propagators only in a gauge where only physical polarizations propagate. In covariant gauges, the additional unphysical polarizations can be "emitted" or "absorbed", giving the individual graphs more complex divergences, such that the scaling behaviour worked out for the trilinear vertices breaks down. Therefore, the use of axial gauge is essential for the proof, but the implications of the result concerning factorization are more general since the choice of gauge must be irrelevant for the final physical cross section.

Renormalization group

Equations (3.12) respectively (3.18) have the structure of a typical relation between bare and renormalized quantities:

$$M_B = M_R \cdot Z_B^{-1} \tag{3.19}$$

where the (divergent) bare quantity $M_B = M \sim \hat{F}^{(i)}$, multiplied by the (divergent) renormalization constant $Z_B = 1 - \mathcal{P}K \sim \Gamma^{-1}$ gives the (finite) renormalized result $M_R = C_0/(1-(1-\mathcal{P})K_0) \sim C^{(i)}$. In this sense, the factorization of mass singularities in dimensional regularization is formally very similar to the ultraviolet OPE technique. This allows to use the powerful methods of the renormalization group.

The procedure of renormalization of collinear divergences is the following: We start the calculation with $p^2 \neq 0$ in $m = 4 - 2\epsilon\,(\epsilon > 0)$ dimensions and subtract the ultraviolet poles. The collinear divergences are regulated by p^2. After ultraviolet subtraction has been performed, we analytically continue the result to $m = 4 - 2\epsilon\,(\epsilon < 0)$ dimensions and take $p^2 = 0$; this operation generates collinear poles in $\hat{F}^{(i)}$. Since the partonic structure function $\hat{F}^{(i)}$ is a "bare" quantity and does not depend on μ, the μ^2 (and therefore Q^2) –dependence of the "renormalized" quantity $C^{(i)}$ is determined by the singularities of $\Gamma^{-1} = Z_B$.
However, renormalization group methods can only be used if $\Gamma\left(x, \alpha_s, \frac{1}{\epsilon}\right) \sim Z_B^{-1}$ is indeed independent of Q^2 (i.e., independent of the upper limit of the dk^2–integral). In the ultraviolet method, the analogous property of Γ (independence of p^2/μ^2) is a direct consequence of the renormalizability of the theory, whereas in this case the Q^2/μ^2 independence of Γ is by no means obvious. In fact, it is one of the most essential points of the whole factorization program in axial gauge, where the finiteness of the kernels K_0, proven in ref. [28], enters in a crucial way. The proof of the Q^2/μ^2 independence of Γ goes as follows [29]: Using the finiteness of the kernels before the last k^2–integration, the structure of Γ is

$$\begin{aligned}\Gamma\left(\frac{Q^2}{\mu^2}, x, \frac{1}{\epsilon}\right) &= \delta(1-x) + \frac{1}{\epsilon}\Gamma_1\left(\frac{Q^2}{\mu^2}, x\right) + \frac{1}{\epsilon^2}\Gamma_2\left(\frac{Q^2}{\mu^2}, x\right) + \ldots \\ &= \delta(1-x) + PP\int_0^{-Q^2} \frac{dk^2}{k^2}\,\Phi(k^2/\mu^2, x, \epsilon) \qquad (3.20)\end{aligned}$$

where

$$\lim_{\epsilon \to 0} \Phi(k^2/\mu^2, x, \epsilon) < \infty \qquad (3.21)$$

Differentiating both sides of Eq. (3.20) over Q^2, using (3.21) and comparing coefficients of the same powers of $1/\epsilon$ on both sides we find $\partial\Gamma/\partial Q^2 = 0$.

Now we can act with the renormalization group operator

$$\begin{aligned}\mathcal{D} &= \mu\frac{\partial}{\partial\mu} + \beta(g,\epsilon)\frac{\partial}{\partial g} \\ \beta(g,\epsilon) &= \beta(g) - \epsilon g \quad (m = 4 - 2\epsilon\,, \epsilon < 0) \qquad (3.22)\end{aligned}$$

on equation (3.18). Since $\hat{F}^{(i)}$ as a physical quantity is independent of μ, we obtain

$$\mathcal{D}\ln\hat{F}^{(i)} = 0 \;=\; \mathcal{D}\ln C^{(i)} + \mathcal{D}\ln\Gamma \qquad (3.23)$$

$$[\mathcal{D} + 2\gamma(N,\alpha_s)]C^{(i)}\left(\frac{Q^2}{\mu^2}, N, \alpha_s\right) \;=\; 0 \qquad (3.24)$$

where $\gamma(N,\alpha_s)$ is defined as

$$\gamma(N,\alpha_s)=\frac{1}{2}\mathcal{D}\ln\Gamma=\frac{1}{2}\beta(g,\epsilon)\frac{\partial}{\partial g}\ln\Gamma(N,\alpha_s,\epsilon)\,. \tag{3.25}$$

Integrating Eq. (3.25) leads to

$$\Gamma(N,\alpha_s,\epsilon)=\exp\left\{-\int_0^{\alpha_s}d\lambda\frac{\gamma(N,\lambda)}{\beta(\lambda)-\epsilon\lambda}\right\} \tag{3.26}$$

From Eq. (3.24) and the finiteness of $C^{(i)}$ and $\mathcal{D}$ in the limit $\epsilon\to 0$, we conclude that $\gamma(N,\alpha_s)$ is also finite in that limit. In the $\overline{\rm MS}$ factorization scheme Γ has the Laurent expansion

$$\Gamma(N,\alpha_s,\frac{1}{\epsilon})=1+\sum_{k=1}^{\infty}\frac{\Gamma^{(k)}(N,\alpha_s)}{\epsilon^k}\,. \tag{3.27}$$

Using (3.22) and (3.24), we find that the anomalous dimension is determined by the simple pole term in the expansion of Γ :

$$\gamma(N,\alpha_s)=-\frac{1}{2}\,g\,\frac{\partial}{\partial g}\Gamma^{(1)}(N,\alpha_s) \tag{3.28}$$

It has been shown [29] that $\gamma(N,\alpha_s)$ calculated in this way coincides with the anomalous dimension of the twist-two non-singlet Wilson operator of DIS calculated with OPE in the $\overline{\rm MS}$ scheme.

Bare and dressed parton densities

In order to construct the *hadronic* structure functions $F_H^{(i)}$, the partonic structure functions $\hat{F}^{(i)}$ should be convoluted with the "bare" density $q_{B,H}(x,\alpha_s,\frac{1}{\epsilon})$ of quarks inside the hadron. According to the generalized ladder expansion, $q_{B,H}$ is given by

$$q_{B,H}(x,\alpha_s,\frac{1}{\epsilon})=x\int\frac{d^mp}{(2\pi)^m}\delta(x-\frac{pn}{p_{\rm h}n})\left[\frac{\not n}{4pn}\mathbf{H}\not p_{\rm h}\right] \tag{3.29}$$

where $\mathbf{H}$ is the 2PI hadron–quark kernel. For our purposes, we need only one property of $\mathbf{H}$, i.e. that it is soft in the following sense:

$$H(p^2,x)=\frac{1}{p^2}\int\frac{d^{m-2}p_\perp}{2(2\pi)^m}\left[\frac{\not n}{4pn}\mathbf{H}\not p_{\rm h}\right]\le\frac{c}{|p^2|^\delta}\,,\ (|p^2|\to\infty,\delta>0).$$

This assumption is consistent with all phenomenological evidence concerning the internal hadron structure. Assuming this property, we can extend the p^2-integral to infinity:

$$q_{B,H}(x,\alpha_s,\frac{1}{\epsilon})=\int^{-Q^2}\frac{dp^2}{p^2}\,H(p^2,x)=\int^{-\infty}\frac{dp^2}{p^2}\,H(p^2,x)+\mathcal{O}[(\frac{\mu^2}{Q^2})^\delta]\,,$$

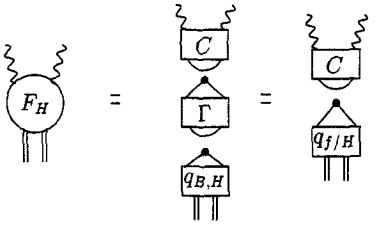

Figure 3.5: The hadronic structure function F^H is obtained by convoluting the partonic quantities $C \cdot \Gamma$ with the bare parton density $q_{B,H}$. The quantity $\Gamma \cdot q_{B,H}$ is then interpreted as the physical parton density $q_{f/H}$.

such that the "bare" density contains only power-like corrections to the Q^2-dependence of the structure functions (higher twists in the Wilson expansion). On the other hand, the lower limit of the dp^2/p^2-integral will generate the mass singularities which, according to the KLN theorem [18] must exactly cancel the divergences of $\Gamma(x, \alpha_s, \frac{1}{\epsilon})$. Therefore, the "dressed" density

$$q_{f/H}(x, Q^2) = (\Gamma \otimes q_{B,H})(x, \alpha_s(Q^2)) \tag{3.30}$$

is free from mass singularities and can be interpreted as the physical (renormalized) density of partons of type f in hadron H. In terms of moments, the convolution in Eq. (3.30) becomes a simple product

$$q_{f/H}(N, Q^2) = \exp\left\{ - \int_0^{\alpha_s(Q^2)} d\lambda \frac{\gamma(N, \lambda)}{\beta(\lambda) - \epsilon\lambda} \right\} q_{B,H}(N, \alpha_s, \epsilon) \tag{3.31}$$

where expression (3.26) for Γ has been used. This factorization is shown diagrammatically in Fig. 3.5.
As can be deduced from relation (3.31), the evolution of the physical parton density $q_{f/H}$ with Q^2 in moment space is given by

$$Q^2 \frac{\partial}{\partial Q^2} q_{f/H}(N, Q^2) = \gamma_{q/q}(N, \alpha_s(Q^2))\, q_{f/H}(N, Q^2) \tag{3.32}$$

where we consider only the non-singlet case for simplicity of notation. With the definition

$$\gamma_{q/q}(N, \alpha_s) = \int_0^1 dx\, x^{N-1} P_{q/q}(x, \alpha_s) \tag{3.33}$$

relation (3.32) in $x-$space reads

$$Q^2 \frac{\partial}{\partial Q^2} q_{f/H}(x,Q^2) = \int_x^1 \frac{dz}{z} P_{q/q}(\frac{x}{z}, \alpha_s(Q^2))\, q_{f/H}(z,Q^2) \tag{3.34}$$

Expanding $P_{q/q}(x,\alpha_s(Q^2))$ in powers of α_s

$$P_{q/q}(x,\alpha_s) = \left(\frac{\alpha_s}{2\pi}\right) P^{(0)}_{q/q}(x) + \left(\frac{\alpha_s}{2\pi}\right)^2 P^{(1)}_{q/q}(x) + \mathcal{O}({\alpha_s}^3) \tag{3.35}$$

we see that Eq. (3.34) is the Altarelli-Parisi equation generalized to all orders, so

$$P^{(0)}_{q/q}(x) = C_F \left(\frac{1+x^2}{1-x}\right)_+$$

Using the expansion (3.35), the density $\Gamma_{q/q}(x,\alpha_s,\frac{1}{\epsilon})$ can be written as

$$\Gamma_{q/q}(x,\alpha_s,\frac{1}{\epsilon}) = \delta(1-x) - \frac{1}{\epsilon}\left\{\left(\frac{\alpha_s}{2\pi}\right) P^{(0)}_{q/q}(x) + \frac{1}{2}\left(\frac{\alpha_s}{2\pi}\right)^2 P^{(1)}_{q/q}(x) + \ldots\right\} + \mathcal{O}\left(\frac{1}{\epsilon^2}\right). \tag{3.36}$$

It will be convenient to treat separately the contribution from Z_F, the renormalization factor of the external leg, and hence to introduce the notation

$$\begin{aligned}
\Gamma_{q/q}(x,\alpha_s,\frac{1}{\epsilon}) &= Z_F\, \hat{\Gamma}_{q/q}(x,\alpha_s,\frac{1}{\epsilon}) \\
\hat{\Gamma}_{q/q}(x,\alpha_s,\frac{1}{\epsilon}) &= \delta(1-x) \\
&- \frac{1}{\epsilon}\left\{\left(\frac{\alpha_s}{2\pi}\right) \hat{P}^{(0)}_{q/q}(x) + \frac{1}{2}\left(\frac{\alpha_s}{2\pi}\right)^2 \hat{P}^{(1)}_{q/q}(x) + \mathcal{O}({\alpha_s}^3)\right\} + \mathcal{O}(\frac{1}{\epsilon^2})
\end{aligned} \tag{3.37}$$

$$Z_F = 1 - \frac{1}{\epsilon}\,\xi_q(\alpha_s) + \mathcal{O}(\frac{1}{\epsilon^2})$$

$$\xi_q(\alpha_s) = \frac{\alpha_s}{2\pi}\xi^{(0)}_q(x) + \frac{1}{2}\left(\frac{\alpha_s}{2\pi}\right)^2 \xi^{(1)}_q(x) + \mathcal{O}({\alpha_s}^3) \tag{3.38}$$

$$P_{q/q}(x,\alpha_s) = \hat{P}_{q/q}(x,\alpha_s) + \xi_q(\alpha_s)\,\delta(1-x). \tag{3.39}$$

An important simplification in the the CFP method is that one has to calculate only $\hat{P}^{(1)}_{a/b}(x)$ because the contribution of the wave function renormalization factor Z_F at $x = 1$ can easily be obtained from fermion number conservation and momentum conservation sum rules.

From Eqs. (3.13), (3.14) and (3.17) we find

$$\Gamma = 1 + \mathcal{P}K_0 + \mathcal{P}(K_0)^2 - \mathcal{P}(K_0\mathcal{P}K_0) + \ldots \tag{3.40}$$

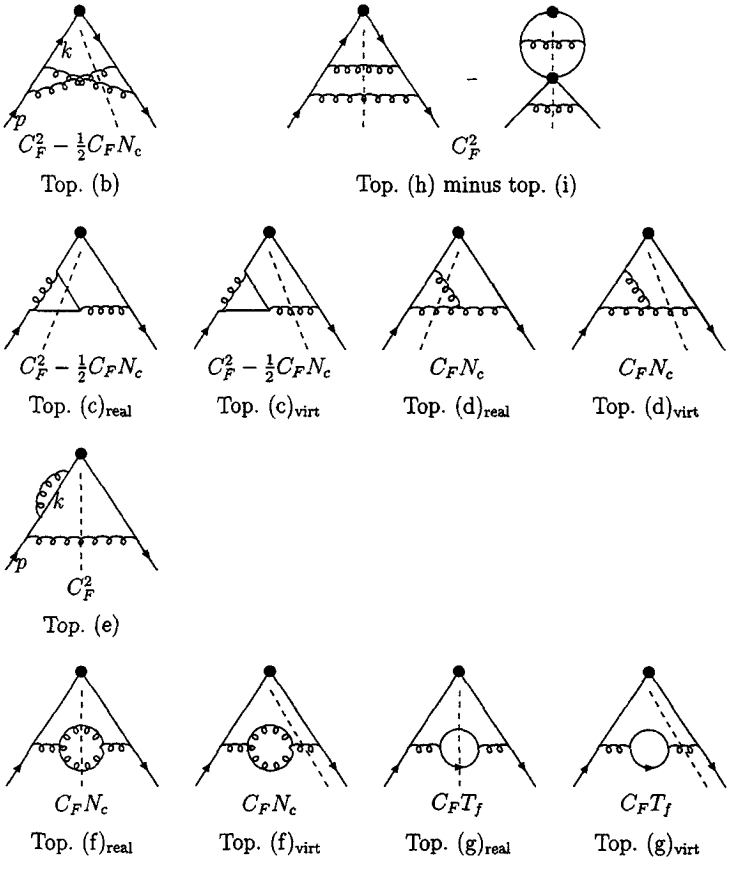

Figure 3.6: Diagrams contributing to $\hat{P}^{(1)}_{q/q}(x)$

This expansion leads to the next-to-leading order diagrams contributing in the CFP scheme to $\hat{P}^{(1)}_{q/q}(x)$, shown in Fig. 3.6.
The labeling of the diagrams follows the conventions of CFP. The solid circle denotes an insertion of the projection operator $\mathcal{P}$. The diagrams where only one internal line is cut contain insertions of virtual one-loop diagrams and therefore will be called virtual diagrams. The real diagrams are the ones where two internal lines are cut.

3.3 Principal value and Mandelstam-Leibbrandt prescription

Axial gauges are characterized by a vector n_μ and the gauge condition

$$n^\mu A^a_\mu(x) = B^a(x) \,.$$

The most common ones are homogeneous axial gauges where $B^a(x) = 0$. They can be classified to be temporal ($n^2 > 0$), space-like ($n^2 < 0$) or light-like ($n^2 = 0$) axial gauges. While temporal and space-like axial gauges exhibit problems already at the free level [41], light-like axial gauge, also called light-cone gauge, can be consistently quantized and renormalized, as will be discussed below.
Performing perturbative QCD calculations in axial gauges has several advantages. One is of course the absence of Faddeev-Popov ghosts. Related to this fact that in axial gauges in general only physical degrees of freedom propagate is the nice feature that those gauges allow to retain the parton interpretation even in higher order calculations.
Within the CFP method, the use of axial gauge is crucial to achieve factorization via the generalized ladder expansion. The use of *light-like* axial gauge in addition reduces the complexity of the calculation by reducing the number of diagrams as well as the complexity of the gluon propagator compared to other axial gauges. It also allows to establish a link to the OPE calculation.
The light-cone gauge formally leads to a gluon propagator of the form

$$D^{ab}_{\mu\nu}(q) = \frac{i\delta^{ab}}{q^2 + i\eta}\{-g_{\mu\nu} + \frac{n_\mu q_\nu + n_\nu q_\mu}{qn}\} = \frac{i\delta^{ab}}{q^2 + i\eta}\, d_{\mu\nu}(q) \,. \tag{3.41}$$

The $1/qn$−factor in the gluon propagator gives rise to the so-called "spurious poles", singular terms which are gauge artifacts in both, the real and the virtual contributions. Although these singular contributions must cancel in gauge invariant quantities, one has to use some regularization method in order to be able to evaluate the individual contributions. As yet, in all calculations based on the CFP method, the principal value (PV) prescription has been used which is defined as

$$\frac{1}{qn} \;\to\; \lim_{\delta\to 0}\frac{1}{2}\left(\frac{1}{qn + i\delta(pn)} + \frac{1}{qn - i\delta(pn)}\right) = \lim_{\delta\to 0}\frac{qn}{(qn)^2 + \delta^2(pn)^2} \tag{3.42}$$

where $\quad pn \neq 0\,;\, \vec{p}_\perp = \vec{0}\,.$

The factor pn in conjunction with the $\delta-$regulator is present in order to keep the δ dimensionless and to preserve the invarinance of the gluon propagator under a rescaling of n. In our calculation we use the parametrization of p and n given in Eq. (2.9) and Appendix B.

It is well-known[1] that by applying the PV prescription, Wick rotation becomes impossible without crossing a spurious pole, since it places the poles in the complex q_0-plane in the first and fourth quadrants. As a consequence the possibility to use power counting theorems breaks down. Nevertheless, the spurious poles appearing as $\ln\delta$, $\ln^2\delta-$terms in individual contributions cancel in the sum of all virtual and all real contributions. Another difficulty of the PV method is related to the ultraviolet renormalization constants which become dependent on longitudinal momentum fractions and on $\ln\delta$. These spurious pole terms in the UV renormalization constants of course will cancel when calculating the full cross section. But in the CFP factorization scheme, the cancellation would have to take place independently in C and Γ in order to preserve the finiteness of the 2PI kernels. In fact, this is not the case, but the spurious poles from Z_F cancel with the photon vertex. This means that the factorizability would be broken in light-cone gauge with PV prescription without local subtraction of the spurious poles in the UV singular terms. On the other hand, if one *does* subtract them, the scheme works, giving the same result as obtained with the OPE technique. CFP call this subtraction procedure a "phenomenological rule", being aware of the fact that there remains some theoretical justification for this procedure to be worked out.

A further reason to mistrust the PV prescription has been provided from a different context: Using the PV prescription in $N = 4$ supersymmetric Yang-Mills theory, there are divergent one-loop contributions remaining [60], at variance with the corresponding covariant gauge calculations which do not exhibit such a singularity [41].

After the work of CFP it was pointed out that the principal value prescription is not consistent with canonical quantization in light-like axial gauge [38, 39]. Canonical quantization leads to the ML prescription [36, 37] defined as

$$\frac{1}{qn} \to \lim_{\eta\to 0^+} \frac{1}{qn + i\eta\,\mathrm{sign}(qn^*)} = \lim_{\eta\to 0^+} \frac{qn^*}{qn\,qn^* + i\eta} \tag{3.43}$$

which introduces a second vector n^*_μ "conjugate" to n_μ which is subject to the conditions

$$(n^*)^2 = 0\,;\, nn^* \neq 0\,.$$

If $n_\mu = (n_0, \vec{n})$ and if we set $nn^* = 1$, then $n^* = (n_0, -\vec{n})/2n_0^2$.

The first definition in Eq. (3.43) has been given by Mandelstam [36], while the second

[1] The subject of quantization and renormalization in noncovariant gauges and their use in perturbation theory is described in refs. [41, 42].

is due to Leibbrandt [37]. The two are identical in the sense of the theory of distributions; therefore one usually simply denotes it by "the ML prescription".

A crucial property of the ML prescription is that the spurious poles are placed in the complex q_0-plane in the same way as the "usual" covariant poles. Therefore, Wick rotation will not produce extra terms and a generalized power counting theorem for UV divergences can be established [41].
The origin of the difference between PV and ML prescription can be traced back to different quantization procedures. This can be sketched by considering the usual Yang-Mills Lagrangian and the gauge fixing term:

$$\mathcal{L} = -\frac{1}{4} F^a_{\mu\nu} F^{a,\mu\nu} - \lambda^a \, n^\mu A^a_\mu \tag{3.44}$$

which leads in the Hamiltonian formalism to an equation of the form [38]

$$\partial_- \lambda^a = 0 \,. \tag{3.45}$$

Following now the null-plane formalism and quantizing the system on the surface $x^+ = 0$, Eq. (3.45) is not an equation of motion, since in this case the derivative $n^\mu \partial_\mu$ can be considered as a spatial derivative. If we now impose the boundary condition that the λ^a should vanish at $x^- = \pm\infty$, we obtain $\lambda^a = 0$ everywhere, and a formalism which cannot be equivalent to the equal time quantized version of the Lagrangian (3.44). Thus we are led to a principal value (or an equivalent one-vector) prescription for the spurious poles [41]. However, according to an analysis done by McCartor and Robertson [39], a careful light-cone quantization implies that the initial conditions $\lambda^a = 0$ at $x^- = \pm\infty$ are too naive in this context: The unphysical degrees of freedom must be initialized on a surface of equal x^-, satisfying equal x^- commutation relations. Thus one is lead to the existence of a second characteristic surface which is related to the second "gauge vector" n^* needed to formulate the ML prescription, and the ML form of the gauge field propagator is recovered.
Hence it can be concluded that even the light-cone quantization does *not* lead unavoidably to the PV prescription. On the other hand, quantizing the theory with equal time commutation relations in the usual space-time coordinates leads unavoidably to the ML prescription [38].
In the usual space-time coordinates, we cannot interpret Eq. (3.45) as a constraint, but rather as a genuine equation of motion since a time derivative is involved. Thus the λ^a describe degrees of freedom propagating on the hypersurface $nq = 0$, tangent to the light-cone. Carrying through the quantization procedure, one finds the gluon propagator in the ML prescription [38]. This propagator can be decomposed into a term corresponding to the propagation of the physical polarizations and into a term which describes the propagation of scalar and longitudinal gluons in the $qn = 0$ plane:

$$< 0|T\{A^a_\mu(x) A^b_\nu(0)\}|0 > = < 0|T\{T^a_\mu(x) T^b_\nu(0)\}|0 > + < 0|T\{L^a_\mu(x) L^b_\nu(0)\}|0 > \tag{3.46}$$

where

$$< 0|T\{T^a_\mu(x)T^b_\nu(0)\}|0 > = \frac{i\delta^{ab}}{(2\pi)^4}\int \frac{d^4q\, e^{iqx}}{q^2+i\eta} \left(-g_{\mu\nu}+\frac{(n_\mu q_\nu + q_\mu n_\nu)}{q_\perp^2}\frac{2qn^*}{nn^*} - \frac{n_\mu g_{0\nu}+n_\nu g_{0\mu}}{q_\perp^2}\,q^2\right)$$

and

$$< 0|T\{L^a_\mu(x)L^b_\nu(0)\}|0 > = -\frac{i\delta^{ab}}{(2\pi)^4}\int \frac{d^4q\, e^{iqx}}{q^2+q_\perp^2+i\eta} \left(\frac{(n_\mu q_\nu + q_\mu n_\nu)}{q_\perp^2}\frac{2qn^*}{nn^*} - \frac{n_\mu g_{0\nu}+n_\nu g_{0\mu}}{q_\perp^2}\,(q^2+q_\perp^2)\right)$$

Adding up these contributions and using $q^2+q_\perp^2 = 2(qn^*)(qn)/nn^*$ we obtain the axial-gauge propagator with ML regularization

$$D^{ab}_{\mu\nu}(x) = \frac{i\delta^{ab}}{(2\pi)^4}\int \frac{d^4q\, e^{iqx}}{q^2+i\eta}\left(-g_{\mu\nu}+\frac{(n_\mu q_\nu + q_\mu n_\nu)\, qn^*}{qn\, qn^* + i\eta}\right). \tag{3.47}$$

The discontinuity of this propagator can be decomposed into the physical axial-gauge contribution and an unphysical contribution:

$$\mathrm{Disc}\, D^{ab}_{\mu\nu}(q) = 2\pi\theta(q_0)\,\delta^{ab}\left\{-g_{\mu\nu}+\frac{2qn^*}{nn^*}\,\frac{(n_\mu q_\nu + n_\nu q_\mu)}{q_\perp^2}\right\}\delta(q^2) \tag{3.48}$$

$$-2\pi\theta(q_0)\,\delta^{ab}\left\{\frac{2qn^*}{nn^*}\,\frac{(n_\mu q_\nu + n_\nu q_\mu)}{q_\perp^2}\right\}\delta(q^2+q_\perp^2)\,. \tag{3.49}$$

As this is an important equation, we will also give its form with light-cone parametrization of the momenta: Using

$$q_\pm = \frac{1}{\sqrt{2}}(q_0 \pm q_3)$$

$$q^2 = 2q_+q_- - q_\perp^2 = \frac{2\,qn\,qn^*}{nn^*} - q_\perp^2$$

one obtains

$$\mathrm{Disc}\, D^{ab}_{\mu\nu}(q) = 2\pi\theta(q_0)\,\delta^{ab}\left\{-g_{\mu\nu}+\frac{(n_\mu q_\nu + n_\nu q_\mu)}{q^+}\right\}\delta(q^2) \tag{3.50}$$

$$-2\pi\theta(q_0)\,\delta^{ab}\left\{2q^-\,\frac{(n_\mu q_\nu + n_\nu q_\mu)}{q_\perp^2}\right\}\delta(q^2+q_\perp^2)\,. \tag{3.51}$$

The term proportional to the delta function $\delta(q^2+q_\perp^2)$ is the so-called *axial ghost* contribution. It has been shown by Bassetto *et al.* [38] that all vectors of the physical

Hilbert-space are annihilated by the creation operator of these degrees of freedom. Therefore, similarly to the Gupta-Bleuler ghosts of QED, they decouple from the S-matrix. The ghosts have negative mass squared, indefinite metric, they live in the $qn = 0$ plane and their polarization sum is

$$\sum_{\lambda=1,2} e_\mu^\lambda(q) e_\nu^\lambda(q) = -\frac{2qn^*}{nn^*} \frac{(n_\mu q_\nu + q_\mu n_\nu)}{q_\perp^2} . \tag{3.52}$$

It should be pointed out that the ghost part of the discontinuity of the gluon propagator is *not* transverse. Note also that the explicit presence of $q_\perp^2$ is a clear manifestation of the Lorentz non-covariance of the gauge, entailing technical complications in loop- and phase space integrals.

On the other hand, in expressions (3.48) and (3.49) for the discontinuity of the propagator with ML prescription, one can identify a cancellation mechanism between the standard axial gauge contribution and the axial ghost contribution: In the limit $q_\perp^2 \to 0$ the spurious poles $1/q_\perp^2$ appearing in Eqs. (3.48) and (3.49) cancel each other. But we will show that this mechanism is more sophisticated in two loops.
Using PV prescription, the second term (3.51) in the discontinuity of the gluon propagator is absent since the PV regulated $1/q^+$ pole does not have the causality structure of propagating degrees of freedom.

One can find a decomposition similar to the one in Eqs. (3.48) and (3.49) also for the virtual contributions with the help of a formula given in refs. [59, 60]. Let us consider the integral

$$J_n^A(k_1 \ldots k_{n-1}) = \int d^m q \frac{1}{[q^2 + i\epsilon]\,[(q+k_1)^2 + i\epsilon] \ldots [(q+k_{n-1})^2 + i\epsilon]\, qn} \tag{3.53}$$

defined and calculated in detail in Appendix A. Using exponential parametrization for the propagator denominator factors and the ML prescription to regulate the $1/qn-$denominator leads to

$$\begin{aligned} J_n^{A,\mathrm{ML}}(k_1 \ldots k_{n-1}) &= \frac{1}{i^n} \int_0^\infty da_0 \ldots da_{n-1} \exp\{i \sum_{j=1}^{n-1} a_j k_j^2 - i\tilde{R}^2/z - z\epsilon\} \\ &\quad \cdot \int d^m q \frac{\exp\{iz\,q^2\}}{q^+ - \tilde{R}^+/z + i\eta\,\mathrm{sign}\,(q^- - \tilde{R}^-/z)} \end{aligned} \tag{3.54}$$

$$\begin{aligned} \tilde{R}^\mu &= a_1 k_1^\mu + \ldots + a_{n-1} k_{n-1}^\mu \\ z &= a_0 + \ldots + a_{n-1} . \end{aligned}$$

The $q-$integral

$$J_q^{ML} = \int dq^+ dq^- d^{(m-2)}\vec{q}_\perp \frac{\exp\{iz\,q^2\}}{q^+ - \tilde{R}^+/z + i\eta\,\mathrm{sign}(q^- - \tilde{R}^-/z)}$$

has been evaluated using the Cauchy theorem and integrating first over dq^+, then over dq^-. The integral over the transverse momenta is a standard Gaussian integral, and one obtains finally

$$J_q^{ML} = \frac{-\pi^{\frac{m}{2}}(iz)^{1-\frac{m}{2}}}{\tilde{R}^+ + i\eta\, z\, \mathrm{sign}\,\tilde{R}^-}\Big\{1 - \exp\{2i\tilde{R}^+\tilde{R}^-/z - 2\eta|\tilde{R}^-|\}\Big\}. \tag{3.55}$$

Rescaling $a_i = z \cdot b_i$ $(i = 0 \ldots n-1)$ and carrying out the $z-$integration we get

$$\begin{aligned} J_n^{A,ML}(k_1 \ldots k_{n-1}) &= i\pi^{\frac{m}{2}}\Gamma(n-\frac{m}{2})(-1)^{n+1}\int db_0 \ldots db_{n-1}\,\delta(1-\sum_{j=0}^{n-1} b_j) \\ &\quad \frac{1}{R^+ + i\eta\,\mathrm{sign}\,R^-}\Big\{[M_n]^{\frac{m}{2}-n} - [M_n - 2R^+R^-]^{\frac{m}{2}-n}\Big\} \qquad (3.56) \\ R^\mu &= \sum_{j=1}^{n-1} b_j\, k_j^\mu \quad ; \quad M_n = R^2 - \sum_{j=1}^{n-1} b_j\, k_j^2 \end{aligned}$$

whereas PV regularization leads to

$$\begin{aligned} J_n^{A,PV}(k_1 \ldots k_{n-1}) &= i\pi^{\frac{m}{2}}\Gamma(n-\frac{m}{2})(-1)^{n+1}\int db_0 \ldots db_{n-1}\,\delta(1-\sum_{j=0}^{n-1} b_j) \\ &\quad \frac{R_+}{R_+^2 + \delta^2 p_+^2}\cdot[M_n]^{\frac{m}{2}-n} \qquad (3.57) \end{aligned}$$

Thus we see that the term proportional to $[M_n - 2R^+R^-]^{\frac{m}{2}-n}$ in (3.56) obtained with ML prescription is completely absent in the PV result (3.57).

In the following, we will distinguish between the "**PV scheme**" and the "**ML scheme**". In the **PV scheme**, all virtual integrals are evaluated by applying the PV prescription defined in Eq. (3.42) before doing the $m-$dimensional integration over the loop momentum q. The same prescription is also used to regulate the spurious poles of the real diagrams. As explained above, axial ghosts are not present in the PV scheme.
In the **ML scheme**, the virtual integrals are evaluated using the ML prescription defined in Eq. (3.43) before doing the $q-$integration. After having carried out the $m-$dimensional integration over the loop momentum, there will be *infrared* spurious poles in the integrals over Feynman parameters. Such infrared spurious poles will also appear in the transverse real diagrams and in the ghost diagrams. We can regulate these poles as we like, as long as we do it in the same way in both, the virtual and the real parts. We will present two different methods to regulate these infrared spurious poles:

1. $\delta-$regularization or PVI–regularization

2. $\epsilon-$regularization.

The $\delta-$regularization introduces a regulator δ for the *spurious* poles whereas the "usual" soft and collinear poles (and ultraviolet poles of course) are still regulated by the dimensional ϵ. In the real part, the $\delta-$regulator is introduced in exactly the same way as has been done for the calculation with PV prescription. Of course, the ghosts, which are not present in the PV scheme, also have to be regulated by the same δ in the ML case. We call the $\delta-$regularization PVI regularization because it is a principal value regularization for the spurious *infrared* poles appearing *within* the ML scheme. The advantage of the PVI regularization originates from the fact that the calculation of the transverse real part then is *identical* to the one in the PV scheme. Besides the obvious advantage of having to do this part of the calculation only once for both schemes, it also allows to identify those subparts which make up the difference between PV and ML schemes.
A similar identification can be done in the virtual part, as will be explained below. This possibility of mapping subparts provided by the PVI regularization is very important for a proof that PV and ML schemes might be equivalent. We will come back to this point in section 3.6.

The $\epsilon-$regularization method uses the ϵ from dimensional regularization as a regulator for all sorts of poles, "usual" and spurious ones. One advantage of this method is of course that we do not have to bother whether we regulate the spurious poles in virtual, transverse real and ghost parts in the same way. The other advantage is of technical nature: Some integrals, being analytical functions of ϵ only instead of ϵ *and* δ, are much easier to calculate using the $\epsilon-$regularization method.

To be concrete, the different regularization methods *within* the ML scheme are implemented in the following way:

1. In the virtual part:
   From Eq. (3.56), we see that all virtual integrals done with ML prescription contain the denominator
   $$\frac{1}{R^+ + i\eta \operatorname{sign} R^-}$$
   where the spurious poles correspond to the limit $R^+ \to 0$. PVI regularization now means to do the replacement
   $$\text{PVI:} \qquad \frac{1}{R^+ + i\eta \operatorname{sign} R^-} \to \frac{R^+}{(R^+)^2 + (\delta p^+)^2} \tag{3.58}$$
   whereas $\epsilon-$regularization means
   $$\epsilon - \text{reg.:} \qquad \frac{1}{R^+ + i\eta \operatorname{sign} R^-} \to \frac{1}{R^+} \tag{3.59}$$

In general, R^+ is some combination of Feynman parameters, say u and y, and the external parameter $x = k^+/p^+$. In the $\epsilon-$regularization method, the limit $R^+ \to 0$ will be regulated by terms like $(a\,u + b\,y)^{-\epsilon}$ stemming from the numerators $[M_n]^{\frac{m}{2}-n}$ and $[M_n - 2R^+R^-]^{\frac{m}{2}-n}$ in Eq. (3.56).
Concrete examples of virtual integrals regulated in both ways are given in Appendix A.2.

Comparing Eq. (3.56) with PVI regularization to Eq. (3.57), we see that the first part of the difference in Eq. (3.56) is then *identical* to the PV result (3.57). Therefore the second term, the one proportional to $[M_n - 2R^+R^-]^{\frac{m}{2}-n}$ in Eq. (3.56), is an additional virtual contribution only present in the ML scheme, similar to the ghosts being an additional real contribution only present in the ML scheme. How these additional ML contributions are related to the extra terms in the PV scheme, arising there due to the special UV renormalization, will be explained in section 3.6.

2. In the real part:
   As the spurious poles in the transverse real part arise from $q^+ \to 0$, whereas those in the ghost part arise from $q_\perp^2 \to 0$, we have the following relations:

$$\begin{aligned} \text{For the transverse part:} \quad \frac{1}{q_+} &\to \frac{q^+}{(q^+)^2 + (\delta\, p^+)^2} \\ \text{which leads, using} \quad q^+ &= \frac{q^2 + q_\perp^2}{2q^-} \quad \text{and} \quad q^2 = 0, \ \text{to} \\ \frac{1}{q_\perp^2} &\to \frac{q_\perp^2}{(q_\perp^2)^2 + \delta^2 (2p^+q^-)^2}\,, \end{aligned} \tag{3.60}$$

   where we could use $q^2 = 0$ because for $q_\perp^2 \to 0$, q^2 also becomes on-shell in the ghost kinematics, as can be seen from Eq. (3.49).

In both, real and virtual parts, the $\delta-$regulator of the PVI regularization gives rise to parameter integrals of the following form, denoted by I_0 and I_1:

$$I_0 = \int_0^1 du \, \frac{u}{u^2 + \delta^2} = -\ln\delta + \mathcal{O}(\delta) \tag{3.61}$$

$$I_1 = \int_0^1 du \, \frac{u \ln u}{u^2 + \delta^2} = -\frac{1}{2}\ln^2\delta - \frac{1}{4}\,Li_2(1) + \mathcal{O}(\delta)\,. \tag{3.62}$$

Note that terms of order $\epsilon\, I_0, \epsilon\, I_1$ can be dropped since they are of order ϵ, whereas with the $\epsilon-$regularization method, I_0 appears as a pole $1/\epsilon_{\text{spurious}}$, and terms of order $\epsilon/\epsilon_{\text{spurious}}$ give a finite contribution.

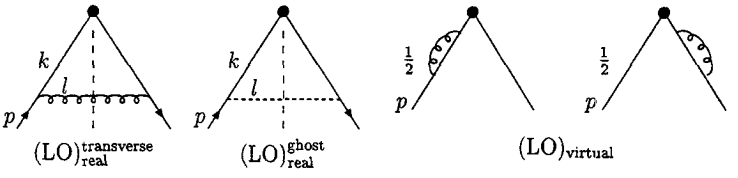

Figure 3.7: Leading order diagrams

3.3.1 Leading order as an example

As a first example, we will rederive the leading order (LO) result for the non-singlet splitting function $P^{(0)}_{q/q}(x)$, with both prescriptions, PV and ML. This is a rather trivial calculation that nevertheless displays the main improvements provided by the use of ML. Furthermore, the virtual graphs in the NLO calculation have the LO kinematics, such that this section also serves to prepare the NLO calculation. We note that the LO example has already been worked out in [40] where collinear poles were regularized by keeping the initial quark off-shell, $p^2 < 0$, rather than by using dimensional regularization. This is perfectly fine at the LO level, but beyond LO it becomes technically too involved to keep $p^2 \neq 0$, and in fact the underlying method of CFP that we are employing has been set up in such a way that it relies on the use of dimensional regularization, yielding final results that correspond to the $\overline{\text{MS}}$ scheme. It therefore seems a useful exercise to sketch the calculation of $P^{(0)}_{q/q}(x)$ if dimensional regularization is used.

From Eq. (3.17) and the expansions (3.13),(3.14) we obtain

$$\begin{aligned}\Gamma_{q/q}\left(x,\alpha,\frac{1}{\epsilon}\right) &= Z_F\left\{\delta(1-x)+PP\,x\int\frac{d^mk}{(2\pi)^m}\,\delta(x-\frac{kn}{pn})\cdot\left[\frac{\not n}{4kn}\,K_0\,\not p\right]\right\}\\ &= Z_F\left\{\delta(1-x)+PP\,I_{qq}\right\}\end{aligned}\tag{3.63}$$

where Z_F is the contribution from the quark selfenergy and PP denotes the pole part. The diagrams which contribute to the kernel K_0 in leading order are shown in Fig. 3.7. The momenta are parametrized as

$$p = (P,\vec{0},P)\quad(P>0)\quad;\quad n=(\frac{pn}{2P},\vec{0},-\frac{pn}{2P})$$

$$k = (\xi P+\frac{k^2+k_\perp^2}{4\xi P},\vec{k}_\perp,\xi P-\frac{k^2+k_\perp^2}{4\xi P})\quad;\quad \xi=\frac{kn}{pn}\quad;\quad k^2<0$$

Real contributions

Inserting the leading order expression for the kernel K_0, the integral I_{qq} is given by

$$\begin{aligned} I_{qq} &= g^2\mu^{2\epsilon}C_F\frac{1}{(k^2)^2}\,x\int\frac{d^mk}{(2\pi)^m}\,\delta(x-\xi)\,Tr\left[\frac{\not n}{4kn}\;\not k\gamma^\mu\;\not p\gamma^\nu\;\not k\right] \\ &\quad\cdot\int d^ml\,\delta(p-k-l)\cdot\mathrm{Disc}\left[\frac{id_{\mu\nu}(l)}{l^2+i\eta}\right] \end{aligned} \tag{3.64}$$

The discontinuity of the gluon propagator in the PV scheme is given by

$$\begin{aligned} \mathrm{Disc}^{PV}\left[\frac{id_{\mu\nu}(l)}{l^2+i\eta}\right] &= 2\pi\theta(l_0)\,\delta(l^2)\cdot d_{\mu\nu}(l) \\ d_{\mu\nu}(l) &= -g_{\mu\nu}+\frac{n_\mu l_\nu+n_\nu l_\mu}{ln} \end{aligned}$$

whereas in the ML scheme, as explained above, we have

$$\begin{aligned} \mathrm{Disc}^{ML}\left[\frac{id_{\mu\nu}(l)}{l^2+i\eta}\right] &= 2\pi\theta(l_0)\left[\delta(l^2)\cdot d_{\mu\nu}(l)+\delta(l^2+l_\perp^2)\cdot s_{\mu\nu}(l)\right] \\ s_{\mu\nu}(l) &= -2l^-\frac{n_\mu l_\nu+n_\nu l_\mu}{l_\perp^2} \end{aligned} \tag{3.65}$$

such that in the ML scheme, we have an additional diagram, denoted by $(\mathrm{LO})^{\mathrm{ghost}}_{\mathrm{real}}$ in Fig. 3.7.

Using the parametrization of momenta given above and evaluating the trace in $m = 4-2\epsilon$ dimensions leads to the following expression for the *transverse* real part [2]

$$\begin{aligned} I_{qq}^{\mathrm{trans}} &= C_F\frac{\alpha_s}{2\pi}\frac{(4\pi\mu^2)^\epsilon}{\Gamma(1-\epsilon)}\cdot P_{q/q}(x,\epsilon)\int_0^{Q^2}\frac{d|k^2|}{|k^2|}\,dk_\perp^2\,(k_\perp^2)^{-\epsilon}\delta(k_\perp^2+(1-x)k^2) \\ &= -\frac{1}{\epsilon}C_F\frac{\alpha_s}{2\pi}\frac{1+x^2}{1-x}(1-x)^{-\epsilon} \quad + \text{ finite} \end{aligned} \tag{3.66}$$

Using the identity

$$(1-x)^{-1-\epsilon} = -\frac{1}{\epsilon}\,\delta(1-x)+\frac{1}{(1-x)_+}-\epsilon\left(\frac{\ln(1-x)}{(1-x)}\right)_+ + \mathcal{O}(\epsilon^2)\,,$$

[2] We can consider the last integral over k^2 as either infrared *or* ultraviolet divergent, depending on how we define the integration range. CFP treat its divergence as a collinear infrared singularity, using an ultraviolet cutoff Q^2, given by the large momentum scale of the process. Collins and Soper [43] instead introduce an infrared cutoff and consider the last integral as an ultraviolet divergent integral. As we only need the pole part of the k^2-integral and since the integrand *before* the k^2-integration is finite, there will be no Q^2-dependence in the final result for $\Gamma_{q/q}(x,\epsilon)$.

where the "plus" distribution has been defined in Eq. (2.22), we obtain

$$PP\{I_{qq}^{\rm trans}\} = -\frac{1}{\epsilon} C_F \frac{\alpha_s}{2\pi} \left\{ -\frac{2}{\epsilon}\delta(1-x) + \frac{1+x^2}{(1-x)_+} \right\} . \tag{3.67}$$

In the PV scheme, we do not regulate the singularity at $x = 1$ in (3.66) with the dimensional ϵ, but with δ, according to [29]

$$\frac{1}{1-x} \to \frac{1-x}{(1-x)^2+\delta^2} = I_0\,\delta(1-x) + \frac{1}{(1-x)_+}$$

such that we have, since $I_{qq}^{\rm trans}$ is the only real contribution in the PV scheme,

$$\Gamma_{q/q}^{PV}\left(x, \alpha_s, \frac{1}{\epsilon}\right) = Z_F \left\{ \delta(1-x) - \frac{1}{\epsilon} C_F \frac{\alpha_s}{2\pi} \left(\frac{1+x^2}{(1-x)_+} + 2I_0\,\delta(1-x) \right) \right\} \tag{3.68}$$

In the ML scheme, we additionally have to calculate the ghost contribution to obtain the full real part. Inserting the matrix element

$$M^{\rm gh} = Tr\left[\frac{\not{n}}{4kn}\, \not{k}\gamma^\mu\, \not{p}\gamma^\nu\, \not{k} \right] s_{\mu\nu}(l) = 4k^2 \cdot \frac{2l^-}{l_\perp^2} , \tag{3.69}$$

stemming from the ghost part of the gluon propagator, into expression (3.64) leads to

$$I_{qq}^{\rm ghost} = -2\,C_F \frac{\alpha_s}{2\pi} \frac{(4\pi\mu^2)^\epsilon}{\Gamma(1-\epsilon)} \delta(1-x) \int_0^{Q^2} \frac{d|k^2|}{|k^2|} \int_0^{|k^2|} dk_\perp^2\, (k_\perp^2)^{-1-\epsilon} \tag{3.70}$$

Note that $l_\perp^2 = k_\perp^2$ and that the factor l^- in (3.69) is cancelled with a factor $1/l^-$ in the ghost phase space, stemming from

$$\delta(l^2 + l_\perp^2) = \delta(2l^+l^-) = \frac{1}{2l^-}\delta(l^+) + \frac{1}{2l^+}\delta(l^-) .$$

The term proportional to $\delta(l^-)$ vanishes when being combined with $M^{\rm gh}$ because of the factor l^- in (3.69).
After the substitution

$$k_\perp^2 = |k^2| \cdot y \quad ; \quad 0 \le y \le 1$$

one arrives at

$$PP\{I_{qq}^{\rm ghost}\} = \frac{2}{\epsilon} C_F \frac{\alpha_s}{2\pi} \delta(1-x) \int_0^1 dy\, y^{-1-\epsilon} = -\frac{1}{\epsilon} C_F \frac{\alpha_s}{2\pi} \delta(1-x) \cdot \frac{2}{\epsilon} \tag{3.71}$$

such that the result for $I_{qq}^{\rm ghost}$ combined with $I_{qq}^{\rm trans}$ from Eq. (3.67) is completely finite in a distributional sense:

$$\begin{aligned} PP\{I_{qq}^{\rm trans} + I_{qq}^{\rm ghost}\} &= -\frac{1}{\epsilon} C_F \frac{\alpha_s}{2\pi} \frac{1+x^2}{(1-x)_+} \\ \Gamma_{q/q}^{ML}\left(x, \alpha_s, \frac{1}{\epsilon}\right) &= Z_F \left\{ \delta(1-x) - \frac{1}{\epsilon} C_F \frac{\alpha_s}{2\pi} \frac{1+x^2}{(1-x)_+} \right\} \end{aligned} \tag{3.72}$$

Therefore, in the ML scheme, the ghost contribution regulates the transverse real part, which in the PV scheme, where these ghosts are not present, is singular at $x = 1$, the singularity being contained in I_0. In the PV scheme, it is the *virtual* contribution which regulates $x = 1$.

Virtual contribution

The contribution Z_F from the quark selfenergy insertion on the legs of the ladder shown in Fig. 3.7 can be extracted in two ways: Either by direct calculation, or by using quark number conservation. In order to guarantee the conservation of quark number, we must have

$$\int_0^1 dx\, \Gamma_{q/q}(x, \alpha_s, \frac{1}{\epsilon}) = 1 \tag{3.73}$$

Therefore the full answer for Γ has to be of the form

$$\Gamma_{q/q}\left(x, \alpha_s, \frac{1}{\epsilon}\right) = \delta(1-x) - \frac{1}{\epsilon} C_F \frac{\alpha_s}{2\pi} \left\{ \frac{1+x^2}{1-x} - \delta(1-x) \int_0^1 dy \frac{1+y^2}{1-y} \right\} \tag{3.74}$$

which is, using the plus prescription

$$\begin{aligned} \Gamma_{q/q}\left(x, \alpha_s, \frac{1}{\epsilon}\right) &= \delta(1-x) - \frac{1}{\epsilon} \frac{\alpha_s}{2\pi} P^{(0)}_{q/q}(x) \\ P^{(0)}_{q/q}(x) &= C_F \left\{ \frac{1+x^2}{(1-x)_+} + \frac{3}{2}\delta(1-x) \right\} = C_F \left[\frac{1+x^2}{1-x} \right]_+ \end{aligned} \tag{3.75}$$

The direct calculation proceeds in the following way:
Z_F is defined as the residue of the pole of the full quark propagator

$$G(p) \sim Z_F \frac{i\, \not{p}}{p^2} \text{ for } p^2 \to 0\,. \tag{3.76}$$

The full quark propagator is related to the selfenergy by

$$G(p) = \frac{i}{\not{p} - i\Sigma}$$

where the general decomposition of Σ into invariant amplitudes has the form

$$\Sigma(p) = A\, \not{p} + B\, \not{n} \frac{p^2}{2pn} + C\, \not{n}^* \frac{p^2}{2pn^*}\,. \tag{3.77}$$

Note that the vector n^* only is present in the ML scheme, so $C \equiv 0$ in the PV scheme. The presence of n^* also influences the possible form of A, B and C: In the PV scheme, A and B can only depend on p^2, pn, ϵ whereas in the ML scheme, A, B and C can depend on $p^2, pn, pn^*, nn^*, \epsilon$, containing therefore the scale invariant dimensionless

quantity
$\chi_p = 2pn\,pn^*/(nn^*p^2)$ which diverges in the limit $p^2 \to 0$. This issue will be very important in two loops.
Inserting the above expression for $\Sigma(p)$ into $G(p)$ one obtains after some algebra

$$G(p) = \frac{i}{1-\sigma}\left\{\frac{\not p}{p^2} - \frac{B}{1-A}\frac{\not n}{2pn} - \frac{C}{1-A}\frac{\not n^*}{2pn^*}\right\} \tag{3.78}$$

$$\sigma = A + B + C + \frac{BC}{\chi_p(1-A)} \tag{3.79}$$

$$\chi_p = \frac{2pn\,pn^*}{nn^*p^2}$$

The general expression for $\Sigma(p)$ in light-cone gauge is given by

$$\begin{aligned}\Sigma(p) &= \Sigma^F(p) + \Sigma^A(p) \\ &= C_F\,g^2 \int \frac{d^mq}{(2\pi)^m} \frac{\gamma_\mu(\not p + \not q)\gamma_\nu}{(p+q)^2\,q^2}\left\{-g_{\mu\nu} + \frac{q_\mu n_\nu + q_\nu n_\mu}{qn}\right\}\end{aligned} \tag{3.80}$$

where Σ^F denotes that part of the expression which stems from the Feynman part (the part proportional to $-g_{\mu\nu}$) of the gluon propagator, Σ^A denotes the remaining axial part. Σ^F can be written in terms of simple loop integrals as

$$\Sigma^F(p) = g^2 C_F \frac{(m-2)}{(2\pi)^m}\left(\not p\, J_2^F(p) + \gamma^\nu J_{2\nu}^F(p)\right) \tag{3.81}$$

$$\Sigma^A(p) = -g^2 C_F \frac{1}{(2\pi)^m}\left(2p^2\ \not n\, J_2^A(p) + \not n\, J_{2\mu}^A(p)\gamma^\mu\ \not p + \not p\, J_{2\mu}^A(p)\gamma^\mu\ \not n\right) \tag{3.82}$$

The integrals can be found in Appendix A.3. In terms of form factors we obtain

$$\Sigma^F(p) = C_F \frac{g^2}{(2\pi)^m} Q_\epsilon^p \frac{(m-2)}{2}\ \not p\, T_0 \tag{3.83}$$

$$\Sigma^A(p) = -C_F \frac{g^2}{(2\pi)^m}\frac{Q_\epsilon^p}{pn}\left\{2\ \not n p^2\,(B_1 - B_0) + 2\,B_2(\not p nn^* + \not n pn^* - \not n^* pn)\right\} \tag{3.84}$$

Selfenergy in the PV scheme

Note that in the PV scheme the form factor B_2 is zero since there is no n^* present in this scheme. In the PV scheme, the form factors are given by

$$\begin{aligned}T_0 &= \frac{2}{\epsilon}\int_0^1 dy\, y^{1-\epsilon}(1-y)^{-\epsilon} = \frac{1}{\epsilon} + 2 + \mathcal{O}(\epsilon) \\ B_1^{PV} &= T_0\end{aligned}$$

$$B_0^{PV} = \frac{1}{\epsilon}\int_0^1 dy\, y^{-\epsilon}(1-y)^{-\epsilon}\frac{y}{y^2+\delta^2}$$
$$= \frac{I_0}{\epsilon} - I_1 + Li_2(1) + \mathcal{O}(\epsilon) \tag{3.85}$$

Hence one obtains, after having subtracted the UV poles and having combined Eqs. (3.83),(3.84) and (3.77)

$$A^{PV} + B^{PV} = -\frac{1}{\epsilon}C_F\frac{\alpha_s}{2\pi}\{\frac{3}{2} - 2I_0 + \mathcal{O}(\epsilon)\} \tag{3.86}$$

such that we have according to Eqs. (3.78) and (3.76)

$$Z_F^{PV} = PP\frac{1}{1-\sigma} = 1 + PP\{A^{PV} + B^{PV}\} + \mathcal{O}({\alpha_s}^2) = 1 - \frac{1}{\epsilon}C_F\frac{\alpha_s}{2\pi}\{\frac{3}{2} - 2I_0\} \tag{3.87}$$

Inserting the result (3.87) for Z_F into expression (3.68) we end up at expression (3.75) again, thus having shown that in the PV scheme it is the virtual contribution which regulates the singularity at $x = 1$ from the real contribution.

Selfenergy with Mandelstam-Leibbrandt prescription

In the ML scheme, we obtain after insertion of the ML form factors into Eqs. (3.83) and (3.84)

$$A^{ML}(p) = C_F\frac{\alpha_s}{2\pi}(-p^2)^{-\epsilon}\Big\{(1+\epsilon)(\frac{1}{2\epsilon_{\rm uv}} + 1) + \frac{\chi_p \ln\chi_p}{1-\chi_p}\Big\} \tag{3.88}$$

$$B^{ML}(p) = C_F\frac{\alpha_s}{2\pi}(-p^2)^{-\epsilon}\Big\{2\,[Li_2(1-\chi_p) - Li_2(1) - \frac{\chi_p\ln\chi_p}{1-\chi_p}]$$
$$+[\frac{\chi_p}{\epsilon_{\rm uv}} + 2\chi_p + \frac{\chi_p^2\ln\chi_p}{1-\chi_p}]\Big\} \tag{3.89}$$

$$C^{ML}(p) = C_F\frac{\alpha_s}{2\pi}(-p^2)^{-\epsilon}\Big\{-\frac{\chi_p}{\epsilon_{\rm uv}} - 2\chi_p - \frac{\chi_p^2\ln\chi_p}{1-\chi_p}\Big\} \tag{3.90}$$

$$\chi_p = \frac{2pn\,pn^*}{nn^*p^2}$$

The extraction of Z_F in the ML scheme is quite different from the one in the PV scheme, since we have $(1-\sigma)^{-1} \neq Z_F$ due to the presence of the n^*−term in Eq. (3.78). In fact, it has been shown [41] that there is an additional renormalization constant $\tilde{Z}_2$ necessary to account for the renormalization of the additional structures due to the presence of n^*. The quark field then is renormalized according to

$$\psi_r = (Z_2\tilde{Z}_2)^{\frac{1}{2}}\,[1 - (1-\tilde{Z}_2^{-1})\frac{\not{n}\,\not{n}^*}{2nn^*}]\,\psi\,. \tag{3.91}$$

In our special case however, one can find the appropriate expression for Z_F by using the fact that n^* has to be proportional to p in the limit $p^2 \to 0, \vec{p}_\perp \to 0$. This is because in the limit $p^2 \to 0$, $\vec{p}_\perp \to 0$, one has three light-like vectors with vanishing transverse components, but only two of them can be independent. So choosing n and p as independent light-like vectors, n^* has to be proportional to p.
In more physical terms, one can argue that for on-shell incoming momentum p, this incoming momentum can always be chosen to be equal to n^*, choosing the axis such that the transverse components are zero.
Then one has according to (3.78)

$$\begin{aligned} G(p) &= \frac{i}{1-\sigma}\left\{\frac{\not p}{p^2} - \frac{B}{1-A}\frac{\not n}{2pn} - \frac{C}{1-A}\frac{pn\,\not n^*}{\chi_p nn^* p^2}\right\} \\ &\longrightarrow \frac{i}{1-\sigma}\left\{\frac{\not p}{p^2} - \frac{B}{1-A}\frac{\not n}{2pn} - \frac{C}{(1-A)\chi_p}\frac{\not p}{p^2}\right\} \text{ for } n^* \to p \end{aligned} \tag{3.92}$$

Thus from (3.76) and (3.92) we conclude

$$\begin{aligned} Z_F^{ML} &= PP\{(1-\sigma)^{-1}(1 - \frac{C}{\chi_p(1-A)})\} \\ &= 1 + PP\{A + B + C(1 - \frac{1}{\chi_p}) + O({\alpha_s}^2)\} \\ &= 1 - \frac{1}{\epsilon} C_F \frac{\alpha_s}{2\pi} \cdot \frac{3}{2} \end{aligned} \tag{3.93}$$

Inserting this result into Eq. (3.72) gives the result (3.75) already obtained in the PV scheme:

$$\Gamma_{q/q}\left(x, \alpha_s, \frac{1}{\epsilon}\right) = \delta(1-x) - \frac{1}{\epsilon} C_F \frac{\alpha_s}{2\pi}\left\{\frac{1+x^2}{(1-x)_+} + \frac{3}{2}\delta(1-x)\right\} \tag{3.94}$$

To summarize, the advantage of the ML prescription at the LO level mainly amounts to producing truly finite results for the 2PI kernels, as required for the CFP method. Furthermore, there is no need for introducing renormalization constants depending on additional singular quantities like I_0 that represent a mix–up in the treatment of UV and IR singularities.

3.3.2 UV renormalization with PV respectively ML prescription

Treating the UV renormalization of the virtual diagrams, it has to be stressed again that in the ML scheme, the UV renormalization procedure is formally solid and well understood, although being not straightforward due to the additional counterterm structures containing n and n^*. In the PV scheme, however, the UV poles have spurious infrared divergent residues I_0 and the renormalization constants depend on the

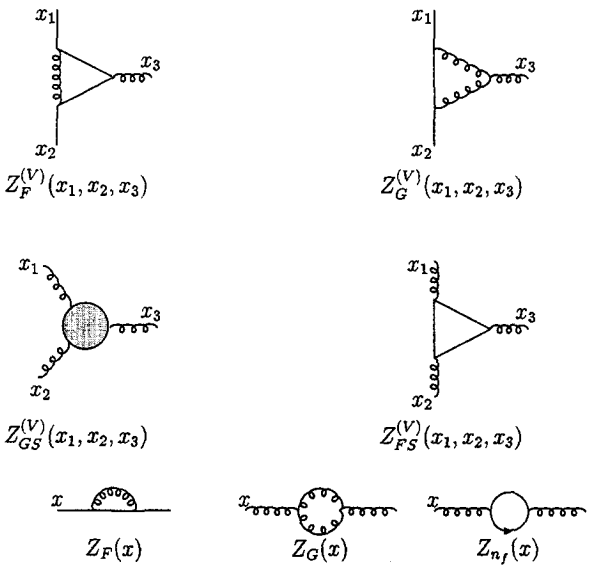

Figure 3.8: UV renormalization constants with PV prescription

longitudinal momentum fraction x. Although the Ward identities are still fulfilled [29], it is not a priori clear how to deal with these spurious poles and $x-$dependent terms in the UV renormalization constants. As we explained in the beginning of Section 3.3, the phenomenological rule of CFP is to subtract them locally, since this preserves the finiteness of the 2PI kernels K_0 and turned out to give the right result. But there is no warranty that this procedure will also work in three loops.
In both, PV and ML schemes, the counterterms are obtained by inserting the UV divergent one-loop structures into the corresponding virtual diagram. In the PV scheme, this leads to an expression proportional to the Born term (the leading order splitting function $P_{i/j}^{(0)}$, $i, j \in \{q, g\}$) times the renormalization constant $Z_{(a)}$ for the corresponding one-loop diagram (a). The one-loop diagrams are collected in Fig. 3.8 and the corresponding renormalization constants in the PV scheme are given by Eqs. (3.95) to (3.100).

$$Z_F^{(V)}(x_1,x_2,x_3) = 1+\frac{\alpha_s}{2\pi}\frac{1}{2\epsilon_{\rm uv}}(C_F-\frac{1}{2}N_c)(-4I_0-2\ln x_1-2\ln x_2+3) \quad (3.95)$$

$$Z_G^{(V)}(x_1,x_2,x_3) = 1+\frac{\alpha_s}{2\pi}\frac{1}{2\epsilon_{\rm uv}}N_c(-4I_0-\ln x_1-\ln x_2-2\ln x_3+\frac{3}{2}) \quad (3.96)$$

$$Z_{GS}^{(V)}(x_1,x_2,x_3) = 1+\frac{\alpha_s}{2\pi}\frac{1}{2\epsilon_{\rm uv}}N_c(-6I_0-2\ln x_1-2\ln x_2-2\ln x_3+\frac{11}{3})$$

$$Z_{FS}^{(V)}(x_1,x_2,x_3) = 1+\frac{\alpha_s}{2\pi}\frac{1}{2\epsilon_{\rm uv}}T_f(-\frac{4}{3}) \quad (3.97)$$

$$Z_F(x) = 1+\frac{\alpha_s}{2\pi}\frac{1}{2\epsilon_{\rm uv}}C_F(4I_0+4\ln x-3) \quad (3.98)$$

$$Z_G(x) = 1+\frac{\alpha_s}{2\pi}\frac{1}{2\epsilon_{\rm uv}}N_c(4I_0+4\ln x-\frac{11}{3}) \quad (3.99)$$

$$Z_{n_f}(x) = 1+\frac{\alpha_s}{2\pi}\frac{1}{2\epsilon_{\rm uv}}T_f(\frac{4}{3}) \quad (3.100)$$

$$C_F = \frac{N_c^2-1}{2N_c} \quad ; \quad T_f=\frac{1}{2}n_f$$

Note that $Z_{GS}^{(V)}$ contains both, the "triangle" and the "swordfish" (see Fig. 3.9) contribution to the three-gluon vertex.

One can check from Eqs. (3.95) to (3.100) that for a physical quantity, only the well-known renormalization of the bare coupling remains:

$$\begin{aligned}\alpha_s{}^{(0)} &= \alpha_s\mu^{2\epsilon}[Z_F^{(V)}(x_1,x_2,x_3)+Z_G^{(V)}(x_1,x_2,x_3)]\cdot\left(Z_F(x_1)Z_F(x_2)[Z_G(x_3)+Z_{n_f}(x_3)]\right)^{\frac{1}{2}} \\ &= \alpha_s\mu^{2\epsilon}\left(1+\frac{\alpha_s}{2\pi}\frac{1}{2\epsilon_{\rm uv}}[-\frac{11}{6}N_c+\frac{2}{3}T_f]+\ldots\right)\end{aligned}$$

Furthermore, the QED Ward identity can be easily checked also for $x-$dependent renormalization constants: Considering topologies $(c)_{\rm virt}$ and (e) of Fig. 3.6 and the counterpart of topology (e) with selfenergy insertion on the $p-$line and using $kn = x$, $pn = 1$, we find the following relation for the one-loop insertions:

$$[Z_F^{(V)}(x)-1]+\frac{1}{2}[Z_F(x)-1]+\frac{1}{2}[Z_F(1)-1]=0$$

But it has to be pointed out here that according to the CFP ladder expansion of 2PI kernels K_0, the diagram with selfenergy insertion on the $p-$line does not contribute since the kernels K_0 do not contain lower lines, whereas the diagram with selfenergy insertion on the $k-$line (topology (e)) does not obtain a factor $1/2$ since the $k-$line is an internal line. This is a subtle point, since we then obtain the following contribution proportional to C_F:

$$[Z_F^{(V)}(x)-1]+[Z_F(x)-1]=\frac{\alpha_s}{2\pi}\frac{1}{\epsilon_{\rm uv}}C_F\cdot\ln x$$

As we will see in section 3.4, this remaining $\ln x$ term is important to obtain the correct answer for the NLO splitting functions in the PV scheme.

In the ML scheme, the renormalization constants are really constant, but the counterterms are *not* proportional to the Born term due to the presence of n^* in the UV divergent one-loop structures. The latter have been calculated in [37, 47, 48, 49, 50] and are given in Fig. 3.9 and Eqs. (3.101) to (3.104). We only show the structures we need for our calculation, details can be looked up in [41, 42]. As expected, the structures are gauge dependent and Lorentz noncovariant. Even more, the expressions for the nonabelian quantities $\Pi^{ab}_{\mu\nu,G}(l)$ and $\Gamma^{G,a}_{\mu}(l)$ as well as some structures contained in $T^{a_1a_2a_3}_{\mu_1\mu_2\mu_3}(p_1,p_2,p_3)$ and $S^{a_1a_2a_3}_{\mu_1\mu_2\mu_3}(p_1,p_2,p_3)$ (see Fig. 3.9) are nonpolynomial in the external momenta, owing to terms like $1/ln$. It is an important feature of the ML prescription that these nonlocal terms exist, but decouple from physical Green functions [55] thanks to the orthogonality of the free propagator with respect to the gauge vector, $n_\mu D^{\mu\nu}(l) = 0$ (this has actually been an important ingredient for the proof [55] of the renormlizability of QCD in the ML light-cone gauge). Thus, the nonlocal terms never appear in our calculation.

$$\Gamma^{F,a}_{\mu}(l) = igT^a(C_F - \frac{N_c}{2})\frac{\alpha_s}{4\pi}\frac{1}{\epsilon_{\rm uv}}\left[\gamma_\mu + \frac{2}{nn^*}[\not{n}n^*_\mu - \not{n}^* n_\mu]\right] \quad (3.101)$$

$$\Gamma^{G,a}_{\mu}(l) = igT^a\frac{N_c}{2}\frac{\alpha_s}{4\pi}\frac{1}{\epsilon_{\rm uv}}\left[\gamma_\mu - \frac{2}{nn^*}[\not{n}n^*_\mu + \not{n}^* n_\mu - 2\not{n}\frac{ln^*}{[ln]}n_\mu]\right] \quad (3.102)$$

$$T^{a_1a_2a_3}_{\mu_1\mu_2\mu_3}(p_1,p_2,p_3) = -ig\frac{N_c}{2}f^{a_1a_2a_3}\frac{\alpha_s}{4\pi}\frac{1}{\epsilon_{\rm uv}}\left[\frac{4}{3}A_{\mu_1\mu_2\mu_3} + 2C_{\mu_1\mu_2\mu_3} + \ldots\right] \quad (3.103)$$

$$S^{a_1a_2a_3}_{\mu_1\mu_2\mu_3}(p_1,p_2,p_3) = -ig\frac{N_c}{2}f^{a_1a_2a_3}\frac{\alpha_s}{4\pi}\frac{1}{\epsilon_{\rm uv}}[6A_{\mu_1\mu_2\mu_3} - 6C_{\mu_1\mu_2\mu_3} + \ldots] \quad (3.104)$$

$$A_{\mu_1\mu_2\mu_3} = g_{\mu_2\mu_3}(p_2-p_3)_{\mu_1} + g_{\mu_3\mu_1}(p_3-p_1)_{\mu_2} + g_{\mu_1\mu_2}(p_1-p_2)_{\mu_3}$$

$$C_{\mu_1\mu_2\mu_3} = g_{\mu_2\mu_3}n^*_{\mu_1}(p_2-p_3)\cdot n + g_{\mu_3\mu_1}n^*_{\mu_2}(p_3-p_1)\cdot n + g_{\mu_1\mu_2}n^*_{\mu_3}(p_1-p_2)\cdot n$$

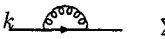

$$\Sigma(k) = i\frac{\alpha_s}{4\pi}\frac{C_F}{\epsilon_{uv}}\left[\not{k} + 2\{\not{n}(kn^*) - \not{n}^*(kn)\}\right]$$

$$\Pi^{ab}_{\mu\nu,G}(l) = i\frac{\alpha_s}{4\pi}\frac{N_c}{\epsilon_{uv}}\delta^{ab}\left[\frac{11}{3}(l^2\, g_{\mu\nu} - l_\mu l_\nu) - 2l^2(\hat{n}_\mu\hat{n}^*_\nu + \hat{n}^*_\mu\hat{n}_\nu)\right]$$

$$\hat{n}_\mu = n_\mu - \frac{ln}{l^2}\, l_\mu\,;\ \hat{n}^*_\mu = n^*_\mu - \frac{ln^*}{[ln]}\, n_\mu$$

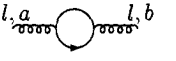

$$\Pi^{ab}_{\mu\nu,F}(l) = -i\frac{\alpha_s}{3\pi}\frac{T_f}{\epsilon_{uv}}\delta^{ab}\left[l^2\, g_{\mu\nu} - l_\mu l_\nu\right]$$

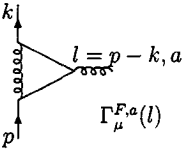

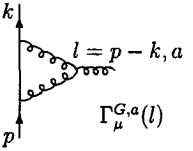

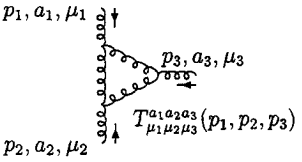

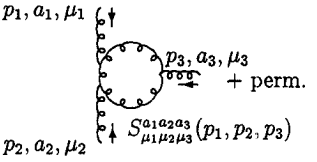

Figure 3.9: UV divergent parts of one-loop diagrams with ML prescription.

3.4 Next-to-leading order for colour structure C_F^2

Since every colour structure defines a gauge invariant contribution, we can first restrict our study of the ML prescription within the CFP scheme to the terms that are proportional to C_F^2 [65]. Besides the obvious advantage of reducing the number of contributing Feynman diagrams, this colour structure has two additional simplifying features: (i) the ultraviolet counterterms satisfy the QED Ward-identities, (ii) the sums of the real and virtual contributions are separately free from soft and collinear singularities and from spurious poles. The axial-ghost contributions, however, remain important and therefore the C_F^2 structure gives a good opportunity to study these contributions in isolation from other complications. In order to be able to exhibit clearly the cancellation mechanism of the spurious poles, we use PVI regularization throughout Section 3.4. Thus all spurious poles appear in terms of I_0 and I_1 defined in Eqs. (3.61) and (3.62), whereas the "physical" ultraviolet and infrared poles are still regulated by dimensional regularization as usual.

As we know from Section 2.1.4, the non-singlet evolution kernel $P_{q/q}^{(1)}$ at NLO is given by

$$P_{q/q}^{(1)} = P_{q/q}^{V,(1)} + P_{q/\bar{q}}^{V,(1)} + 2n_f\, P_{q/\bar{q}}^{S,(1)} \tag{3.105}$$

The diagrams contributing to $P_{q/\bar{q}}^{(1)}$ are the same with PV and ML prescription since they do not contain any virtual loop or cut gluon line. Therefore we do not need to consider $P_{q/\bar{q}}^{(1)}$ in the following.

The Feynman diagrams contributing to the part of $\hat{P}_{q/q}^{V,(1)}$ being proportional to C_F^2 are shown in Fig. 3.10. We recall that, as indicated in Eq. (3.39), the "hat" means that we do not include the contributions at $x = 1$ here. The axial ghosts are denoted by dotted lines replacing cut gluon lines.

Virtual corrections

The virtual part of the C_F^2 colour structure is given by topologies $(c)_{\text{virt}}$ and (e) in Fig. 3.10.

One special feature of the C_F^2 virtual part is that in the ML scheme, the UV poles cancel between the C_F^2 part of the vertex diagram $(c)_{\text{virt}}$ and the quark selfenergy diagram (e), whereas in the PV scheme, this cancellation is incomplete due to the fact that the UV poles depend on I_0 and logarithms of the longitudinal momentum fraction x, as has been shown in the previous section. We will see that this difference in the treatment of the UV poles leads to extra terms in the PV scheme, which in the ML scheme will be accounted for by the ghost contributions.

The second special feature of the C_F^2 virtual part is given by the fact that each virtual integral appearing in this part is separately free from spurious poles. The reason for

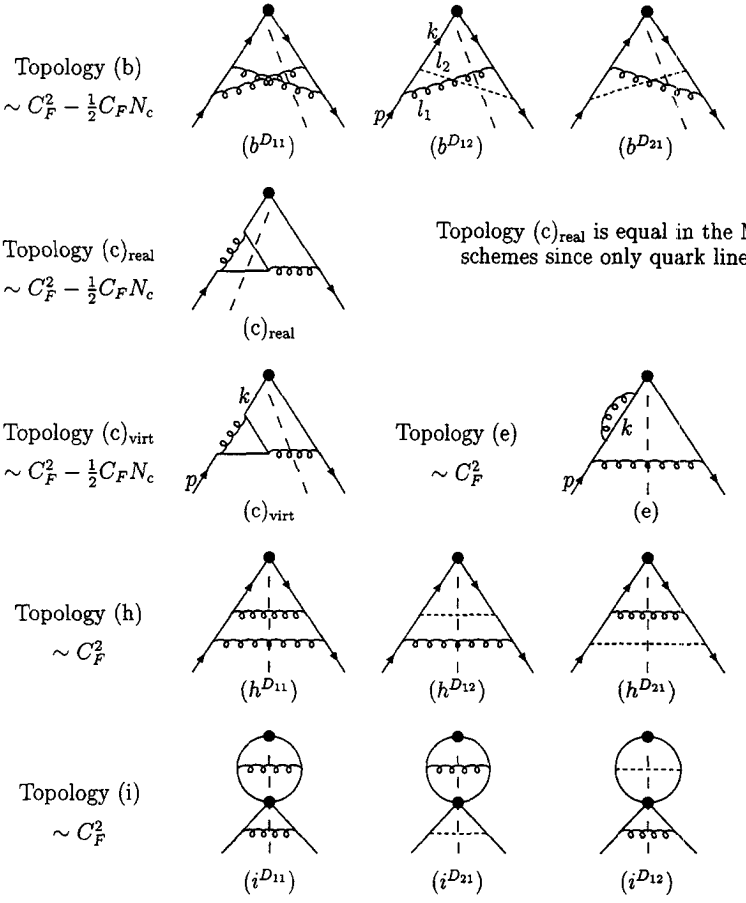

Figure 3.10: Diagrams contributing to $\hat{P}_{q/q}^{V,(1)}(x)$ with colour factor C_F^2

this can be deduced from Eq. (3.56): Consider the term

$$\frac{1}{R^+ + i\eta \,\mathrm{sign}\, R^-}\Big\{[M_n]^{\frac{m}{2}-n} - [M_n - 2R^+R^-]^{\frac{m}{2}-n}\Big\} \tag{3.106}$$

This expression is vanishing in the limit $R^+ \to 0$, $R^+ = 0$ being the spurious singularity, as long as there is no conflict with the limit $M_n \to 0$. In the C_F^2 part, M_n is always different from zero, such that the spurious poles appearing in the first part of the difference in (3.106) will always be cancelled by the ones contained in the second part, no matter how we regulate them.

In the following, we will give explicit expressions for the virtual diagrams in a scheme independent way by using the integral form factors defined and given in Appendix A. Inserting the form factors obtained in the PV scheme, the well-known result for the virtual part of the CFP calculation is reproduced. We will proceed by first calculating the one-loop insertions, extracting their UV poles, and then evaluating the UV renormalized contribution to $\hat{\Gamma}^{(1)}_{q/q}(x,\epsilon)$.

Quark selfenergy

The quark selfenergy (see topology (e) in Fig. 3.10) already has been calculated for the leading order and is given by Eqs. (3.83) and (3.84), where the external momentum of the selfenergy insertion is now k instead of p. Furthermore, we set $p = n^*$ since p has to be proportional to n^* if we have $pn \neq 0$ and $\vec{p}_\perp = 0$, as has been explained in Section 3.3.1. For all virtual diagrams we use the condition $l^2 = 0$ coming from the one-body phase space. Using these kinematics and $m = 4 - 2\epsilon$ we have

$$\begin{aligned}
\Sigma(k) &= \Sigma^F(k) + \Sigma^A(k) \\
\Sigma^F(k) &= C_F \frac{g^2}{(2\pi)^m} Q_\epsilon^k \frac{(m-2)}{2} \not{k}\, T_0 \\
\Sigma^A(k) &= -C_F \frac{g^2}{(2\pi)^m} \frac{Q_\epsilon^k}{kn} \left(2\, \not{n} k^2 (P_1 - P_0) + P_2(\not{n}\, \not{p}\, \not{k} + \not{k}\, \not{p}\, \not{n})\right) \\
&= -C_F \frac{g^2}{(2\pi)^m} \frac{Q_\epsilon^k}{kn} \Big(2\, \not{n} k^2 (P_1 - P_0) + 2P_2(\not{k}\, pn - \not{p}\, kn + \frac{k^2}{2}\, \not{n})\Big)
\end{aligned} \tag{3.107}$$

Inserting the above expression for $\Sigma(k)$ into the full diagram leads to

$$\begin{aligned}
T^{(e)}(x,k^2,\epsilon) &:= -C_F \frac{ig^2}{(k^2)^2} Tr\,[\frac{\not{n}}{4kn}\, \not{k}\Sigma\, \not{k}\gamma^\mu\, \not{p}\gamma^\nu\, \not{k}]\, d_{\mu\nu}(p-k) \\
&= C_F^2\, {\alpha_s}^2\, (4\pi)^\epsilon \Gamma(1+\epsilon)\, (-k^2)^{-\epsilon} \\
&\quad \cdot \frac{2}{x}\Big\{\hat{P}_{q/q}(x,\epsilon)\,[T_0\,(\epsilon-1) + 4\,(P_1 - P_0) + \frac{2}{x} P_2] \\
&\quad + 2P_2 \frac{(1+x)}{1-x}\Big\}
\end{aligned} \tag{3.108}$$

$$\hat{P}_{q/q}(x,\epsilon) = \frac{1+x^2}{1-x} - \epsilon\,(1-x) =: p_{qq}(x) - \epsilon\,(1-x)\,; \quad x < 1\,. \tag{3.109}$$

Vertex correction

The vertex insertion in diagram $(c)_{\rm virt}$ can also be split into a Feynman part and an axial part:

$$\begin{aligned}
\Gamma_{\mu,b} &= \Gamma^F_{\mu,b} + \Gamma^A_{\mu,b} \\
\Gamma^F_{\mu,b} &= T_b\,(C_F - \frac{N_c}{2})\frac{2g^3}{(2\pi)^m}\Big\{[\not p\gamma_\mu\ \not k\, J_3^F(k,p) + \not p\gamma_\mu\gamma^\nu J^F_{3\nu}(k,p) + \gamma^\nu\gamma_\mu\ \not k J^F_{3\nu}(k,p) \\
&\qquad +\gamma^\lambda\gamma_\mu\gamma^\sigma J^F_{3\lambda\sigma}(k,p)] \\
&\quad -\epsilon\,[\not k\gamma_\mu\ \not p\, J_3^F(k,p) + \gamma^\nu\gamma_\mu\ \not p J^F_{3\nu}(k,p) + \not k\gamma_\mu\gamma^\nu J^F_{3\nu}(k,p) + \gamma^\lambda\gamma_\mu\gamma^\sigma J^F_{3\lambda\sigma}(k,p)]\Big\}
\end{aligned}$$

$$\Gamma^A_{\mu,b} =: T_b\,(C_F - \frac{N_c}{2})(\Gamma^A_{1\mu} + \Gamma^A_{2\mu})$$

$$\Gamma^A_{1\mu} = \frac{g^3}{(2\pi)^m}\{\not n\ \not k\gamma_\mu\, J_2^A(k) + \not n\gamma^\nu\gamma_\mu\, J^A_{2\nu}(k) + \gamma_\mu\ \not p\ \not n\, J_2^A(p) + \gamma_\mu\gamma^\nu\ \not n\, J^A_{2\nu}(p)\}$$

$$\begin{aligned}
\Gamma^A_{2\mu} &= -\frac{g^3}{(2\pi)^m}\{k^2\gamma_\mu\ \not p\ \not n\, J_3^A(k,p) + k^2\gamma_\mu\gamma^\nu\, J^A_{3\nu}(k,p)\ \not n \\
&\quad +\ \not k\gamma^\nu\, J^A_{3\nu}(k,p)\,\gamma_\mu\ \not p\ \not n + \not k\gamma^\nu\gamma_\mu\gamma^\lambda\, J^A_{3\nu\lambda}(k,p)\ \not n\}
\end{aligned}$$

Inserting the expression for $\Gamma_{\mu,b}$ into the full diagram and defining $T^{(c)_{\rm v}}$ analogous to $T^{(e)}$ above, we obtain for the Feynman part

$$\begin{aligned}
T^{(c)_{\rm v},{\rm Fey}}(x,k^2,\epsilon) &= C_F(C_F - \frac{N_c}{2})\,{\alpha_s}^2\,(4\pi)^\epsilon\Gamma(1+\epsilon)\,(-k^2)^{-\epsilon} \\
&\quad \cdot\frac{4}{x}\Big\{\{R_1 - R_0 + (2-\epsilon)R_2 - (1-\epsilon)(R_4+R_5)\}\,[x+\epsilon\,(1-x)] \\
&\quad +2\,R_6\,(1-\epsilon)^2\,\hat P_{q/q}(x,\epsilon)\Big\}
\end{aligned} \tag{3.110}$$

and for the axial part

$$\begin{aligned}
T^{(c)_{\rm v},{\rm Ax}}(x,k^2,\epsilon) &= C_F(C_F - \frac{N_c}{2})\,{\alpha_s}^2\,(4\pi)^\epsilon\Gamma(1+\epsilon)\,(-k^2)^{-\epsilon} \\
&\quad \cdot\Big\{\frac{4}{x}\left((P_0 - P_1)\,\hat P_{q/q}(x,\epsilon) - P_2\,\frac{1+x}{1-x}\right) \\
&\quad +(p^2/k^2)^{-\epsilon}\,\frac{4}{x}\,(B_0 - B_1 - B_2)\,\hat P_{q/q}(x,\epsilon) \\
&\quad +\frac{2}{x}\Big[(S_1 + S_4 + (2-x)\,S_2 - 2\,S_0 + R_0)\,\hat P_{qq}(x,\epsilon) \\
&\quad -2(R_1 + R_2 - R_0)\,\frac{1+x}{1-x}\Big]\Big\}.
\end{aligned} \tag{3.111}$$

The form factors are defined and given in Appendix A.3 both for PV and ML prescription.

Ultraviolet renormalization

We use dimensional regularization to regulate both the ultraviolet and the infrared singularities. Doing the loop integrals we first must assume that in $m = 4 - 2\epsilon$, ϵ is positive. After adding the UV counterterms for the quark selfenergy and vertex one-loop subdiagrams we obtain an ultraviolet finite answer. Then we can analytically continue the result to negative values of ϵ and go on with the evaluation of the Feynman parameter integrals. Thus we should keep p off-shell first and set it on-shell only after ultraviolet renormalization. It is known that the sum of the two ultraviolet counterterms for the vertex and quark selfenergy diagrams in regular gauges vanishes as a consequence of Abelian gauge invariance.

Inserting the UV divergent one-loop structures given in Section 3.3.2 into the corresponding full diagrams, we obtain the counterterms for these diagrams. In particular, we find for the C_F^2−case:[3]

$$\begin{aligned}
T_{\rm UV}^{(e),ML} &= C_F^2 {\alpha_s}^2 \frac{1}{\epsilon_{\rm uv}} \frac{2}{x} [3\,\hat{P}_{q/q}(x,\epsilon) - 2] \\
T_{\rm UV}^{(c)_{\rm v},ML} &= C_F (C_F - \frac{N_c}{2})\, {\alpha_s}^2 \frac{1}{\epsilon_{\rm uv}} \frac{2}{x} [-3\,\hat{P}_{q/q}(x,\epsilon) + 2] \\
T_{\rm UV}^{(e),PV} &= C_F^2 {\alpha_s}^2 \frac{1}{\epsilon_{\rm uv}} \frac{2}{x} \hat{P}_{q/q}(x,\epsilon)\, [3 - 4I_0 - 4\ln x] \\
T_{\rm UV}^{(c)_{\rm v},PV} &= C_F (C_F - \frac{N_c}{2})\, {\alpha_s}^2 \frac{1}{\epsilon_{\rm uv}} \frac{2}{x} \hat{P}_{q/q}(x,\epsilon)\, [-3 + 4I_0 + 2\ln x]
\end{aligned}$$

and so

$$\begin{aligned}
T_{{\rm UV},C_F^2}^{(e+c_{\rm v}),ML} &= 0 \\
T_{{\rm UV},C_F^2}^{(e+c_{\rm v}),PV} &= -C_F^2 {\alpha_s}^2 \frac{1}{\epsilon_{\rm uv}} \frac{4}{x} \hat{P}_{q/q}(x,\epsilon)\, \ln x. \qquad (3.112)
\end{aligned}$$

This is an essential difference between the PV and ML schemes. The leftover UV singularity (3.112) in the PV scheme is a remainder from the contributions of the spurious poles to the UV renormalization constants. In the ML prescription, there are terms in the UV pole parts of the single diagrams which are even not proportional to the Born term $p_{qq}(x)$, stemming from the n^*−part of the virtual integrals, but those terms completely cancel when summing up diagrams contributing to a gauge invariant subpart. Therefore it does not matter in the ML case whether they are subtracted or not. In the C_F^2 part we even have

$$T_{\rm ren}^{(e+c_{\rm v}),ML} = T_{\rm bare}^{(e+c_{\rm v}),ML} = T^{(e+c_{\rm v}),ML}$$

[3]Note that the ϵ−dependence in $\hat{P}_{q/q}(x,\epsilon)$, stemming from the trace of the diagram with the one-loop counterterm insertion, has to be kept to obtain the complete counterterm.

and the contribution to $\hat{\Gamma}^{(1)}_{q/q}(x,\epsilon)$ is, according to Eqs. (3.17) and (3.37), given by[4]

$$\begin{aligned}\hat{\Gamma}^{(1,e+c_v),ML}_{q/q}(x,\epsilon) &= PP\{\frac{1}{16\pi^2}\frac{(4\pi)^\epsilon}{\Gamma(1-\epsilon)}\int_0^{Q^2} d|k^2|\,|k^2|^{-1-\epsilon}\,x\,(1-x)^{-\epsilon} \\ &\quad \cdot 2\,T^{(e+c_v),ML}(x,k^2,\epsilon)\} \qquad (3.113)\end{aligned}$$

Details about the phase space integral are given in Appendix B.1.
In the PV case however, the leftover term in (3.112) leads to an additional contribution to the splitting function in the following way: The renormalized expression for the sum of diagrams $(c)_{\text{virt}}$ and (e) is given by

$$T^{(e+c_v),PV}_{\text{ren}} = T^{(e+c_v),PV} - T^{(e+c_v),PV}_{\text{UV}}. \qquad (3.114)$$

Note that $T^{(e+c_v),PV}$ contains a factor of $|k^2|^{-\epsilon}$ whereas $T^{(e+c_v),PV}_{\text{UV}}$ does not. Inserting the UV subtracted expression (3.114) into the k^2–integral (3.113) and disregarding for the moment the finite parts of $T^{(e+c_v),PV}_{\text{ren}}$ we obtain

$$\begin{aligned}& PP\{\frac{1}{16\pi^2}\frac{(4\pi)^\epsilon}{\Gamma(1-\epsilon)}\int_0^{Q^2} d|k^2||k^2|^{-1-\epsilon}\,x\,(1-x)^{-\epsilon}\cdot 2\,T^{(e+c_v),PV,\text{sing}}_{\text{ren}}\} \\ &= C_F^2(\frac{\alpha_s}{2\pi})^2(1-x)^{-\epsilon}\int_0^{Q^2} d|k^2||k^2|^{-1-\epsilon}\hat{P}_{q/q}(x,\epsilon)\left[-2|k^2|^{-\epsilon}\frac{\ln x}{\epsilon}+2\frac{\ln x}{\epsilon}\right] \\ &= -\frac{1}{2\epsilon}C_F^2(\frac{\alpha_s}{2\pi})^2\left(\frac{2\ln x}{\epsilon}p_{qq}(x)-2\ln x\,[1-x+p_{qq}(x)\ln(1-x)]+\mathcal{O}(\epsilon)\right)\end{aligned}$$

The double pole term has to be dropped since $\hat{P}^{(1)}_{q/q}(x)$ is defined through simple poles in ϵ (see Eq. (3.37)). But the single pole term gives a contribution to $\hat{P}^{(1)}_{q/q}(x)$ which is exactly the difference of the virtual contributions $(\text{PV–ML})_{\text{virt}}$ obtained by using PV respectively ML prescription, as can be seen in Tables 3.1 and 3.4. This difference will be compensated by the ghost diagrams present only in the ML case.
The complete contributions of the virtual diagrams to $\hat{P}^{(1)}_{q/q}(x)$ are listed in Table 3.1. Virtual diagrams where the cut line is a ghost line would give a contribution at $x=1$ only, so they do not contribute to $\hat{P}^{(1)}_{q/q}(x)$ according to Eq. (3.39).

Real contributions

Now we will give some details concerning the calculation of the contributions from the diagrams of topologies (b),$(c)_{\text{real}}$,(h) and (i). Topology (i) represents the subtraction term $\mathcal{P}(K_0\mathcal{P}K_0)$ in Eq. (3.40) and consists of two Born diagrams linked by an additional projection. Diagram $(c)_{\text{real}}$ has no cut gluon lines, therefore it contains no axial ghosts.

[4] A factor of two has to be included for diagrams which are not symmetric.

C_F^2						
Finite part						
	e_{ML}	$c_{v,ML}$	e_{PV}	$c_{v,PV}$	$(e+c_v)_{ML}$	$(e+c_v)_{PV}$
$p_{qq}(x)$	6	-6	7	-7	0	0
$p_{qq}(x)\ln^2 x$	0	0	-2	2	0	0
$p_{qq}(x)\ln x \ln(1-x)$	0	0	-4	2	0	-2
$p_{qq}(x)\ln x$	-1	1	0	0	0	0
$p_{qq}(x)\ln(1-x)$	3	-3	3	-3	0	0
$p_{qq}(x)\,Li_2(1-x)$	4	-2	0	2	2	2
$p_{qq}(x)\,\pi^2/3$	-2	2	-2	2	0	0
$x/(1-x)$	2	-2	0	0	0	0
x	-2	3	-3	4	1	1
1	-2	2	3	-3	0	0
$x\ln x$	-1	1	4	-2	0	2
$\ln x$	1	-1	-4	2	0	-2
$\ln(1-x)$	-2	2	0	0	0	0
Spurious poles						
$p_{qq}(x)\,I_0\ln(1-x)$	0	0	-4	4	0	0
$p_{qq}(x)\,I_0\ln x$	0	0	-4	4	0	0
$p_{qq}(x)\,I_0$	0	0	0	0	0	0
$p_{qq}(x)\,I_1$	0	0	4	-4	0	0
$x\,I_0$	0	0	4	-4	0	0
I_0	0	0	-4	4	0	0
Ultraviolet poles						
$p_{qq}(x)\,I_0/\epsilon_{uv}$	0	0	-4	4	0	0
$p_{qq}(x)\ln x/\epsilon_{uv}$	0	0	-4	2	0	-2
$p_{qq}(x)/\epsilon_{uv}$	3	-3	3	-3	0	0
$1/\epsilon_{uv}$	-2	2	0	0	0	0

Table 3.1: Contributions to $\hat{P}^{(1)}_{q/q}(x)$ from the virtual diagrams proportional to C_F^2.

The calculation will be divided into transverse real part and axial ghost part. The spurious poles present in transverse and ghost parts will be shown to cancel. This cancellation can be regarded as being twofold:

1. Within a given topology:
   The spurious poles of the transverse contributions are always regulated by the corresponding ghost contributions of the same topology.

2. Within transverse part and ghost part separately:

The sum of all transverse real diagrams is free from spurious poles as well as the sum of all ghost diagrams.

Note that these two properties are only true in the case of the C_F^2 colour structure. In the $C_F N_c$ and N_c^2 colour structures treated in the next section, the spurious poles do not cancel separately in virtual and real parts in the ML scheme, and therefore the feature that all spurious poles in the transverse real part are directly regulated by the corresponding ghost diagrams *within* the real part is destroyed. As a consequence, it is important there to regulate the spurious poles in real and virtual parts in the same way.

But in the case of the C_F^2 colour structure, due to the fact that the virtual part is separately free from spurious poles, we can choose in the real part PVI– or ϵ–regularization, independently from what we did in the virtual part. We did the calculation with both regularization methods, but only the result obtained with the PVI regularization method will be shown here since this is the method where the cancellation mechanism for the spurious poles is exhibited in the clearest way.

Physical contributions

The physical contributions to the real part, containing only transverse gluon propagators, are given by topologies $(b^{D_{11}})$, $(c)_{\text{real}}$, $(h^{D_{11}})$ and $(i^{D_{11}})$ shown in Fig. 3.10. The typical integral we have to evaluate for topologies (b),$(c)_{\text{real}}$ and (h) can be written as

$$I^{(a)} = \frac{1}{2}\frac{g^4}{(2\pi)^m}\int \frac{dk^2}{k^4}\, d\vec{k}_\perp \int d\Phi(l_1,l_2)\cdot M^{(a)}(x,l_1,l_2,k,\epsilon) \tag{3.115}$$

where $d\Phi(l_1,l_2)$ is the two-body phase space for the two cut lines and $M^{(a)}$ the matrix element for topology (a).

All details about the phase space are given in Appendix B.2.1. The matrix elements have been evaluated by using FORM [61], the phase space integrations have been implemented in Mathematica [62].

The results for the individual diagrams are shown in Tables 3.2 and 3.3.

Ghost contributions

The diagrams considered in this section are given by topologies $b^{D_{12}}, h^{D_{12}}, h^{D_{21}}, i^{D_{12}}$ and $i^{D_{21}}$) in Fig. 3.10. Topology $(b^{D_{21}})$ leads to the same result as $(b^{D_{12}})$ because the diagrams are symmetric under exchange of $l_1 \leftrightarrow l_2$. Diagrams with two cut ghost lines only give a contribution at $x = 1$, which has been omitted since it can be obtained more easily from fermion number conservation.

The phase space for diagrams with one ghost line and one gluon line cut is given by (for details see Appendix B.2.2)

$$\begin{aligned} PS^{\text{ghost}} &= F_\epsilon\, |k^2|^{2-2\epsilon}\, x^{-1+\epsilon}(1-x)^{-\epsilon}\int_0^1 du\, u^{-\epsilon}(1-u)^{1-\epsilon}\int_0^1 dy\, y^{-\epsilon} \\ &\quad \frac{1}{B(\frac{1}{2}-\epsilon,\frac{1}{2}-\epsilon)}\int_0^1 dw\, [w(1-w)]^{-\frac{1}{2}-\epsilon}. \end{aligned} \tag{3.116}$$

The results for the ghost diagrams are given in Tables 3.2 and 3.3. Table 3.4 shows the results for both, the real and the virtual part in the PV and ML schemes, where real means standard *plus* ghost contributions in the ML case.

Comparison of PV and ML schemes for the C_F^2 part

It is instructive to make a detailed comparison of the C_F^2 part results obtained in the PV respectively ML scheme. The necessary informations are summarized in Tables 3.1 to 3.4. In evaluating one-loop insertions in the ML scheme, the spurious poles cancel within the loop integrals, whereas the PV integrals can be recovered as a subpart of the ML integrals, this subpart being plagued by spurious singularities (see Eqs. (3.56),(3.57) and Table 3.1). Nevertheless, the sum of all virtual contributions in the PV scheme is free from spurious poles. The difference $(\text{ML–PV})_{\text{virt}}$ of the sums of all virtual contributions calculated in the ML respectively PV scheme is due to the second term in (3.56) which is not present in the PV case (3.57) *and* due to the difference in the UV counterterms.

The differences in the real contributions can be organized according to the expressions (3.50) and (3.51). The first term is the standard axial gauge contribution, the second term defines the axial ghost contribution. Using PVI regularization, the transverse real contributions are exactly the same in the PV and the ML scheme, such that the difference $(\text{ML–PV})_{\text{real}}$ is entirely made up by the ghost contributions present only in the ML scheme. These ghost contributions exactly compensate the difference found in the virtual part, as can be seen from Table 3.4.

From Tables 3.2 and 3.3, we see that the individual terms in the ML scheme are more regular than in the PV scheme. If we combine the contributions of the diagrams $(b^{D11}, b^{D12}, b^{D21})$ or $((h-i)^{D11}, (h-i)^{D12}, (h-i)^{D21})$, their sum is separately finite, whereas in the PV scheme, only the contributions $(b^{D11}, h^{D11}, i^{D11})$ exist, which are finite only when combining the different topologies. Consequently, the sums of the ghost and non-ghost diagrams in the ML scheme are also separately finite.

In summary, the evaluation of the C_F^2 part of the two-loop splitting functions in the ML scheme is a consistent method. The axial ghost contributions are important to get the correct answer. It is remarkable that the phenomenological rule of CFP for subtracting all ultraviolet contributions (spurious and non-spurious ones) leads to the same additional terms as provided by the axial ghost contributions in the ML scheme. It is interesting to see the differences between the two schemes and the higher consistency of the ML scheme also for the remaining colour structures, treated in the following sections.

	C_F^2											
	transverse				ghosts						transv.	ghosts
	$b^{D_{11}}$	c_r	$h^{D_{11}}$	$i^{D_{11}}$	$b^{D_{12}}$	$b^{D_{21}}$	$h^{D_{12}}$	$h^{D_{21}}$	$i^{D_{12}}$	$i^{D_{21}}$	$(b+h-i)_{\rm tr}$	$(b+h-i)_{\rm gh}$
$p_{qq}(x)\,\ln^2(1-x)$	0	0	6	6	0	0	0	0	0	0	0	0
$p_{qq}(x)\,\ln^2 x$	-1	-1	0	-2	1/2	1/2	1	0	2	0	1	0
$p_{qq}(x)\,\ln x \ln(1-x)$	0	0	-2	-2	0	0	-2	0	0	0	0	-2
$p_{qq}(x)\,\ln(1-x)$	4	0	-4	0							0	0
$p_{qq}(x)\,\ln x$	0	-3/2	0	0							0	0
$p_{qq}(x)\,Li_2(1-x)$	0	-2	0	0	1	1	-2	0	0	0	0	0
$p_{qq}(x)\,\pi^2/3$	0	0	-2	-2							0	0
$x\,\ln^2 x$	0	0	-1/2	0							-1/2	0
$\ln^2 x$	0	0	-1/2	0							-1/2	0
$x\,\ln x$	2	-7/2	-4	0	0	0	2	0	0	0	-2	2
$\ln x$	2	-7/2	0	-2	0	0	-2	0	0	0	4	-2
$(1+x)Li_2(1-x)$	0	0	2	2							0	0
$1-x$	0	-7	1	-2							3	0
1	0	-1	0	0							0	0
$x^2\,\ln x \ln(1-x)/(1-x)$	0	0	-4	-4							0	0
Spurious poles												
$p_{qq}(x)\,I_0$	4	0	0	4	-2	-2	0	0	0	-4	0	0
$p_{qq}(x)\,I_0\,\ln x$	0	0	-4	-4	0	0	2	2	4	0	0	0
$p_{qq}(x)\,I_0\,\ln(1-x)$	0	0	4	4	0	0	-2	-2	0	-4	0	0
$p_{qq}(x)\,I_1$	0	0	4	4	0	0	-2	-2	-4	0	0	0
$I_0 \cdot x/(1-x)$	0	0	-8	-8	0	0	4	4	0	8	0	0

Table 3.2: The contributions to $\hat{P}^{(1)}_{q/q}(x)$ from real diagrams $\sim C_F^2$ with ML prescription and PVI regularization. The result obtained within the PV scheme also can be read off from this table since it is entirely given by the transverse contributions. Note that the contributions from topology (i) have to be *subtracted.*

	C_F^2											
	transverse				ghosts						transv.	ghosts
	$b^{D_{11}}$	c_r	$h^{D_{11}}$	$i^{D_{11}}$	$b^{D_{12}}$	$b^{D_{21}}$	$h^{D_{12}}$	$h^{D_{21}}$	$i^{D_{12}}$	$i^{D_{21}}$	$(b+h-i)_{\rm tr}$	$(b+h-i)_{\rm gh}$
$p_{qq}(x)\, I_0/\epsilon$	0	0	-4	-4	0	0	2	2	2	2	0	0
$p_{qq}(x)\, \ln x/\epsilon$	0	0	0	0	0	0	2	0	2	0	0	0
$p_{qq}(x)\, \ln(1-x)/\epsilon$	0	0	-4	-4	0	0	0	0	0	0	0	0
$(1+x)\, \ln x/\epsilon$	0	0	-1	-1	0	0	0	0	0	0	0	0
$(1-x)/\epsilon$	0	0	2	2	0	0	0	0	0	0	0	0

Table 3.3: Singular parts of real diagrams in the ML scheme with PVI regularization

	C_F^2						
	sum of real diagrams		$\text{diff}_{\text{real}}$	sum of virtual diagrams		$\text{diff}_{\text{virt}}$	
	$(b+h-i)_{\text{ML}}$	$(b+h-i)_{\text{PV}}$	$(\text{ML–PV})_{\text{real}}$	$(e+c_{\text{v}})_{\text{ML}}$	$(e+c_{\text{v}})_{\text{PV}}$	$(\text{ML–PV})_{\text{virt}}$	sum of ghosts only
$p_{qq}(x)\ \ln^2 x$	1	1	0	0	0	0	0
$p_{qq}(x)\ \ln x \ln(1-x)$	-2	0	-2	0	-2	2	-2
$p_{qq}(x)\ Li_2(1-x)$	0	0	0	2	2	0	0
$x\ \ln^2 x$	-1/2	-1/2	0	0	0	0	0
$\ln^2 x$	-1/2	-1/2	0	0	0	0	0
$x\ \ln x$	0	-2	2	0	2	-2	2
$\ln x$	2	4	-2	0	-2	2	-2
1	3	3	0	0	0	0	0
x	-3	-3	0	1	1	0	0

Table 3.4: Comparison of real and virtual parts proportional to C_F^2 in PV and ML schemes

3.5 NLO techniques and results for $C_F T_f$, $C_F N_c$ and N_c^2 parts

The following three subsections treat the remaining colour structures $C_F T_f$ and $C_F N_c$ of the non-singlet splitting functions and the contributions proportional to N_c^2 of the gluon-gluon splitting functions.
The calculation of the $C_F N_c$ part turned out to be considerably more complicated than the C_F^2 part calculation. Especially the real diagrams of topology (d) where one cut gluon line is an axial ghost (see Fig. 3.14) turned out to be technically too involved to be calculated analytically. Therefore we had to recur to another method, which we will call "imaginary part method": Instead of calculating all real diagrams via the two-body phase space described in Appendix B.2, we calculated the full two-loop diagram and then extracted the discontinuities, the latter corresponding to all possible cuts of the given diagram. This turned out to be the most convenient method for all topologies which have two cuts, leading to a real and a virtual diagram, as it is the case for topologies (f) and (d) in the $C_F N_c$ part (see Fig. 3.14). Using this method, unitarity is manifest: The sum of all cuts of a certain topology is free from soft and collinear poles and, even more important in our context, is *free from spurious poles*.
But it has to be stressed that the cancellation mechanism of the spurious poles in the $C_F N_c$ part is quite different from the one in the C_F^2 part. It is no longer the case that the spurious poles of the transverse real part are fully regulated by the corresponding ghost contributions. Thus, besides the well-known fact that the usual soft and collinear poles cancel between real and virtual cuts of the same topology, we also found that there are spurious poles in both, real and virtual parts, which cancel only in the sum.

The main virtue of the "imaginary part method" is given by the fact that the discontinuity corresponding to the real-cut diagram already contains both, transverse and axial ghost contributions, such that for example the diagrams $(\mathrm{d})^{\mathrm{tr.}}_{\mathrm{real}}$ and $(\mathrm{d})^{\mathrm{gh.}}_{\mathrm{real}}$ can be done in one step. Nevertheless, it is quite interesting to have separate results for transverse and ghost parts. We will explain in Section 3.6 how we managed to obtain separate results for ghost– and non-ghost parts even when applying the imaginary part method.

The key features of the imaginary part method can be studied considering the colour structure $C_F T_f$ to which at $x < 1$ only topology (g) in Fig. 3.6 contributes. The calculation is rather trivial since the inner loop contains no gluons and thus no ML or PV prescription is needed for this subpart. Therefore we will consider the colour structure $C_F T_f$ very explicitly, as a pedagogical example, in Section 3.5.1. In addition, we will calculate the full contribution at $x = 1$ for the $C_F T_f$ part, which requires the calculation of the two-loop quark selfenergy contribution shown in Fig. 3.13. As in all previous calculations the contributions at $x = 1$ have never been explicitly

calculated, but instead have been deduced from fermion number conservation, our calculation constitutes not only a test of the ML prescription in a wider range, but even a more fundamental test of the CFP method itself, since only after inclusion of the $x = 1$ contributions the crucial issue of the finiteness of the 2PI kernels in the light-cone gauge will be fully checked. This finiteness even at $x = 1$ actually has been checked [66] for all colour structures treated in Sections 3.4 and 3.5, but we will show it explicitly only for the $C_F T_f$ part, where we have also calculated the finite contributions at $x = 1$.

After having set up the imaginary part method in the $C_F T_f$ colour structure as a pedagogical example, we will apply it to the $C_F N_c$ part in Section 3.5.2. This completes the calculation of the *non-singlet* splitting functions in next-to-leading order. Then we will have tested all possible one-loop structures of QCD except the non-Abelian three-gluon vertex. In order to include also this last and most involved structure, we will present the calculation of the N_c^2 part of the gluon-gluon splitting function $P_{g/g}^{(1)}$ in Section 3.5.3. This accomplishes the task to show that all NLO splitting functions can be obtained within the CFP scheme by applying the ML prescription, which is the only formally solid method in this context. The remaining contributions, that is, the functions $P_{q/g}^{(1)}$ and $P_{g/q}^{(1)}$ as well as the remaining parts of $P_{g/g}^{(1)}$, do not contain any new feature compared to the most complicated cases we studied.

We used the $\epsilon-$regularization method in all calculations presented in Section 3.5 for two reasons: First because the integrals of the $C_F N_c$ and N_c^2 parts are quite involved, thus being almost impossible to do if two different regulators, ϵ and δ, are present. Second, it seemed appealing to us to show that no additional regulator to the dimensional ϵ is really needed when using the ML prescription.

3.5.1 Colour structure $C_F T_f$ and endpoint contributions

Quark vacuum polarization contribution

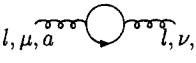

Figure 3.11: $\Pi_{\mu\nu}^{ab}(l)$

The expression for the fermion loop shown in Fig. 3.11 is given by

$$\begin{aligned}\Pi_{\mu\nu}^{ab}(l) &= -g^2 T_f \delta^{ab} \int \frac{d^m q}{(2\pi)^m} \frac{Tr[\gamma_\mu \not{q} \gamma_\nu (\not{l} + \not{q})]}{[q^2 + i\eta]\,[(q+l)^2 + i\eta]} \\ &= -\frac{4g^2}{(2\pi)^m} T_f \delta^{ab} \left\{ l_\mu J_{2\nu}^F(l) + l_\nu J_{2\mu}^F(l) + 2 J_{2\mu\nu}^F(l) + g_{\mu\nu} \frac{l^2}{2} J_2^F(l) \right\} \quad (3.117)\end{aligned}$$

where a statistical factor 1/2, a factor minus one for the fermion loop and a factor two for antifermions has been included.

Inserting the expression for $\Pi^{ab}_{\mu\nu}(l)$ into the full diagram (topology (g) in Fig. 3.6) leads to

$$\begin{aligned} T_{\text{floop}} &= -g^2 T^a T^b \frac{1}{|k^2|^2} \frac{1}{(l^2+i\eta)^2} Tr[\frac{\not n}{4kn} \not k \gamma_\alpha \not p \gamma_\beta \not k] \, d^{\alpha\mu}(l) \, \Pi^{ab}_{\mu\nu}(l) \, d^{\nu\beta}(l) \\ &= \frac{g^2}{(2\pi)^m} C_F T_f \, |k^2|^{-1} \, Q^l_\epsilon T_0 \left\{ \frac{F_k(x,\epsilon)}{|k^2|} + \frac{F_l(x,\epsilon,ln)}{l^2+i\eta} \right\} \end{aligned} \tag{3.118}$$

$$\begin{aligned} Q^l_\epsilon &= i\pi^{\frac{m}{2}} \Gamma(1+\epsilon)(-l^2)^{-\epsilon} \\ T_0 &= \frac{1}{\epsilon} + 2 + \epsilon(4 - \frac{\pi^2}{6}) \\ F_k(x,\epsilon) &= \frac{8}{3} - \frac{32}{9}\epsilon + \frac{8}{27}\epsilon^2 \\ F_l(x,\epsilon,ln) &= \frac{A_l(x,\epsilon)}{[ln]} + B_l(x,\epsilon) \\ A_l(x,\epsilon) &= (1+x)[-\frac{8}{3} + \frac{8}{9}\epsilon + \frac{16}{27}\epsilon^2] \\ B_l(x,\epsilon) &= -\frac{8}{3}\epsilon + \frac{8}{9}\epsilon^2 + \frac{1}{x}[-\frac{8}{3} + \frac{32}{9}\epsilon - \frac{8}{27}\epsilon^2] \end{aligned}$$

where the symbol $1/[ln]$ means that this factor has to be regularized, in our example here according to the ML prescription, defined by

$$\frac{1}{[ln]} \to \frac{1}{ln + i\eta \, \text{sign}(ln^*)} \tag{3.119}$$

The tensor integrals appearing in $\Pi^{ab}_{\mu\nu}(l)$ have been reduced to scalar integrals by Passarino-Veltman reduction [63].
The contribution to the splitting function is given by the pole part of the integral

$$\begin{aligned} I_{fl} &= x \cdot \int \frac{d^m k}{(2\pi)^m} \delta(x - \frac{kn}{pn}) \int d^m l \, \delta(p-k-l) \, \theta(l^0) \cdot T_{\text{floop}} \\ &= \frac{1}{32\pi^3} \frac{(4\pi)^\epsilon}{\Gamma(1-\epsilon)} \int d|k^2| \, dk_\perp^2 (k_\perp^2)^{-\epsilon} \int d^m l \, \delta(p-k-l) \, \theta(l^0) \cdot T_{\text{floop}} \end{aligned}$$

Inserting the expression (3.118) for T_{floop} leads to

$$\begin{aligned} I_{fl} &= i \, C_F T_f (\frac{\alpha_s}{2\pi})^2 \frac{1}{8\pi} (4\pi)^{2\epsilon} \frac{\Gamma(1+\epsilon)}{\Gamma(1-\epsilon)} T_0 \int \frac{d|k^2|}{|k^2|} \, dk_\perp^2 (k_\perp^2)^{-\epsilon} \\ &\int d^m l \, \delta(p-k-l) \, \theta(l^0) (-l^2)^{-\epsilon} \Big\{ |k^2|^{-1} F_k(x,\epsilon) \end{aligned}$$

$$
\begin{aligned}
&+\frac{1}{l^2+i\eta}\left[\frac{A_l(x,\epsilon)}{ln+i\eta\,\mathrm{sign}(ln^*)}+B_l(x,\epsilon)\right]\Big\} \\
&= i\,C_F T_f(\frac{\alpha_s}{2\pi})^2\frac{1}{8\pi}(4\pi)^{2\epsilon}\frac{\Gamma(1+\epsilon)}{\Gamma(1-\epsilon)}\,T_0\int\frac{d|k^2|}{|k^2|}\,dk_\perp^2(k_\perp^2)^{-\epsilon} \\
&\int d^m l\,\delta(p-k-l)\,\theta(l^0)(-l^2)^{-\epsilon}\Big\{|k^2|^{-1}F_k(x,\epsilon) \\
&+\{PV(\frac{1}{l^2})-i\pi\delta(l^2)\}\left[A_l(x,\epsilon)\{PV(\frac{1}{ln})-i\pi\,\mathrm{sign}(ln^*)\,\delta(ln)\}+B_l(x,\epsilon)\right]\Big\}
\end{aligned}
\tag{3.120}
$$

Now we keep only the terms proportional to $i\pi$ and write for simplicity $PV(1/z) = 1/z$. Note that the term $(-l^2)^{-\epsilon}$ gives an imaginary part only for $l^2 > 0$, stemming from the expansion

$$
\lim_{\eta\downarrow 0}(-l^2-i\eta)^{-\epsilon} = (l^2)^{-\epsilon}\{1-\frac{\epsilon^2}{2}\pi^2+i\epsilon\pi(1-\epsilon^2\frac{\pi^2}{6})+\mathcal{O}(\epsilon^4)\}\,. \tag{3.121}
$$

So the discontinuity of I_{fl} is given by [5]

$$
\begin{aligned}
\mathrm{Disc}\,I_{fl} &= C_F T_f(\frac{\alpha_s}{2\pi})^2\frac{1}{4}(4\pi)^{2\epsilon}\frac{\Gamma(1+\epsilon)}{\Gamma(1-\epsilon)}\,T_0\int\frac{d|k^2|}{|k^2|}\,dk_\perp^2(k_\perp^2)^{-\epsilon}\int d^m l\,\delta(p-k-l)\,\theta(l^0) \\
&\Big\{-\epsilon\,(l^2)^{-\epsilon}(1-\epsilon^2\frac{\pi^2}{6})\left(|k^2|^{-1}F_k(x,\epsilon)+\frac{1}{l^2}\left[\frac{A_l(x,\epsilon)}{ln}+B_l(x,\epsilon)\right]\theta(l^2)\right) \\
&+(-l^2)^{-\epsilon}\mathrm{sign}(ln^*)\,\delta(ln)(l^2)^{-1}\cdot A_l(x,\epsilon) \\
&+(-l^2)^{-\epsilon}\delta(l^2)\left(\frac{A_l(x,\epsilon)}{ln}+B_l(x,\epsilon)\right)\Big\} \\
&=: C_F T_f(\frac{\alpha_s}{2\pi})^2\frac{1}{4}(4\pi)^{2\epsilon}\frac{\Gamma(1+\epsilon)}{\Gamma(1-\epsilon)}\int\frac{d|k^2|}{|k^2|}\left\{I^{(r)}+I^{(vgh)}+I^{(v)}\right\}
\end{aligned}
\tag{3.122}
$$

The integrals $I^{(r)}$, $I^{(vgh)}$ and $I^{(v)}$ correspond to the diagrams shown in Fig. 3.12. Note that for the virtual loops, the counterterms also have to be included. After UV renormalization, $I^{(v)}$ will be zero since it is proportional to $(-l^2)^{-\epsilon}$ with $l^2 = 0$ and $\epsilon < 0$.

Now the contributions from the integrals defined in (3.122) will be calculated explicitly, starting with $I^{(r)}$.

[5] Note that I_{fl}/i has to be multiplied by $2i$ to obtain the discontinuity, according to the relations

$$
\mathrm{Disc}\,I(q^2) = \lim_{\eta\downarrow 0}\{I(q^2+i\eta)-I(q^2-i\eta)\} = 2i\lim_{\eta\downarrow 0}\Im m\,I(q^2+i\eta)
$$

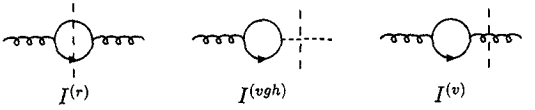

Figure 3.12: Diagrams corresponding to the different imaginary parts

Note that $I^{(r)}$ has only an imaginary part for

$$l^2 = \frac{1}{x}(|k^2|\tilde{x} - k_\perp^2) > 0$$

Therefore, when substituting

$$k_\perp^2 = |k^2|\tilde{x}\cdot\kappa \quad ; \quad (\tilde{x} = 1-x)$$

we know that $\kappa_{\max} = 1$. Thus we have

$$\begin{aligned} I^{(r)} &= -\epsilon(1-\epsilon^2\frac{\pi^2}{6})\,T_0\,|k^2|^{-2\epsilon}x^\epsilon\tilde{x}^{-2\epsilon}\int_0^1 d\kappa\,\kappa^{-\epsilon}(1-\kappa)^{-\epsilon}\Big\{\tilde{x}F_k(x,\epsilon) \\ &\quad +x\,(1-\kappa)^{-1}\,[\frac{A_l(x,\epsilon)}{\tilde{x}} + B_l(x,\epsilon)]\Big\} \\ &= -\epsilon(1-\epsilon^2\frac{\pi^2}{6})\,T_0\,|k^2|^{-2\epsilon}x^\epsilon\Big\{\tilde{x}^{1-2\epsilon}\mathrm{Beta}(1-\epsilon,1-\epsilon)\,F_k \\ &\quad +x\cdot\mathrm{Beta}(-\epsilon,1-\epsilon)\,\Big[A_l\{-\frac{1}{2\epsilon}\delta(1-x)+\frac{1}{(1-x)_+}-2\epsilon\left(\frac{\ln\tilde{x}}{\tilde{x}}\right)_+\}+\tilde{x}^{-2\epsilon}\,B_l\Big]\Big\} \end{aligned}$$

where we used the expansion

$$\begin{aligned} (1-z)^{-1-\epsilon} &= -\frac{1}{\epsilon}\delta(1-z)+\frac{1}{(1-z)_+}-\epsilon\left(\frac{\ln(1-z)}{(1-z)}\right)_+ + \mathcal{O}(\epsilon^2) \\ \text{and}\ \ \mathrm{Beta}(a,b) &= \frac{\Gamma(a)\Gamma(b)}{\Gamma(a+b)}. \end{aligned}$$

Inserting now the functions $F_k(\epsilon), A_l(x,\epsilon)$ and $B_l(x,\epsilon)$ leads to

$$\begin{aligned} I^{(r)} &= 4|k^2|^{-2\epsilon}\Big\{p_{qq}^+(x)[-\frac{1}{\epsilon}\frac{2}{3}-\frac{10}{9}]-\frac{2}{3}p_{qq}(x)\ln x+\frac{4}{3}(1+x^2)\left(\frac{\ln(1-x)}{1-x}\right)_+ \\ &\quad +\delta(1-x)\left[\frac{1}{\epsilon^2}\frac{2}{3}+\frac{1}{\epsilon}\frac{10}{9}+\frac{56}{27}-\frac{\pi^2}{3}\right]\Big\} \qquad (3.123) \\ p_{qq}^+(x) &= \frac{1+x^2}{(1-x)_+} \quad ; \quad p_{qq}(x) = \frac{1+x^2}{1-x} \end{aligned}$$

The virtual diagram where the cut line is a ghost is given by

$$\begin{aligned} I^{(vgh)} &= T_0 \int dk_\perp^2 (k_\perp^2)^{-\epsilon} \int d^m l\, \delta(p-k-l)\, \theta(l^0)(-l^2)^{-\epsilon}\, \delta(ln)(l^2)^{-1} A_l(x,\epsilon) \\ &= -T_0 \int dk_\perp^2 (k_\perp^2)^{-\epsilon} \int dl^+ dl^- d\vec{l}_\perp \delta(1-x-l^+)\delta(k^- + l^-)\delta(\vec{k}_\perp + \vec{l}_\perp)\delta(l^+) \\ &\quad \cdot\theta(l^+ + l^-)\,(-2l^+l^- + l_\perp^2)^{-1-\epsilon} \cdot A_l(x,\epsilon) \qquad (3.124) \\ &= -T_0 \delta(1-x) \int dk_\perp^2 (k_\perp^2)^{-1-2\epsilon} \theta(|k^2| - k_\perp^2) \cdot A_l(1,\epsilon) \end{aligned}$$

Note that we used $\mathrm{sign}(ln^*) = +1$, which follows from $ln^* \sim l^-$ and the constraints $\delta(l^+)\theta(l^+ + l^-)$ in (3.124).

Now we substitute

$$k_\perp^2 = |k^2| \cdot y$$

From the θ–function we know that $y_{\max} = 1$. Then

$$\begin{aligned} I^{(vgh)} &= -T_0 \delta(1-x) |k^2|^{-2\epsilon} \int_0^1 dy\, y^{-1-2\epsilon} A_l(1,\epsilon) \\ &= \delta(1-x)\, 4|k^2|^{-2\epsilon} \Big[-\frac{1}{\epsilon^2}\frac{2}{3} - \frac{1}{\epsilon}\frac{10}{9} - \frac{56}{27} + \frac{\pi^2}{9} \Big] \qquad (3.125) \end{aligned}$$

The counterterm for $I^{(vgh)}$ is obtained by replacing T_0 by $1/\epsilon_{\mathrm{uv}}$ and $(-l^2)^{-\epsilon}$ by one. Furthermore, the $\mathcal{O}(\epsilon)$ terms stemming from the virtual integrals have to be dropped, whereas those stemming from the trace have to be kept. This can be achieved in the present case by the substitution $F_k(\epsilon), A_l(x,\epsilon), B_l(x,\epsilon) \to F_k(0), A_l(x,0), B_l(x,0)$ and multiplication with the factor

$$\begin{aligned} P_\epsilon &=: \hat{P}^+_{q/q}(x,\epsilon)/p^+_{qq}(x) \\ \hat{P}^+_{q/q}(x,\epsilon) &= p^+_{qq}(x) - \epsilon \cdot (1-x) \end{aligned} \qquad (3.126)$$

Note that this difference of $\mathcal{O}(\epsilon)$ is vanishing when multiplied with $\delta(1-x)$, but it will be important for the non-ghost virtual integral $I^{(v)}$.
So the counterterm $I^{(vgh)}_{\mathrm{counter}}$ is given by

$$\begin{aligned} I^{(vgh)}_{\mathrm{counter}} &= -\delta(1-x)|k^2|^{-\epsilon} \frac{1}{\epsilon_{\mathrm{uv}}} \int_0^1 dy\, y^{-1-\epsilon} A_l(1,0) \\ &= \delta(1-x)\, 4|k^2|^{-\epsilon} \frac{1}{\epsilon^2} \cdot \left(-\frac{4}{3}\right) \qquad (3.127) \end{aligned}$$

where we have set $\epsilon_{\mathrm{uv}} = \epsilon$ in the last step.

The integral $I^{(v)}$ is given by

$$I^{(v)} = T_0 \int dk_\perp^2 (k_\perp^2)^{-\epsilon} \int d^m l\, \delta(p-k-l)\, \theta(l^0)(-l^2)^{-\epsilon}\, \delta(l^2) \left(\frac{A_l(x,\epsilon)}{1-x} + B_l(x,\epsilon) \right) \tag{3.128}$$

which is zero for $l^2 = 0, \epsilon < 0$, such that the only contribution comes from the counterterm of the virtual non-ghost diagram. Doing the steps explained above to obtain the counterterm leads to

$$\begin{aligned} I^{(v)}_{\text{counter}} &= \frac{1}{\epsilon_{\text{uv}}} \int dk_\perp^2 (k_\perp^2)^{-\epsilon} \delta(\frac{1}{x}(|k^2|\tilde{x} - k_\perp^2))\, P_\epsilon \left(\frac{A_l(x,0)}{1-x} + B_l(x,0) \right) \\ &= \frac{1}{\epsilon_{\text{uv}}} |k^2|^{-\epsilon} P_\epsilon\, x \left(A_l(x,0) \{ -\frac{1}{\epsilon}\delta(1-x) + \frac{1}{(1-x)_+} - \epsilon \left(\frac{\ln \tilde{x}}{\tilde{x}} \right)_+ \} + \tilde{x}^{-\epsilon} B_l(x,0) \right) \\ &= 4|k^2|^{-\epsilon} \Big\{ -\frac{1}{\epsilon}\frac{2}{3} p_{qq}^+(x) + \frac{2}{3}(1+x^2) \left(\frac{\ln \tilde{x}}{\tilde{x}} \right)_+ + \frac{2}{3}(1-x) \\ &\quad + \delta(1-x) \frac{1}{\epsilon^2} \frac{4}{3} \Big\} \end{aligned} \tag{3.129}$$

Inserting now the results for the different integrals into Eq. (3.122), we obtain

$$\begin{aligned} \text{Disc}\, I_{fl} &= C_F T_f (\frac{\alpha_s}{2\pi})^2 (4\pi)^{2\epsilon} \frac{\Gamma(1+\epsilon)}{\Gamma(1-\epsilon)} \int d|k^2| |k^2|^{-1-\epsilon} \\ &\quad \cdot \Big\{ |k^2|^{-\epsilon} \Big(p_{qq}^+(x) [-\frac{1}{\epsilon}\frac{2}{3} - \frac{10}{9}] - \frac{2}{3} p_{qq}(x) \ln x \\ &\quad + \frac{4}{3}(1+x^2) \left(\frac{\ln \tilde{x}}{\tilde{x}} \right)_+ - \delta(1-x) \frac{2\pi^2}{9} \Big) \\ &\quad - \left(-\frac{1}{\epsilon_{\text{uv}}} \frac{2}{3} p_{qq}^+(x) + \frac{2}{3}(1+x^2) \left(\frac{\ln \tilde{x}}{\tilde{x}} \right)_+ + \frac{2}{3}(1-x) \right) \Big\} \end{aligned} \tag{3.130}$$

The contribution to $\Gamma^{(1)}_{q/q,C_F T_f}(x,\epsilon)$ is given by the coefficient of the single pole of the $|k^2|$−integral:

$$\begin{aligned} \Gamma^{(1)}_{q/q,C_F T_f}(x,\epsilon) &= -\frac{1}{2\epsilon} C_F T_f (\frac{\alpha_s}{2\pi})^2 \cdot P^{(1)}_{q/q,C_F T_f}(x) \\ P^{(1)}_{q/q,C_F T_f}(x) &= -\frac{10}{9} p_{qq}^+(x) - \frac{2}{3} p_{qq}(x) \ln x - \frac{4}{3}(1-x) - \delta(1-x) \frac{4}{3} \zeta(2) \\ \zeta(2) &= \frac{\pi^2}{6} \end{aligned} \tag{3.131}$$

Two-loop quark selfenergy contribution

In the PV calculations [29, 30, 45] of the two-loop splitting functions the contributions proportional to $\delta(1-x)$ were never directly calculated, but inferred from fermion

number conservation, expressed by the requirement

$$\int_0^1 dx \left(P_{q/q}^{V,(1)}(x) - P_{q/\bar{q}}^{V,(1)}(x) \right) = 0 \,. \tag{3.132}$$

In general, we proceed in the same way, but in the case of the $C_F T_f$ part, the calculation we have performed with the ML prescription allows us to go beyond this pragmatic approach, since we have always picked up the finite amounts $\sim \delta(1-x)$ contributed by the 2PI kernels in the preceding calculation. If we now perform the calculation of the graph shown in Fig. 3.13 which is the only graph contributing to the $C_F T_f$ part of $\xi_q^{(1)}$ (see Eq. (3.38)), we have all terms $\sim \delta(1-x)$ in the $C_F T_f$ part of the flavour non-singlet splitting function and can check for this colour structure whether indeed (3.132) is correctly reproduced.

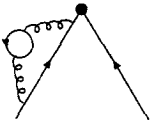

Figure 3.13: Two-loop quark selfenergy contribution $\sim C_F T_f$ at $x = 1$

Let us first establish what we have to obtain for the $C_F T_f$ part of $\xi_q^{(1)}$. The coefficient of $\delta(1-x)$ in the NLO splitting function, which we will denote by C_δ, was determined in [52, 45] via (3.132) to be

$$C_\delta = C_F^2 \left(\frac{3}{8} - 3\zeta(2) + 6\zeta(3) \right) + C_F T_f \left(-\frac{1}{6} - \frac{4}{3}\zeta(2) \right) + C_F N_C \left(\frac{17}{24} + \frac{11}{3}\zeta(2) - 3\zeta(3) \right) \tag{3.133}$$

Considering only the $C_F T_f$ part, we have from Eq. (3.131):

$$C_{\delta, C_F T_f} = \xi_{q, C_F T_f}^{(1)} + C_F T_f \left(-\frac{4}{3}\zeta(2) \right) \,. \tag{3.134}$$

Comparing Eqs. (3.133) and (3.134), we get the following prediction for the $C_F T_f$ part of $\xi_q^{(1)}$ in the light-cone gauge with ML prescription:

$$\xi_{q, C_F T_f}^{(1)} = -\frac{1}{6} C_F T_f \tag{3.135}$$

which is the result we have to obtain from the calculation of the diagram shown in Fig. 3.13.
The calculation is relatively easy since the inner quark loop has obviously no light-cone gauge propagator and can in fact be calculated exactly. Inserting the integrals

in Eq. (3.117) we obtain

$$\Pi^{ab}_{\mu\nu}(r) = -iT_f\delta^{ab}\frac{\alpha_s}{4\pi}(4\pi)^\epsilon 8\Gamma(\epsilon)\frac{\Gamma^2(2-\epsilon)}{\Gamma(4-2\epsilon)}\left(-r^2\right)^{-\epsilon}\left[r^2 g_{\mu\nu} - r_\mu r_\nu\right]. \tag{3.136}$$

This selfenergy can then be renormalized with the help of the counterterm in Fig. 3.9. The renormalized loop is then inserted into the outer loop. Here it is very convenient that $\Pi_{\mu\nu}$ is transverse, that is,

$$d^{\alpha\mu}(r)\left[r^2 g_{\mu\nu} - r_\mu r_\nu\right] d^{\nu\beta}(r) = -r^2\, d^{\alpha\beta}(r)\,. \tag{3.137}$$

In other words, the whole calculation is not very different from a simple one-loop calculation of the quark selfenergy, the only exception being that we now need loop integrals with the extra factor $(-r^2)^{-\epsilon}$ present in (3.136). The integrals we need if we embed the whole graph into the Dirac trace according to Fig. 3.13 are collected in Appendix A.4. Since we have renormalized the inner loop, the left-over divergence after loop integration determines the two-loop counterterm and thus the contribution to $\xi_q^{(1)}$. We find in the $\overline{\rm MS}$ scheme

$$Z_q^{C_F T_f} = 1 + \left(\frac{\alpha_s}{2\pi}\right)^2 C_F T_f \left(-\frac{1}{2\epsilon^2} + \frac{1}{12\epsilon}\right). \tag{3.138}$$

Comparing to Eq. (3.38) this implies that the $C_F T_f$ part of $\xi_q^{(1)}$ is exactly what we expected it to be in (3.135):

$$\xi^{(1)}_{q,C_F T_f} = -\frac{1}{6} C_F T_f\,. \tag{3.139}$$

This result clearly demonstrates the consistency of the whole approach: Our example shows that the light-cone gauge method of CFP is also able to determine the contributions
$\sim \delta(1-x)$ to the splitting functions by explicit calculation. It would be interesting in this context to calculate also the other contributions to $\xi_q^{(1)}$; Actually, the C_F^2 part of Eq. (3.133) could be confirmed already [66] by using the results obtained by [53, 54] for the two-loop quark selfenergy diagrams $\sim C_F^2$ with ML prescription.
It is important to note at this point that the ability to obtain the correct endpoint contributions is not restricted to the ML prescription; this is also possible for the PV prescription. With PV prescription, the coefficient of $\delta(1-x)$ in the $C_F T_f$ part of $P^{(1)}_{q/q}$ reads

$$C^{\rm PV}_{\delta,C_F T_f} = \xi^{(1),\rm PV}_{q,C_F T_f} - C_F T_f \frac{20}{9} I_0 \tag{3.140}$$

where $\xi^{(1),\rm PV}_{q,C_F T_f}$ denotes the $C_F T_f$ part of $\xi_q^{(1)}$ when the PV prescription is used. The explicit calculation gives

$$Z^{\rm PV}_{F,C_F T_f} = 1 + \left(\frac{\alpha_s}{2\pi}\right)^2 C_F T_f \left[-\frac{1}{2\epsilon^2}\left(1 - \frac{4}{3} I_0\right) + \frac{1}{\epsilon}\left(\frac{1}{12} + \frac{2}{3}\zeta(2) - \frac{10}{9} I_0\right)\right] \tag{3.141}$$

that is

$$\xi_{q,C_FT_f}^{(1),\mathrm{PV}} = C_F T_f \left(-\frac{1}{6} - \frac{4}{3}\zeta(2) + \frac{20}{9} I_0 \right) . \tag{3.142}$$

It is interesting to see how upon combining Eqs. (3.140) and (3.142) the I_0 terms drop out, and the $C_F T_f$ part of the endpoint contributions comes out correctly as in (3.133) also for the PV prescription. We note, however, that again this happens at the expense of having renormalization constants depending on singular quantities like I_0 that represent a mix-up in the treatment of UV and IR singularities.

3.5.2 Colour structure $C_F N_c$

Now we will turn to the $C_F N_c$ part which is the most complicated part of the non-singlet splitting functions. The contributing diagrams are shown in Fig. 3.14. Topologies (f) and (d) have been calculated by extracting the imaginary parts of the uncut diagram.

Virtual part

The virtual diagrams, which correspond (for $x < 1$) to the discontinuity $\sim i\pi\delta(l^2)$ of topologies (f) and (d), will first be given in a scheme independent form, that is, the final answer contains the integral form factors given in Appendix A, which can be inserted then according to the PV or the ML scheme.
An important qualitative difference between the PV and the ML scheme can be observed in this way: In the PV scheme, k^2 and l^2 are the only possible scales, whereas in the ML scheme, terms like $2ln^* ln/n^*n = l^2 + l_\perp^2$ are also present, which are non-vanishing even for $l^2 = 0$. Therefore, considering for instance diagram $(\mathrm{f})_{\mathrm{virt}}$, its scale dependence in the PV scheme is identical to the one in covariant gauges. Thus calculating the diagram with off-shell l^2, renormalizing it and then taking the limit $l^2 \to 0$, almost all contributions of the diagram will vanish since all loop integrals have to be proportional to $(-l^2)^{-\epsilon}$ ($\epsilon < 0$) on dimensional grounds. Only the contribution from the $\overline{\mathrm{MS}}$ counterterm remains because this is the only quantity not proportional to $(-l^2)^{-\epsilon}$. In contrast to this, in the ML scheme $l_\perp^2$ sets an extra mass scale. For graph $(\mathrm{f})_{\mathrm{virt}}$ one therefore encounters terms $\sim (-l^2)^{-\epsilon}$, but also terms of the form $\sim (l^2 + l_\perp^2)^{-\epsilon}$. Since $l_\perp^2 = k_\perp^2$, the latter terms yield non-vanishing contributions to the virtual part *even* at $l^2 = 0$.
Furthermore, if we included also the contributions at $x = 1$, we would obtain an additional contribution from an axial ghost momentum with kinematics $l^2 + l_\perp^2 = 0$ running into the loop, in the same way as has been explained for $I^{(vgh)}$ (see Fig. 3.12) in the previous section, and in contrast to the PV scheme, where this contribution is completely absent.

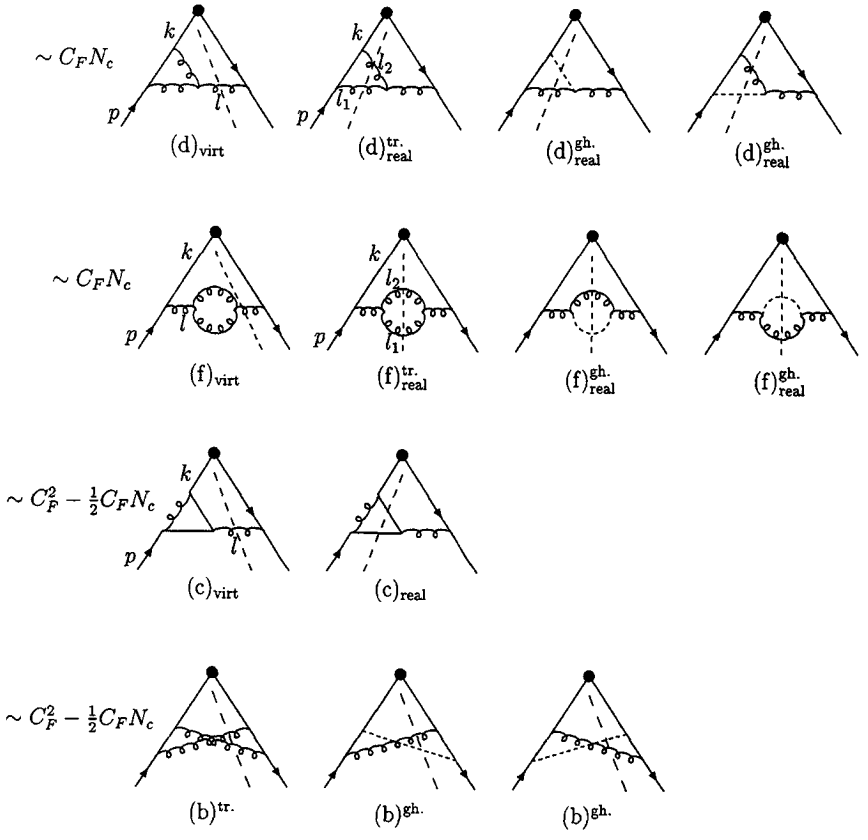

Figure 3.14: Diagrams contributing to the $C_F N_c$ part

Gluon selfenergy

The one-loop gluon selfenergy $\Pi^{ab}_{\mu\nu}(l)$ is given by

$$\begin{aligned}
\Pi^{ab}_{\mu\nu}(l) &= \frac{g^2}{2(2\pi)^m} N_c\,\delta^{ab}\Big\{ J_2^F(l)\,[8l^2\,g_{\mu\nu} - (m+6) l_\mu l_\nu] \\
&\quad + J^F_{2\mu\nu}(l)\,(4m-8) \\
&\quad + J_2^A(l)\cdot 8\,l^2\{\frac{l^2}{nl} n_\mu n_\nu + nl\,g_{\mu\nu} - (n_\mu l_\nu + n_\nu l_\mu)\} \\
&\quad + l^\lambda J^A_{2\lambda}(l)\,\{8\frac{l^2}{nl} n_\mu n_\nu - 4(n_\mu l_\nu + n_\nu l_\mu)\} \\
&\quad + 4\,nl\,\{l_\mu J^A_{2\nu}(l) + l_\nu J^A_{2\mu}(l)\} \\
&\quad - 4\,l^2\{n_\mu J^A_{2\nu}(l) + n_\nu J^A_{2\mu}(l)\}\Big\} \qquad (3.143)
\end{aligned}$$

The integrals are given in Appendix A. The UV divergent part of expression (3.143) with ML prescription already has been given in Section 3.3.2. With PV prescription one obtains

$$\begin{aligned}
\Pi^{ab,UV\,div}_{\mu\nu,PV}(l) &= \frac{i}{2\epsilon_{\rm uv}} \frac{\alpha_s}{2\pi} \delta^{ab} N_c \Big\{ \frac{11}{3}(l^2\,g_{\mu\nu} - l_\mu l_\nu) \\
&\quad + 4\,l^2\,(I_0 + \log(ln))\,[-g_{\mu\nu} + \frac{l_\mu n_\nu + l_\nu n_\mu}{ln} - \frac{l^2}{(ln)^2} n_\mu n_\nu] \\
&\quad + 4\,[l_\mu l_\nu - l^2(\frac{l_\mu n_\nu - l_\nu n_\mu}{ln} + \frac{l^2}{(ln)^2} n_\mu n_\nu)]\Big\} \qquad (3.144)
\end{aligned}$$

The UV counterterm is obtained by inserting $\Pi^{ab,UV\,div}_{\mu\nu}(l)$ into the full diagram, using $n^* = p$:

$$\begin{aligned}
T^{glu}_{\rm counter} &=: \frac{ig^2}{k^4} T^a T^b\, Tr\,[\frac{\not n}{4kn}\; \not k \gamma_\mu\; \not p \gamma_\nu\; \not k\,] \frac{d^{\mu\rho}(l)}{l^2}\, \Pi^{ab,UV\,div}_{\rho\lambda}(l)\, d^{\lambda\nu}(l) \\
&= (\frac{\alpha_s}{2\pi})^2\, C_F N_c\, |k^2|^{-1}\, \frac{16\pi^2}{x} \cdot G^{(f)_{\rm virt}}_{UV} \\
G^{(f)_{\rm virt},ML}_{UV} &= \frac{1}{\epsilon_{\rm uv}} \{ \frac{11}{6} \cdot P_{q/q}(x,\epsilon) - \frac{2\,x(1+x)}{1-x} \} \qquad (3.145) \\
G^{(f)_{\rm virt},PV}_{UV} &= \frac{1}{\epsilon_{\rm uv}} P_{q/q}(x,\epsilon) \{ \frac{11}{6} - 2I_0 - 2\ln(1-x) \} \qquad (3.146)
\end{aligned}$$

After having subtracted the UV counterterm $T^{glu}_{\rm counter}$, one can go to the infrared region where $l^2 = 0, \epsilon < 0$. As already explained, we see that in the PV scheme the whole infrared part is vanishing since it is proportional to $(-l^2)^{-\epsilon}$ and $\epsilon < 0$, $l^2 = 0$ in

the infrared region. With ML prescription, the axial part integrals contain a factor $(2ln^*\,ln/n^*n)^{-\epsilon} = (2l^+l^-)^{-\epsilon} = (l^2+l_\perp^2)^{-\epsilon}$ which will *not* vanish in the infrared region (for details see Appendix A.2). Therefore, there is a remaining nonzero contribution in the ML scheme, given by

$$\begin{aligned} T^{glu,ML} &= \frac{ig^2}{k^4} T^a T^b\, Tr\,[\frac{\not n}{4kn}\ \not k\gamma_\mu\ \not p\gamma_\nu\ \not k\,]\,\frac{d^{\mu\rho}(l)}{l^2}\,\Pi^{ab}_{\rho\lambda}(l)\,d^{\lambda\nu}(l) \\ &=: C_F N_c\,(\frac{\alpha_s}{2\pi})^2(4\pi)^\epsilon\Gamma(1+\epsilon)|k^2|^{-1-\epsilon}\,\frac{16\pi^2}{x}\cdot\tilde{T}^{glu,ML} \\ \tilde{T}^{glu,ML} &= -2\,P_{q/q}(x,\epsilon)\,C_0^{\rm ir} + 2\frac{x(1+x)}{1-x}\,C_1^{\rm ir} \end{aligned} \tag{3.147}$$

The phase space for the virtual diagrams is given by (see Appendix B.1 for details)

$$\begin{aligned} PS^{virt} &= 2\pi\, z\int\frac{d^m k}{(2\pi)^m}\,\delta(x-z)\,\delta((p-k)^2) \\ &= \frac{1}{16\pi^2}\,\frac{(4\pi)^\epsilon}{\Gamma(1-\epsilon)}\int_0^{Q^2} d|k^2|\,|k^2|^{-\epsilon}\,x\,(1-x)^{-\epsilon} \end{aligned} \tag{3.148}$$

such that the contribution from the gluon selfenergy diagram $(f)_{\rm virt}$ to $\hat{\Gamma}^{(1)}_{q/q}(x,\epsilon)$ is given by

$$\begin{aligned} \hat{\Gamma}^{(1,f_{\rm v})}_{q/q}(x,\epsilon) &= PP\Big\{\frac{1}{16\pi^2}\,\frac{(4\pi)^\epsilon}{\Gamma(1-\epsilon)}\int_0^{Q^2} d|k^2|\,|k^2|^{-\epsilon}\,x\,(1-x)^{-\epsilon}\cdot \\ &\quad [T^{glu}(x,k^2,\epsilon) - T^{glu}_{\rm counter}(x,k^2,\epsilon)]\Big\} \\ &= PP\Big\{C_F N_c\,(\frac{\alpha_s}{2\pi})^2\frac{\Gamma(1+\epsilon)}{\Gamma(1-\epsilon)}\,(4\pi)^{2\epsilon}\int_0^{Q^2} d|k^2|\,|k^2|^{-1-\epsilon}(1-x)^{-\epsilon}\cdot \\ &\quad [|k^2|^{-\epsilon}\tilde{T}^{glu}(x,\epsilon) - G^{(f)_{\rm virt}}_{UV}(x,\epsilon)]\Big\} \end{aligned} \tag{3.149}$$

where in the PV scheme $\tilde{T}^{glu}(x,\epsilon)\equiv 0$ according to the discussion above.

Vertex, non-Abelian part

The vertex insertion in topology $(\mathrm{d})_{\rm virt}$ is given by

$$\begin{aligned} \Gamma^a_\mu &= g^3 T^a\frac{N_c}{2}\int\frac{d^m q}{(2\pi)^m}\,\frac{\gamma_\rho\,\not q\,\gamma_\sigma}{q^2(k+q)^2(p+q)^2}\,d^{\nu\rho}(k+q)\,d^{\lambda\sigma}(p+q) \\ &\quad\cdot V_{3g}(\mu,-l;\nu,-(k+q);\lambda,p+q) \end{aligned}$$

Using the results of Section 3.3.2, the UV counterterms are of the form

$$T^{(\mathrm{d})_{\rm v}}_{\rm counter} = -T^a\,\frac{ig}{|k^2|^2}\,Tr\,[\frac{\not n}{4kn}\ \not k\,\Gamma^{a,UV\,div}_{\mu,C_A}\ \not p\gamma_\nu\ \not k\,]\,d^{\mu\nu}(p-k)$$

$$= (\frac{\alpha_s}{2\pi})^2 C_F N_c |k^2|^{-1} \frac{16\pi^2}{x} \cdot V_{UV}^{(d)_v}$$

$$V_{UV}^{(d)_v,ML} = \frac{1}{\epsilon_{uv}} \Big\{ -\frac{1}{4} P_{q/q}(x,\epsilon) + \frac{1}{2} \frac{x(1+x)}{1-x} \Big\} \tag{3.150}$$

$$V_{UV}^{(d)_v,PV} = \frac{1}{\epsilon_{uv}} \frac{1}{2} P_{q/q}(x,\epsilon) \Big\{ -\frac{3}{2} + 4I_0 + 2\ln(1-x) + \ln x \Big\} \tag{3.151}$$

Note that the term proportional to $n_\mu ln^*/[ln]$ in (3.102) does not contribute to $T_{\text{counter}}^{(d)_v,ML}$ because of $n_\mu d^{\mu\nu}(l) = 0$.

The expression for the vertex in the infrared region is obtained by inserting Γ_μ^a into the full diagram (topology $(d)_{\text{virt}}$), using $n^* = p$ and $l^2 = 0$:

$$\begin{aligned} T^{(d)_v} &= -T^a \frac{ig}{|k^2|^2} Tr\,[\frac{\not{n}}{4kn}\, \not{k} \Gamma_\mu^a\, \not{p} \gamma_\nu\, \not{k}\,]\, d^{\mu\nu}(p-k) \\ &=: C_F N_c (\frac{\alpha_s}{2\pi})^2 (4\pi)^\epsilon \Gamma(1+\epsilon) |k^2|^{-1-\epsilon} \frac{16\pi^2}{x} \cdot \tilde{T}^{(d)_v} \end{aligned}$$

$$\begin{aligned} \tilde{T}^{(d)_v} &= T_0 \frac{-1-x-3x^2-2x\epsilon\,(2-x)}{4(1-x)} \\ &\quad -\frac{1}{4} P_{q/q}(x,\epsilon) \cdot \{U_0 - 3\,C_0^{\text{ir}} - 3\,P_0 - D_0^{\text{ir}} + R_0\} \\ &\quad -C_1^{\text{ir}} \frac{x(1+x)}{1-x} \\ &\quad -\frac{1}{4} ((2-x)\,P_1 + P_2) \frac{1-\epsilon\,(1-x)}{1-x} \Big\} \end{aligned} \tag{3.152}$$

Note that $P_2, D_0^{\text{ir}}, C_0^{\text{ir}}$ and C_1^{ir} are zero in the PV scheme because P_2 is the coefficient of n^* and $D_0^{\text{ir}}, C_0^{\text{ir}}$ and C_1^{ir} are proportional to $(-p^2)^{-\epsilon}$ resp. $(-l^2)^{-\epsilon}$. For details see Appendix A.
Including a combinatorial factor of two for the vertex diagram yields the following contribution to $\hat{\Gamma}_{q/q}^{(1)}(x,\epsilon)$:

$$\begin{aligned} \hat{\Gamma}_{q/q}^{(1,d_v)}(x,\epsilon) &= PP\Big\{ \frac{1}{16\pi^2} \frac{(4\pi)^\epsilon}{\Gamma(1-\epsilon)} \int_0^{Q^2} d|k^2|\, |k^2|^{-\epsilon}\, x\,(1-x)^{-\epsilon} \cdot \\ &\quad 2\,[T^{(d)_v}(x,k^2,\epsilon) - T_{\text{counter}}^{(d)_v}(x,k^2,\epsilon)] \Big\} \\ &= PP\Big\{ C_F N_c (\frac{\alpha_s}{2\pi})^2 \frac{\Gamma(1+\epsilon)}{\Gamma(1-\epsilon)} (4\pi)^{2\epsilon} \int_0^{Q^2} d|k^2|\, |k^2|^{-1-\epsilon} (1-x)^{-\epsilon} \cdot \\ &\quad 2\,[|k^2|^{-\epsilon} \tilde{T}^{(d)_v}(x,\epsilon) - V_{UV}^{(d)_v}(x,\epsilon)] \Big\} \end{aligned} \tag{3.153}$$

Vertex, Abelian part

The vertex diagram $(c)_{virt}$ containing no three-gluon-vertex is proportional to $C_F^2 - \frac{1}{2}C_F N_c$, so it already has been treated in Section 3.4.
The results for the virtual diagrams are given in Table 3.5.

	$C_F N_c$					
	$(f)^{ML}_{virt}$	$(d)^{ML}_{virt}$	$(c)^{ML}_{virt}$	ML^{sum}_{virt}	PV^{sum}_{virt}	$(PV\text{-}ML)_{virt}$
$p_{qq}(x)\ln^2(1-x)$	-2	1/2	0	-3/2	-2	-1/2
$p_{qq}(x)\ln(1-x)$	11/3	-3/2	3/2	11/3	11/3	0
$p_{qq}(x)\ln x$	0	1/2	-1/2	0	0	0
$p_{qq}(x)\,Li_2(1-x)$	0	-2	1	-1	-2	-1
$p_{qq}(x)\,\pi^2/3$	3/2	3/4	-1	5/4	3/2	1/4
$p_{qq}(x)$	-4	1/2	7/2	0	0	0
$x\ln(1-x)$	2	0	0	2	2	0
$\ln(1-x)$	-2	1	-1	-2	-2	0
$x\ln x$	0	1/2	-1/2	0	0	0
$\ln x$	0	-1/2	1/2	0	0	0
x	-11/3	0	-1	-14/3	-14/3	0
1	23/3	-5/2	-3/2	11/3	11/3	0

Table 3.5: Contributions $\sim C_F N_c$ to $\hat{P}^{(1)}_{q/q}(x)$ from virtual diagrams.

Real part

The diagrams contributing to the real $C_F N_c$ part are given by topologies $(f)^{tr.}_{real}$, $(f)^{gh.}_{real}$, $(d)^{tr.}_{real}$, $(d)^{gh.}_{real}$ and $(b)^{tr.}_{real}$, $(b)^{gh.}_{real}$. Topology (b), being proportional to $C_F^2 - \frac{1}{2}C_F N_c$, already has been calculated in Section 3.4. Note that we used PVI regularization in Section 3.4 whereas here we use $\epsilon-$regularization, but the calculation of topology (b) with $\epsilon-$regularization via the two-body phase space given in Appendix B.2 has no new features such that we only will quote the result.
Diagrams $(f)_{real}$ and $(d)_{real}$ also have been tried to be calculated using the two-body phase space, but the phase space integrals for the ghost contributions became extremely complicated. For graph $(f)^{gh.}_{real}$ it was still possible to obtain the right result in this way, but for graphs $(d)^{gh.}_{real}$, this seemed a forbidding task. The main reason is the presence of the denominator $1/l^2$ which can go through zero and change sign: The

kinematics for a physical gluon imposes $l^2 > 0$, but the ghosts have the kinematics $l^2 = -l_\perp^2$, such that a singularity at $l^2 = 0$ appears *within* the range of the phase space integrals.
Of course, this singularity still is present when evaluating these graphs via the imaginary part of the full two-loop diagram. But in this case, it could be treated uniquely by using a principal value regulator[6] λ, leading to a perfectly well-defined, λ−independent result. This result includes both, transverse and ghost-like real contributions.
Nevertheless, it is possible to obtain separate expressions for those diagrams which have only transverse cut gluon lines (graphs $(\mathrm{f})^{\mathrm{tr.}}_{\mathrm{real}}$ and $(\mathrm{d})^{\mathrm{tr.}}_{\mathrm{real}}$) and those which have one transverse and one ghost line cut (graphs $(\mathrm{f})^{\mathrm{gh.}}_{\mathrm{real}}$ and $(\mathrm{d})^{\mathrm{gh.}}_{\mathrm{real}}$). How this can be achieved will be explained in Section 3.6.
Note that the ML results for the transverse real diagrams are not identical to the PV results with $\delta \neq 0$ if we use ϵ−regularization, they are only identical if we use PVI regularization. Nevertheless, in the final sum of all diagrams, real and virtual ones, we reproduce the PV result also with ϵ−regularization, thus showing that there is no need for an additional regulator when using the ML prescription.

The detailed results for the real diagrams are given in Table 3.6.

[6]To avoid confusion, we emphasize at this point that this principal value regulator has nothing to do with the principal value prescription for the light-cone gauge denominator.

	$C_F N_c$										
	$(b)^{trans.}$	$(b)^{ghost}$	$(c)_{real}$	$(d)^{trans.}_{real}$	$(d)^{ghost}_{real}$	$(f)^{trans.}_{real}$	$(f)^{ghost}_{real}$	sum of ghosts only	sum of all real ML	sum of all real PV	$(PV\text{-}ML)_{real}$
$p_{qq}(x)\ \ln^2(1-x)$	0	0	0	-1	1/2	4	-2	-3/2	3/2	2	1/2
$p_{qq}(x)\ \ln^2 x$	1/2	-1/2	1/2	-7/2	7/2	1	-1	2	1/2	1/2	0
$p_{qq}(x)\ \ln x \ln(1-x)$	0	0	0	4	-2	-4	2	0	0	0	0
$p_{qq}(x)\ \ln x$	2	-3/2	3/4	-19/4	11/2	23/6	-4	0	11/6	11/6	0
$p_{qq}(x)\ \ln(1-x)$	-4	2	0	8	-6	-23/3	4	0	-11/3	-11/3	0
$p_{qq}(x)\ Li_2(1-x)$	0	-1	1	-5	8	0	-2	5	1	2	1
$p_{qq}(x)\ \pi^2/3$	0	0	0	3	-13/4	-3	3/2	-7/4	-7/4	-2	-1/4
$p_{qq}(x)$	4	-4	0	-10	8	175/18	-4	0	67/18	67/18	0
$x \ln x$	-1	1/2	7/4	-7/4	3/2	2	-2	0	1	1	0
$\ln x$	-1	1/2	7/4	9/4	-9/2	-2	4	0	1	1	0
$x \ln(1-x)$	0	0	0	2	-2	-4	2	0	-2	-2	0
$\ln(1-x)$	0	0	0	-2	4	4	-4	0	2	2	0
x	2	-2	-7/2	-9/2	4	4	-2	0	-2	-2	0
1	-2	2	4	5	-4	-4	2	0	3	3	0

Table 3.6: Contributions $\sim C_F N_c$ to $\hat{P}^{(1)}_{q/q}(x)$ from real diagrams with ML prescription.

3.5.3 Colour structure N_c^2 of the gluon-gluon splitting function

Let us now turn to the calculation of $P_{g/g}^{(1)}$. We restrict ourselves to its N_c^2 part, since the contributions $\sim C_F T_f$, $N_c T_f$ are essentially trivial as far as the investigation of the ML prescription is concerned: The $C_F T_f$ part comprises no gluon emission at all, and all diagrams contributing to the $N_c T_f$ part contain a quark loop and the emission of at most *one* gluon. Such diagrams with one–gluon emission have the LO kinematics and will not reveal any new features as compared to what we have already discussed. In contrast to this, the N_c^2 part of $P_{g/g}^{(1)}$ requires the renormalization of the highly nontrivial three-gluon-vertex and therefore really provides a further challenge for the ML prescription.

The diagrams contributing to the N_c^2 part of $\hat{P}_{g/g}^{(1)}$ at NLO are shown in Fig. 3.15. We do not show here the axial ghosts explicitly, having kept in mind that each cut gluon line has a transverse and a ghost contribution.

The calculation of the various real and virtual diagrams proceeds in exactly the same way as before. For the renormalization of the triangle graph $(\mathrm{d})_{\mathrm{virt}}$ and the "swordfish" ones $(\mathrm{s}_1)_{\mathrm{virt}}$ and (s_2), we need the UV counterterm for the three-gluon-vertex in the light-cone gauge with ML prescription, which already has been discussed in Section 3.3.2.

Concerning the real cuts, we mention that graphs (h),(b),(j) and (k) are most conveniently calculated using the two-body phase space. For topologies (d),(f) and (s_1) which have two cuts, a real and a virtual one, it is much more convenient to calculate the real diagrams with the imaginary part method.

We have again verified that in the ML scheme all 2PI graphs give truly finite contributions to $\Gamma_{g/g}$ before the final integration over $|k^2|$ is performed. Tables 3.7 and 3.8 present the contributions of the various diagrams to $\hat{P}_{g/g}^{(1)}$, where we have defined

$$
\begin{aligned}
p_{gg}(x) &= \frac{(1-x+x^2)^2}{x(1-x)} \\
S_2(x) &= \int_{\frac{x}{1+x}}^{\frac{1}{1+x}} \frac{dz}{z} \ln\left(\frac{1-z}{z}\right) = -2\,Li_2(-x) - 2\ln x \ln(1+x) + \frac{1}{2}\ln^2 x - \frac{\pi^2}{6}\,.
\end{aligned}
$$

We mention in passing that topology (j) and the "swordfish" diagram (s_1) give vanishing contributions to $\hat{P}_{g/g}^{(1)}$ if the PV prescription is used, but are non-vanishing for the ML prescription, where finite contributions arise from their ghost parts.

It also has to be noted that no separate results for ghost– and transverse parts of topology (i) can be given when using $\epsilon-$regularization, since only the combination of both parts leads to a well-defined result.

As for the case of $\hat{P}_{q/q}^{(1)}$, the full result for the N_c^2 part of $\hat{P}_{g/g}^{(1)}$, given by the column "Sum" in Table 3.8, is in agreement with the PV result of [30], which in turn coincides

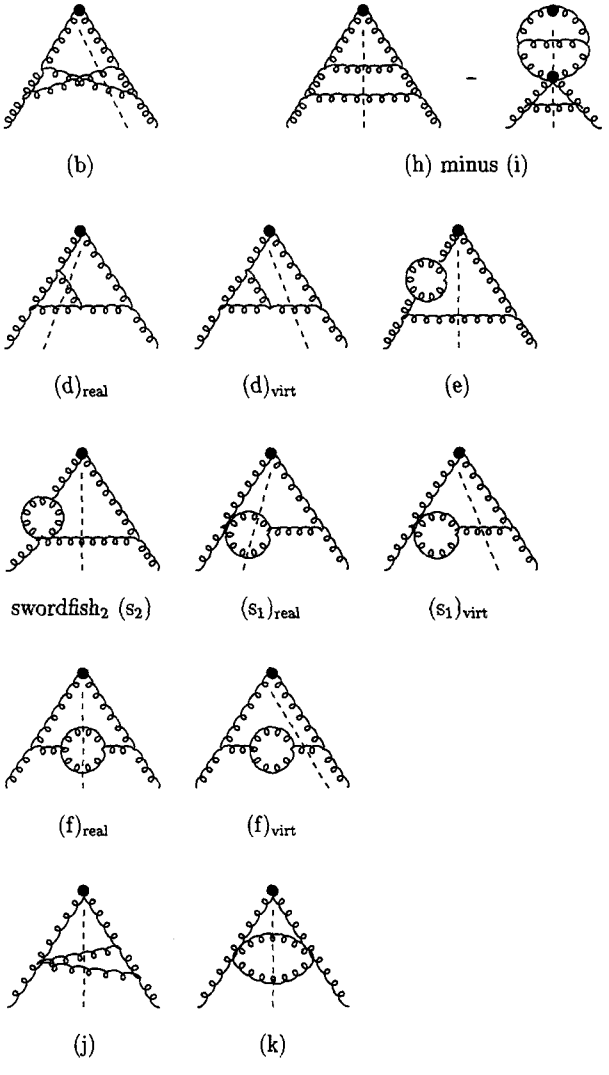

Figure 3.15: Diagrams contributing to the N_c^2 part of $\hat{P}_{g/g}^{(1)}$.

with the OPE one [33, 34]. Thus, the CFP method with ML prescription has also led to the correct final answer in this case, which clearly constitutes a further nontrivial and complementary check.

	N_c^2														
	top. (b)		top. (d)			swordfish$_1$			top. (f)			top. (j)		top. (k)	
	real		virt.	real		virt.	real		virt.	real		real		real	
	tr.	gh.		tr.	gh.		tr.	gh.		tr.	gh.	tr.	gh.	tr.	gh.
$p_{gg}(x)\ \ln^2(1-x)$	0	0	1	-2	1	0	0	0	-4	8	-4	0	0	0	0
$p_{gg}(x)\ \ln^2 x$	-1	1	0	-8	7	0	0	0	0	2	-2	0	0	0	0
$p_{gg}(x)\ \ln x \ln(1-x)$	0	0	8	-4	0	0	0	0	0	-8	4	0	0	0	0
$p_{gg}(x)\ Li_2(1-x)$	0	2	-6	-12	16	0	0	0	0	0	-4	0	0	0	0
$p_{gg}(x)\ \pi^2/3$	0	0	7/2	6	-13/2	0	0	0	3	-6	3	0	0	0	0
$p_{gg}(-x)\ S_2(x)$	2	0	0	0	0	0	0	0	0	0	0	0	0	0	0
$p_{gg}(x)$	-8	8	-62/9	-20	16	0	0	0	-8	175/9	-8	0	0	0	0
x^2	136/9	0	-3	22/3	0	9/2	0	0	-7	1/3	0	0	0	0	0
x	-105/8	0	8/3	-8	0	0	0	0	12	-5/12	0	0	0	-9/8	0
1	105/8	0	3/2	25/3	0	-9/2	0	0	-9	5/12	0	0	0	9/8	0
$1/x$	-136/9	0	0	-22/3	0	0	0	0	8	-1/3	0	0	0	0	0
$p_{gg}(x)\ \ln x$	-4	5/2	5/2	-35/3	11	0	0	0	0	23/3	-8	0	3/2	0	0
$x^2 \ln x$	-11/3	-3/2	5	-11/3	1/2	0	0	3/2	0	0	-3	0	3/2	0	0
$x\ \ln x$	-17/2	1/2	-7	-23/6	-13/2	0	0	0	0	0	6	0	0	0	0
$\ln x$	-17/2	0	13/2	-23/6	6	0	0	-3/2	0	0	-5	0	3/2	0	0
$\ln x/x$	-11/3	-1/2	-5/2	-11/3	-5	0	0	0	0	0	4	0	-3/2	0	0
$p_{gg}(x)\ \ln(1-x)$	8	-4	-22/3	16	-12	0	0	0	22/3	-46/3	8	0	0	0	0
$x^2 \ln(1-x)$	0	0	-5/2	0	-3/2	0	0	-3/2	0	0	3	0	0	0	0
$x\ \ln(1-x)$	0	0	7	0	6	0	0	0	0	0	-6	0	0	0	0
$\ln(1-x)$	0	0	-6	0	-13/2	0	0	3/2	0	0	5	0	0	0	0
$\ln(1-x)/x$	0	0	4	0	4	0	0	0	0	0	-4	0	0	0	0

Table 3.7: Detailed results for real and virtual cuts as well as ghosts (except for the (h-i)–case) of those topologies which have two cuts and/or ghost contributions.

	N_c^2									
	(b)	(d)	(s_2)	(s_1)	(e)	(f)	(h-i)	(j)	(k)	Sum
$p_{gg}(x)\ \ln^2 x$	0	-1	0	0	0	0	2	0	0	1
$x\ \ln^2 x$	0	0	0	0	0	0	4	0	0	4
$\ln^2 x$	0	0	0	0	0	0	4	0	0	4
$p_{gg}(x)\ \ln x \ln(1-x)$	0	4	0	0	0	-4	-4	0	0	-4
$p_{gg}(x)\ Li_2(1-x)$	2	-2	0	0	8	-4	-4	0	0	0
$p_{gg}(x)\ \pi^2/3$	0	3	0	0	-4	0	0	0	0	-1
$p_{gg}(-x)\ S_2(x)$	2	0	0	0	0	0	0	0	0	2
$p_{gg}(x)$	0	-98/9	0	0	134/9	31/9	0	0	0	67/9
x^2	136/9	13/3	9/2	9/2	1	-20/3	-46/3	0	0	67/9
x	-105/8	-16/3	-9	0	-6	139/12	19/2	0	-9/8	-27/2
1	105/8	59/6	0	-9/2	12	-103/12	-19/2	0	9/8	27/2
$1/x$	-136/9	-22/3	0	0	-8	23/3	46/3	0	0	-67/9
$p_{gg}(x)\ \ln x$	-3/2	11/6	-3/2	0	-1	-1/3	1	3/2	0	0
$x^2 \ln x$	-31/6	11/6	-3	3/2	-2	-3	-19/3	3/2	0	-44/3
$x\ \ln x$	-8	-52/3	3	0	4	6	16	0	0	11/3
$\ln x$	-17/2	26/3	-3/2	-3/2	-5	-5	3	3/2	0	-25/3
$\ln x/x$	-25/6	-67/6	3/2	0	1	4	31/3	-3/2	0	0
$p_{gg}(x)\ \ln(1-x)$	4	-10/3	0	0	22/3	0	-8	0	0	0
$x^2 \ln(1-x)$	0	-4	3/2	-3/2	1	3	0	0	0	0
$x\ \ln(1-x)$	0	13	-3	0	-4	-6	0	0	0	0
$\ln(1-x)$	0	-25/2	0	3/2	6	5	0	0	0	0
$\ln(1-x)/x$	0	8	0	0	-4	-4	0	0	0	0

Table 3.8: Contributions $\sim N_c^2$ to $\hat{P}^{(1)}_{g/g}(x)$ with ML prescription. Different cuts of the same topology are summed.

3.6 Relations between PV and ML schemes

We have shown in the previous sections that the application of the ML prescription to calculate the next-to-leading order splitting functions within the CFP scheme [28, 29] is a *consistent method*, since the ML prescription has a solid field-theoretical foundation and there is no need to recur to "phenomenological rules" to obtain the correct result. On the other hand, the complexity of the calculation with ML prescription exceeds the one with PV prescription considerably. Therefore it seems to be appealing to use the insights gained from doing the calculation with both prescriptions in order to find out the deeper reason why the "phenomenological rules" used in the PV case worked so well. An important step towards answering this question is given by our observation that certain subparts of the structures appearing in the ML calculation can be mapped to the structures present in the PV calculation. This can be done in the virtual as well as in the real diagrams contributing to the NLO splitting functions. The key observation is based on the expressions (3.56) and (3.57) obtained for the virtual integrals with ML respectively PV prescription. From Eq. (3.56), we see that any one-loop integral calculated with ML prescription appears as the difference of two terms, one being proportional to

$$\frac{[M_n]^{\frac{m}{2}-n}}{R^+ + i\eta \,\mathrm{sign}\, R^-} \,,$$

the second proportional to

$$\frac{[M_n - 2R^+R^-]^{\frac{m}{2}-n}}{R^+ + i\eta \,\mathrm{sign}\, R^-} \,,$$

which we will call part I and part II respectively. Furthermore, we observe that part I with $\eta \to 0$ is *identical* to the PV result (3.57) with $\delta \to 0$. In general, we can say that part I of any ML integral with $\epsilon-$regularization is the same as the PV integral with $\delta = 0$, and part I of any ML integral with PVI regularization is the same as the PV result for this integral with $\delta \neq 0$. This observation also has been checked by explicit calculation for all virtual integrals.

Using this result as a starting point, it is not difficult to realize why in the PV scheme we have to subtract ultraviolet poles which contain spurious singularities, whereas in the ML scheme we don't: In the ML scheme, it is the second term proportional to $[M_n - 2R^+R^-]^{\frac{m}{2}-n}$ which always provides this subtraction automatically. To be more explicit, consider again expressions (3.56) and (3.57). We know that the limit $R^+ \to 0$ corresponds to the spurious pole. From Eq. (3.56), we see that no ML integral can ever have a spurious pole as a residue of an UV pole, since the limit $R^+ \to 0$ is finite in (3.56) even for $\eta = 0$ as long as $[M_n]^{\frac{m}{2}-n}$ is nonvanishing, but $[M_n]^{\frac{m}{2}-n}$ is *always* nonvanishing in the *UV region.*[7]

[7] In the infrared region, where some of the momenta are on-shell, this term of course *can* vanish, which was one reason for the new features and technical difficulties encountered in the $C_F N_c$ part,

On the other hand, in the PV integral (Eq. (3.57)) we do not have a second term which regulates the first one in the limit $R^+ \to 0$. Therefore one had to introduce the δ to regulate the spurious pole, which will appear as a coefficient of the possible UV pole and thus – by lack of a "natural" subtraction term which contains exactly the same $1/R^+$ pole, as we have it in the ML case – one has to subtract this mixture of spurious pole and UV pole by hand when performing UV renormalization. This is the situation in the virtual part.

Concerning the real part, we already explained that a mapping of subparts can be achieved by exploiting Eqs. (3.48) and (3.49). The discontinuity given by Eq. (3.48) is the only one present in the PV scheme. If we now do the ML calculation with PVI regularization, we regulate the spurious poles in the real part exactly in the same way as in the PV scheme, such that the *transverse* real parts are *identical* in the ML and the PV case. Then the difference $(\text{ML-PV})_{\text{real}}$ is entirely given by the ghost contributions which are not present with PV prescription.

Therefore it suggests itself to investigate whether the two additional stuctures in the ML scheme – the second term $\sim [M_n - 2R^+R^-]^{\frac{m}{2}-n}$ in the virtual part and the additional "ghost" term $\sim \delta(2q^+q^-)$ of the discontinuity of the gluon propagator in the real part – are related. Indeed, the following relation could be shown by using the imaginary part method: With this method, the discontinuities of part I of any virtual integral appearing in a certain diagram correspond to the real diagram where only *transverse* gluon lines are cut, since those are the only ones present in the PV scheme. The discontinuities of part II then have to correspond to the real diagram where one of the cut lines is an axial ghost. As a corroboration of this result, it is instructive to consider topologies $(\text{c})_{\text{real}}$ and $(\text{g})_{\text{real}}$ (see Fig. 3.6): They cannot contain ghost lines since only fermion lines are cut. The one-loop integrals for the vertex and the fermion loop insertions with ML prescription of course are of the form part I minus part II as usual. But doing the second loop integration over $l^2 \sim (1-\kappa)$ (for details see Appendix C), the integral over part II in these diagrams has *no imaginary part*. Therefore the contribution from part II is zero, such that we get no real ghost diagrams for these topologies, as expected.

Thus the imaginary part method allows a rather clear insight into the relation of the ML to the PV scheme for those topologies which have two cuts, a real and a virtual one:

In the virtual–cut diagram with ML prescription, there is always the difference between two terms, part I minus part II, from the virtual ML integrals. Both parts separately contain spurious ultraviolet poles which exactly cancel in the difference. In the same virtual diagram with PV prescription, only part I is present. As a consequence, the spurious UV poles contained in part I have to be subtracted by hand.

In the real–cut diagram, we have the discontinuities of part I and of part II with ML prescription, which directly correspond to the transverse and the ghost contributions

but the occurrence of spurious *infrared* poles is unavoidable in the light-cone gauge and does not constitute a principal problem.

respectively. With PV prescription, we only have the discontinuity from part I since part II is absent in the virtual PV integrals, therefore we obtain no ghost contributions in the PV case.
Hence, if we assume that it was not by accident that the PV prescription together with the recipe of CFP for handling the spurious UV poles lead to the right result, we conclude that there must be a general argument why in the ML case the additional parts II in the virtual integrals and their discontinuities in the real parts (respectively the ghost contributions in topologies which have only a real cut), always nearly add up to zero – but not exactly: The remaining terms are just equal to the ones produced in the PV scheme by doing this special UV subtraction, such that we obtain the correct result in both, ML and PV schemes.
The following Tables as well as Tables 3.5 and 3.6 illustrate the above arguments and exhibit the cancellation mechanisms of the poles in the ML respectively PV scheme for the two most sophisticated colour structures $C_F N_c$ and N_c^2.

	$C_F N_c$										
	$(f)_{virt}$	$(f)^{tr.}_{real}$	$(f)^{gh.}_{real}$	$(f)_{sum}$	$(d)_{virt}$	$(d)^{tr.}_{real}$	$(d)^{gh.}_{real}$	$(c)_{virt}$	$(c)_{real}$	(c+d)	(f+c+d)
	Double poles										
$1/\epsilon^2\, p_{qq}(x)$	-1	2	-1	0	-1/2	-1	3/2	0	0	0	0
	Ultraviolet poles										
$1/\epsilon_{uv}\, p_{qq}(x)$	11/6			11/6	-1/2			1/2		0	11/6
$1/\epsilon_{uv}\, \frac{x(1+x)}{(1-x)}$	-2			-2	1			1		2	0
	Poles of final result after UV subtraction										
$1/\epsilon\, p_{qq}(x)$	-8/3	11/6	-1	-11/6	1	-3	5/2	-1/2	0	0	-11/6
$1/\epsilon\, \frac{x(1+x)}{(1-x)}$	2	0	0	2	-1	0	0	-1	0	-2	0
$1/\epsilon\, p_{qq}(x) \ln(1-x)$	2	-4	2	0	0	2	-2	0	0	0	0
$1/\epsilon\, p_{qq}(x) \ln x$	0	2	-2	0	0	-2	2	0	0	0	0
$1/\epsilon\, x/(1-x)$	-2	4	-2	0	-1	-2	3	0	0	0	0

Table 3.9: Double and single poles of $C_F N_c$ part with ML prescription.

	$C_F N_c$							
	$(f)^{PV}_{virt}$	$(f)^{PV}_{real}$	$(d)^{PV}_{virt}$	$(d)^{PV}_{real}$	$(c)^{PV}_{virt}$	$(c)^{PV}_{real}$	$(b)^{PV}$	Sum
	Double poles							
$1/\epsilon^2\, p_{qq}(x)$	0	0	-1	1	0	0	0	0
	Ultraviolet poles							
$\frac{p_{qq}(x)}{\epsilon_{uv}}\, I_0$	-2		4		-2			0
$\frac{p_{qq}(x)}{\epsilon_{uv}} \ln(1-x)$	-2		2		0			0
$\frac{p_{qq}(x)}{\epsilon_{uv}} \ln x$	0		1		-1			0
$\frac{p_{qq}(x)}{\epsilon_{uv}}$	11/6		-3/2		3/2			11/6
	Single poles of final result after UV subtraction							
$\frac{p_{qq}(x)}{\epsilon}\, I_0$	4	-2	-6	2	2	0	0	0
$\frac{p_{qq}(x)}{\epsilon} \ln(1-x)$	4	-2	-2	0	0	0	0	0
$\frac{p_{qq}(x)}{\epsilon} \ln x$	0	0	-1	0	1	0	0	0
$\frac{p_{qq}(x)}{\epsilon}$	-11/3	11/6	3/2	0	-3/2	0	0	-11/6
$\frac{1-x}{\epsilon}$	0	0	1	-1	0	0	0	0
	Spurious poles							
$p_{qq}(x)\, I_1$	0	2	-2	-2	2	0	0	0
$p_{qq}(x)\, I_0$	0	-2	0	4	0	0	-2	0
$p_{qq}(x)\, I_0 \ln(1-x)$	-4	2	6	-2	-2	0	0	0
$p_{qq}(x)\, I_0 \ln x$	0	-2	2	2	-2	0	0	0
$I_0\,(1-x)$	-4	2	6	-2	-2	0	0	0

Table 3.10: Spurious poles and poles in ϵ of $C_F N_c$ part with PV prescription.

	N_c^2													
	topology (b)		topology (d)			(e)	(s_2)	(s_1)			topology (f)			Sum
	real		virt.	real		virt.	virt.	virt.	real		virt.	real		
	tr.	gh.		tr.	gh.				tr.	gh.		tr.	gh.	
	Double poles													
$1/\epsilon^2\, p_{gg}(x)$	0	0	-1	-2	3	0	0	0	0	0	-2	4	-2	0
	Ultraviolet poles													
$1/\epsilon_{\rm uv}\, p_{gg}(x)$			-10/3			22/3	0	0			-1/3			11/3
$1/\epsilon_{\rm uv}\, x^2$			-1			1	3/2	3/2			-3			0
$1/\epsilon_{\rm uv}\, x$			1			-4	-3	0			-3			0
$1/\epsilon_{\rm uv}$			1/2			6	0	-3/2			-5			0
$1/\epsilon_{\rm uv}\, \frac{1}{x}$			0			-4	0	0			4			0
	Poles of final result after UV subtraction													
$1/\epsilon\, p_{gg}(x)$	-4	4	10/3	-8	8	-22/3	0	0	0	0	-10/3	23/3	-4	-11/3
$1/\epsilon\, x^2$	0	0	1	0	0	-1	-3/2	-3/2	0	0	3	0	0	0
$1/\epsilon\, x$	0	0	-1	0	0	4	3	0	0	0	3	0	0	0
$1/\epsilon$	0	0	-1/2	0	0	-6	0	3/2	0	0	5	0	0	0
$1/\epsilon\, \frac{1}{x}$	0	0	0	0	0	4	0	0	0	0	-4	0	0	0
$1/\epsilon\, p_{gg}(x) \ln(1-x)$	0	0	0	4	-4	0	0	0	0	0	4	-8	4	0
$1/\epsilon\, p_{gg}(x) \ln x$	0	0	0	-4	4	0	0	0	0	0	0	4	-4	0

Table 3.11: Double and single poles appearing in the calculation of $\hat{P}^{(1)}_{g/g}(x)$ with ML prescription.

	N_c^2						
	topology (b)	topology (d)		topology (e)	topology (f)		Sum
	real	virt.	real	virtual	virt.	real	
	Double poles						
$1/\epsilon^2\, p_{gg}(x)$	0	-2	2	0	0	0	0
	Ultraviolet poles						
$1/\epsilon_{\rm uv}\, p_{gg}(x)$		-11/3		11/3	11/3		11/3
$1/\epsilon_{\rm uv}\, p_{gg}(x) I_0$		6		-4	-4		-2
$1/\epsilon_{\rm uv}\, p_{gg}(x) \ln(1-x)$		2		0	-4		-2
$1/\epsilon_{\rm uv}\, p_{gg}(x) \ln x$		2		-4	0		-2
	$1/\epsilon$ poles of final result after UV subtraction						
$1/\epsilon\, p_{gg}(x)$	0	22/3	0	-22/3	-22/3	11/3	-11/3
$1/\epsilon\, p_{gg}(x) I_0$	0	-16	4	8	8	-4	0
$1/\epsilon\, p_{gg}(x) \ln(1-x)$	0	-4	0	0	8	-4	0
$1/\epsilon\, p_{gg}(x) \ln x$	0	-4	0	8	0	0	4
	Spurious poles						
$p_{gg}(x) I_0$	0	0	8	0	0	-4	0
$p_{gg}(x) I_1$	0	-8	-4	8	0	4	0
$p_{gg}(x) I_0 \ln(1-x)$	0	16	-4	-8	-8	4	0
$p_{gg}(x) I_0 \ln x$	0	8	4	-8	0	-4	0

Table 3.12: Double, single and spurious poles appearing in the calculation of $\hat{P}^{(1)}_{g/g}(x)$ with PV prescription.

	N_c^2			
	sum real ML	sum virtual ML	sum real PV	sum virtual PV
$p_{gg}(x)\ \ln^2(1-x)$	3	-3	4	-4
$p_{gg}(x)\ \ln^2 x$	1	0	1	0
$x\ \ln^2 x$	4	0	4	0
$\ln^2 x$	4	0	4	0
$p_{gg}(x)\ \ln x \ln(1-x)$	-4	0	0	-4
$p_{gg}(x)\ Li_2(1-x)$	-2	2	0	0
$p_{gg}(x)\ \pi^2/3$	1	-2	-4	3
$p_{gg}(-x)\ S_2(x)$	2	0	2	0
$p_{gg}(x)$	67/9	0	67/9	0
x^2	49/9	2	67/9	0
x	-67/6	-7/3	-79/6	-1/3
1	29/2	-1	27/2	0
$1/x$	-67/9	0	-67/9	0
$p_{gg}(x)\ \ln x$	0	0	0	0
$x^2 \ln x$	-44/3	0	-44/3	0
$x\ \ln x$	11/3	0	11/3	0
$\ln x$	-25/3	0	-25/3	0
$\ln x/x$	0	0	0	0
$p_{gg}(x)\ \ln(1-x)$	-22/3	22/3	-22/3	22/3
$x^2 \ln(1-x)$	0	0	0	0
$x\ \ln(1-x)$	0	0	0	0
$\ln(1-x)$	0	0	0	0
$\ln(1-x)/x$	0	0	0	0

Table 3.13: PV and ML results for $\hat{P}^{(1)}_{g/g}(x)$ compared in virtual and real parts

Chapter 4

Conclusions and outlook

We have performed the first calculation with the Mandelstam-Leibbrandt prescription [36, 37] of the flavour non-singlet splitting function and the N_c^2 part of the gluon-gluon splitting function in next-to-leading order within the light-cone gauge method of CFP [28, 29]. In all previous calculations [29, 30, 45], the PV prescription has been used to regulate the spurious poles generated by the gluon propagator in the light-cone gauge. Although the PV prescription has several features that could raise doubts on its reliability – like the breakdown of power counting or the dependence on longitudinal momenta of the renormalization constants – CFP obtained the right result by giving recipes how to handle the spurious poles and the UV subtraction mainly based on physical intuition, being aware of the fact that a formal justification of these "phenomenological rules" remains to be provided.

By doing the calculation with the ML prescription, which has a solid field theoretical foundation, we contributed to a progress in several respects:
First we could confirm the usefulness of the CFP method [28, 29] to calculate the splitting functions in next-to-leading order. We were able to show that neither the "phenomenological rules" to treat the UV poles nor additional regulators apart from dimensional regularization are needed when using the ML prescription.
Furthermore, we tested the ML prescription itself in a highly nontrivial application. We found that with ML prescription, the individual topologies contributing to the 2PI kernels which allow to extract the splitting functions are in general more regular than with PV prescription. This is mainly due to the presence of the so-called axial ghosts, which soften the spurious singular infrared behaviour of the discontinuities of the gluon propagator with ML prescription, and which do not exist in the PV case.

The NLO contributions at $x = 1$ never had been calculated before, they were deduced from the sum rules expressing fermion number conservation. Since we explicitly calculated the full $x = 1$ contribution, including the finite part, for the gauge invariant subpart proportional to $C_F T_f$, with ML as well as with PV prescription, we were able to check the consistency with the sum rules, thus corroborating the viability of the CFP method *and* of the ML prescription. We even could show the finiteness of the

2PI kernels at $x = 1$ for all colour structures considered [66].

One has to admit that the calculation with ML prescription, while being much more satisfactory than with PV prescription from a formal point of view, is technically by far more complicated. This is due to the fact that the ML prescription is a two-vector prescription – containing the vector n_μ^* in addition to the gauge vector n_μ, which entails the existence of additional structures – and due to the presence of the ghost contributions. Therefore we had to develop methods which had not been used before to be able to surmount these technical difficulties. These techniques could be very useful in view of an extension of the calculation to three loops.
As the three-loop result will be really required for the collider physics of the near future, we have to judge which methods are viable for this task. First of all it has to be emphasized that the application of two independent methods is almost mandatory in order to control such a complex calculation. The OPE method, after the recent development [33, 34], surely is conceptually solid. Its algebraic complexity is enormous, but a number of programs serving to develop a machinery which can treat the algebraic part systematically already exists [24, 35].
The CFP method with ML prescription has achieved a status of formal solidity comparable to the one of OPE due to the present work, but at the expense of a growth in technical complexity as compared to the PV case. Nevertheless, there is a considerable chance that this complexity still can be reduced. At the present status, it could not be exploited that the axial ghosts decouple from physical quantities since the anomalous dimensions are non-physical, the scheme dependence cancelling only in combination with the coefficient functions. But a first attempt to define *physical anomalous dimensions*, which are certain combinations of anomalous dimensions and coefficient functions, already exists in the literature [64]. Thus there is some prospective that a further development could reduce the complexity of the ML calculation by establishing a sort of "decoupling theorem" which assures that a major part of the ghost contributions does not have to be calculated since it will cancel to zero anyhow.

At present, the CFP method with PV prescription is the one with the least technical complexity, but its formal solidity is not satisfactory. The insights gained from the calculation with ML prescription however could serve to give a formal justification for the PV "recipes". It has been shown above that one can map subparts of the structures appearing with ML prescription to the ones present with PV prescription. If one could also show that the additional structures present only in the ML case always have to cancel, no matter in which order of the perturbative expansion we do the calculation, one could be sure that the PV prescription is safe. Of course, this again would mean nothing else than a confirmation of the reliability of the ML prescription together with a reduction of its complexity down to the PV level.

In any case, there is some room for further development, since it might be some as yet unexploited underlying structure that leads to such considerable cancellations when combining the various contributions to the final result. In this sense, the present

work can give some inspirations and guidelines concerning the development of methods to calculate higher order anomalous dimensions which are both, highly efficient and formally solid.

Appendix A

Virtual integrals

A.1 Definitions and sample calculation

We define general n-point integrals, containing no axial denominator $1/qn$, by

$$J_n^{F\mu_1\cdots\mu_s}(k_1\ldots k_{n-1}) = \int d^m q \frac{q^{\mu_1}\ldots q^{\mu_s}}{[q^2+i\epsilon]\,[(q+k_1)^2+i\epsilon]\ldots[(q+k_{n-1})^2+i\epsilon]}$$

and n-point integrals containing one axial denominator $1/qn$ by

$$\begin{aligned} J_n^{A\mu_1\cdots\mu_s}(k_1\ldots k_{n-1}) &= \int d^m q \frac{q^{\mu_1}\ldots q^{\mu_s}}{[q^2+i\epsilon]\,[(q+k_1)^2+i\epsilon]\ldots[(q+k_{n-1})^2+i\epsilon]\,qn} \\ I_n^{A\mu_1\cdots\mu_s}(k_1\ldots k_n) &= \int d^m q \frac{q^{\mu_1}\ldots q^{\mu_s}}{[(q+k_1)^2+i\epsilon]\ldots[(q+k_n)^2+i\epsilon]\,qn} \end{aligned}$$

The integrals $J_n^{F\mu_1\cdots\mu_s}(k_1\ldots k_{n-1})$ are called Feynman part integrals since they arise from the $g_{\mu\nu}$−part of the gluon propagator in axial gauge.

The $1/qn$ factor in the axial part integrals has to be regularized with ML or PV prescription. In order to exhibit the effect of the ML respectively PV prescription on the virtual loop integral over q, we will give the calculation of the axial part integral $J_n^{A\mu_1\cdots\mu_s}(k_1\ldots k_{n-1})$ with both prescriptions in detail here.

Calculation of virtual integrals with ML and PV prescription

In this section we give the detailed calculation of the axial integral $J_n^{A\mu_1\cdots\mu_s}(k_1\ldots k_{n-1})$ with both, PV and ML prescription. We evaluate the integrals in Minkowski space. They also have been evaluated via Wick rotation, but the difference between ML and PV prescription can be seen more directly if the calculation is done in the way given below.

The covariant denominator factors of $J_n^A(k_1 \dots k_{n-1})$ will be written in the exponential parametrization, exploiting the relation

$$\frac{1}{x+i\epsilon} = \frac{1}{i}\int_0^\infty da\, e^{ia(x+i\epsilon)}$$

This parametrization is leading to

$$\begin{aligned}
J_n^A(k_1 \dots k_{n-1}) &= \frac{1}{i^n}\int_0^\infty da_0 \dots da_{n-1} \int d^m q \frac{1}{qn} \exp\{-z\epsilon\} \exp\{zq^2 + 2Xq + \sum_{j=1}^{n-1} a_j k_j^2\} \\
&= \frac{1}{i^n}\int_0^\infty da_0 \dots da_{n-1} \exp\{-z\epsilon\} \exp\{i\sum_{j=1}^{n-1} a_j k_j^2\} \exp\{-iX^2/z\} \\
&\quad \cdot \int d^m q \frac{1}{qn} \exp\{iz(q+X/z)^2\} \\
X_\mu &= \sum_{j=1}^{n-1} a_j k_{j\mu} \quad ; \quad z = \sum_{j=0}^{n-1} a_j
\end{aligned}$$

Now substitute $q' = q + \frac{X}{z}$, then

$$\begin{aligned}
J_n^A(k_1 \dots k_{n-1}) &= \frac{1}{i^n}\int_0^\infty da_0 \dots da_{n-1} \exp\{-z\epsilon\} \exp\{i\sum_{j=1}^{n-1} a_j k_j^2\} \exp\{-iX^2/z\} \\
&\quad \cdot \int d^m q' \frac{1}{q'n - Xn/z} \exp\{izq'^2\} \\
&= \frac{1}{i^n}\int_0^\infty da_0 \dots da_{n-1} \exp\{-z\epsilon\} \exp\{i\sum_{j=1}^{n-1} a_j k_j^2\} \exp\{-iX^2/z\} \\
&\quad \cdot \int d^{m-2}\vec{q}_\perp \exp\{-iz q_\perp^2\} \int dq^+ dq^- \frac{1}{q^+ - X^+/z} \exp\{2izq^+q^-\}
\end{aligned} \tag{A.1}$$

The integral $J_{q^\pm}$ over q^+ and q^-

$$J_{q^\pm} = \int dq^+ dq^- \frac{1}{q^+ - X^+/z} \exp\{2izq^+q^-\} \tag{A.2}$$

now has to be regulated according to the ML or the PV prescription.

$$\textbf{ML:} \quad \frac{1}{q^+} \to \frac{1}{q^+ + i\eta\, \mathrm{sign}(q^-)} \tag{A.3}$$

$$\textbf{PV:} \quad \frac{1}{q^+} \to \frac{q^+}{(q^+)^2 + \delta^2 (p^+)^2} \tag{A.4}$$

The calculation of $J_{q^\pm}$ will be given below. The results are:

$$J_{q^\pm}^{ML} = -\pi \frac{1}{X^+ + i\eta\, z\, \mathrm{sign}(X^-)} \Big\{ 1 - \exp\{2iX^+X^-/z - 2\eta|X^-|\} \Big\} \quad \text{(A.5)}$$

$$J_{q^\pm}^{PV} = -\pi \frac{X^+}{(X^+)^2 + z^2\delta^2(p^+)^2} \quad \text{(A.6)}$$

Inserting the result for $J_{q^\pm}^{ML}$ into Eq. (A.1) and performing the Gaussian integration over $\vec{q}_\perp$

$$\int_{-\infty}^{\infty} d^{m-2}\vec{q}_\perp \exp\{-iz q_\perp^2\} = \left(\frac{\pi}{iz}\right)^{\frac{m-2}{2}}$$

one obtains

$$J_n^{A,\mathrm{ML}}(k_1 \ldots k_{n-1}) = \frac{-\pi^{\frac{m}{2}}}{i^{n+\frac{m}{2}-1}} \int_0^\infty da_0 \ldots da_{n-1} \exp\{i \sum_{j=1}^{n-1} a_j k_j^2 - z\epsilon\} \cdot z^{1-\frac{m}{2}}$$
$$\cdot \frac{\exp\{-i\, X^2/z\}}{X^+ + i\eta\, z\, \mathrm{sign}\, X^-} \Big\{ 1 - \exp\{2iX^+X^-/z - 2\eta|X^-|\} \Big\}$$

Rescaling $a_i = z \cdot b_i$ $(i = 0 \ldots n-1)$ and carrying out the $z-$integration results in

$$J_n^{A,\mathrm{ML}}(k_1 \ldots k_{n-1}) = i\pi^{\frac{m}{2}} \Gamma(n - \frac{m}{2})(-1)^{n+1} \int db_0 \ldots db_{n-1}\, \delta(1 - \sum_{j=0}^{n-1} b_j)$$
$$\cdot \frac{1}{R^+ + i\eta\, \mathrm{sign}\, R^-} \Big\{ [M_n]^{\frac{m}{2}-n} - [M_n - 2R^+R^-]^{\frac{m}{2}-n} \Big\} \quad \text{(A.7)}$$

$$R^\mu = \sum_{j=1}^{n-1} b_j\, k_j^\mu \quad ; \quad M_n = R^2 - \sum_{j=1}^{n-1} b_j\, k_j^2$$

whereas PV regularization leads to

$$J_n^{A,\mathrm{PV}}(k_1 \ldots k_{n-1}) = i\pi^{\frac{m}{2}} \Gamma(n - \frac{m}{2})(-1)^{n+1} \int db_0 \ldots db_{n-1}\, \delta(1 - \sum_{j=0}^{n-1} b_j)$$
$$\frac{R_+}{R_+^2 + \delta^2 p_+^2} \cdot [M_n]^{\frac{m}{2}-n} \quad \text{(A.8)}$$

Calculation of the integrals $J_{q^\pm}^{ML}$ and $J_{q^\pm}^{PV}$

With ML prescription

Applying the ML prescription to $J_{q^\pm}$ (see Eq. (A.2)) leads to

$$J_{q^\pm}^{ML} = \int dq^+ dq^- \frac{1}{q^+ - X^+/z + i\eta\, \mathrm{sign}(q^- - X^-/z)} \exp\{2izq^+q^-\} \quad \text{(A.9)}$$

Substituting $q' = q - \frac{X}{z}$ gives

$$\begin{aligned} J^{ML}_{q^\pm} &= \exp\{2iX^+X^-/z\} \int dq^+dq^- \frac{1}{q^+ + i\eta\,\mathrm{sign}(q^-)} \exp\{2i\,[zq^+q^- + X^+q^- + X^-q^+]\} \\ &= \exp\{2iX^+X^-/z\} \int dq^- \exp\{2iX^+q^-\} \cdot I_{q^+} \\ I_{q^+} &= \int dq^+ \frac{\exp\{2iq^+[zq^- + X^-]\}}{q^+ + i\eta\,\mathrm{sign}(q^-)} \end{aligned} \tag{A.10}$$

The integral I_{q^+} has a pole at $q^+ = -i\eta\,\mathrm{sign}(q^-)$ with residue $\exp\{2\eta\,\mathrm{sign}(q^-)[zq^- + X^-]\}$. Now two cases have to be considered:

1. $zq^- + X^- > 0$
   The contour has to be closed in the upper half plane; the pole is inside the contour for $q^- < 0$.

2. $zq^- + X^- < 0$
   The contour has to be closed in the lower half plane; the pole is inside the contour for $q^- > 0$. There will be a minus sign for the opposite orientation of the contour relative to case 1.

Using the Cauchy theorem yields

$$\begin{aligned} I_{q^+} &= 2\pi i \exp\{2\eta\,\mathrm{sign}(q^-)[zq^- + X^-]\}\{\theta(-q^-)\theta(zq^- + X^-) - \theta(q^-)\theta(-zq^- - X^-)\} \\ &\text{and so} \\ J^{ML}_{q^\pm} &= 2\pi i \exp\{2iX^+X^-/z\}\Big\{ \int_{-\infty}^{0} dq^- \exp\{2iX^+q^-\} \exp\{-2\eta\,[zq^- + X^-]\}\theta(zq^- + X^-) \\ &\quad - \int_0^\infty dq^- \exp\{2iX^+q^-\} \exp\{2\eta\,[zq^- + X^-]\}\theta(-zq^- - X^-)\Big\} \end{aligned}$$

Substituting $\tilde{q} = -q^-$ in the first part leads to

$$\begin{aligned} J^{ML}_{q^\pm} &= 2\pi i \exp\{2iX^+X^-/z\}\Big\{ \int_0^\infty d\tilde{q} \exp\{-2i\tilde{q}[X^+ + i\eta z]\} \exp\{-2\eta\,X^-\}\theta(-z\tilde{q} + X^-) \\ &\quad - \int_0^\infty dq^- \exp\{2iq^-[X^+ - i\eta z]\} \exp\{2\eta\,X^-\}\theta(-zq^- - X^-)\Big\} \\ &= 2\pi i \exp\{2iX^+X^-/z\}\Big\{\theta(X^-) \int_0^{X^-/z} dq \exp\{-2iq[X^+ + i\eta z]\} \exp\{-2\eta\,X^-\}\Big\} \\ &\quad -\theta(-X^-) \int_0^{-X^-/z} dq \exp\{2iq[X^+ - i\eta z]\} \exp\{2\eta\,X^-\}\Big\} \\ &= 2\pi i \exp\{2iX^+X^-/z\} \exp\{-2\eta\,|X^-|\}\Big\{\theta(X^-) \frac{-(\exp\{-2iX^-/z[X^+ + i\eta\,z]\} - 1)}{2i(X^+ + i\eta\,z)} \end{aligned}$$

$$
\begin{aligned}
& -\theta(-X^-)\frac{(\exp\{-2iX^-/z[X^+ - i\eta\, z]\} - 1)}{2i(X^+ - i\eta\, z)}\Big\} \\
= \; & -\pi \exp\{2iX^+X^-/z\} \\
& \exp\{-2\eta\,|X^-|\}\left(\exp\{-2iX^+X^-/z + 2\eta|X^-|\} - 1\right)\cdot\left\{\frac{\theta(X^-)}{X^+ + i\eta z} + \frac{\theta(-X^-)}{X^+ - i\eta z}\right\} \\
= \; & -\pi\left(1 - \exp\{2iX^+X^-/z - 2\eta\,|X^-|\}\right)\cdot\frac{1}{X^+ + i\eta\, z\,\mathrm{sign}(X^-)} \qquad \text{(A.11)}
\end{aligned}
$$

With PV prescription

Applying the PV prescription to $J_{q^\pm}$ leads to

$$
J^{PV}_{q^\pm} = \int dq^+dq^-\frac{q^+ - X^+/z}{(q^+ - X^+/z)^2 + \delta^2(p^+)^2}\exp\{2izq^+q^-\} \qquad \text{(A.12)}
$$

Now doing the q^+−integration, one has to evaluate

$$
\begin{aligned}
I_{q^+} &= \int dq^+\frac{q^+ - X^+/z}{(q^+ - X^+/z)^2 + \delta^2(p^+)^2}\exp\{2izq^+q^-\} \\
&= \frac{1}{2}\int dq^+\exp\{2izq^+q^-\}\left(\frac{1}{(q^+ - \frac{X^+}{z}) - i\delta p^+} + \frac{1}{(q^+ - \frac{X^+}{z}) + i\delta p^+}\right)
\end{aligned} \qquad \text{(A.13)}
$$

Two cases have to be distinguished:

1. $q^- > 0$
   The contour has to be closed in the upper half plane, so the pole at $q^+ = \frac{X^+}{z} + i\delta p^+$ contributes and the residue of the pole is $\exp\{2iq^-(X^+ + iz\delta p^+)\}$
2. $q^- < 0$
   The contour has to be closed in the lower half plane, so the pole at $q^+ = \frac{X^+}{z} - i\delta p^+$ contributes and the residue of the pole is $\exp\{2iq^-(X^+ - iz\delta p^+)\}$

Then the integral (A.13) can be written as

$$
\begin{aligned}
I_{q^+} &= \frac{1}{2}\int dq^+\exp\{2izq^+q^-\}\left(\frac{1}{(q^+ - \frac{X^+}{z}) - i\delta p^+} + \frac{1}{(q^+ - \frac{X^+}{z}) + i\delta p^+}\right) \\
&= i\pi\left\{\theta(q^-)\exp\{2iq^-(X^+ + iz\delta p^+)\} - \theta(-q^-)\exp\{2iq^-(X^+ - iz\delta p^+)\}\right\}
\end{aligned}
$$

Now the dq^- integration will be done to obtain the final expression for the integral $J^{PV}_{q^\pm}$:

$$
J^{PV}_{q^\pm} = \frac{1}{2}\int_{-\infty}^{\infty} dq^-dq^+\exp\{2izq^+q^-\}\left(\frac{1}{(q^+ - \frac{X^+}{z}) - i\delta p^+} + \frac{1}{(q^+ - \frac{X^+}{z}) + i\delta p^+}\right)
$$

$$= i\pi \int_0^\infty dq^- \exp\{2iq^-(X^+ + iz\delta p^+)\} - i\pi \int_{-\infty}^0 dq^- \exp\{2iq^-(X^+ - iz\delta p^+)\}$$

The substitution $\tilde{q} = -q^-$ in the second integral leads to

$$J_{q^\pm}^{PV} = i\pi \int_0^\infty dq^- \exp\{2iq^-(X^+ + iz\delta p^+)\} - i\pi \int_0^\infty d\tilde{q} \exp\{-2i\tilde{q}(X^+ - iz\delta p^+)\}$$

Renaming $\tilde{q}$ into q^- yields

$$\begin{aligned} J_{q^\pm}^{PV} &= i\pi \int_0^\infty dq^- \left\{\exp\{2iq^-(X^+ + iz\delta p^+)\} - \exp\{-2iq^-(X^+ - iz\delta p^+)\}\right\} \\ &= i\pi \int_0^\infty dq^- \exp\{-2q^- z\delta p^+\} \left\{\exp\{2iq^- X^+\} - \exp\{-2iq^- X^+\}\right\} \\ &= -2\pi \int_0^\infty dq^- \exp\{-2q^- z\delta p^+\} \sin(2q^- X^+) \end{aligned}$$

Now we use the formula (Gradshteyn/Ryzhik integral no. 3.893.1)

$$\int_0^\infty dy e^{-Ay} \sin By = \frac{B}{A^2 + B^2} \quad \text{for} \quad A > 0$$

The condition $A > 0$ is fulfilled because of $0 < q^- < \infty$; $z, \delta, p^+ > 0$. Hence we obtain

$$J_{q^\pm}^{PV} = \frac{-\pi X^+}{(X^+)^2 + z^2\delta^2 p^{+2}}.$$

A.2 Two-point integrals in the ultraviolet and infrared regions

In this subsection, we will show through the calculation of the integral $J_2^A(l)$, appearing for example in the gluon selfenergy, what happens in the ML scheme when doing the analytical continuation in ϵ from the UV to the IR region.

From the general integral (A.7), one obtains the following expression for $J_2^A(l)$ with ML prescription:

$$J_2^{A,ML}(l) = -i\pi^{\frac{m}{2}}\Gamma(\epsilon) \int_0^1 \frac{du}{ul^+ + i\eta} \left\{[-l^2 u(1-u)]^{-\epsilon} - [-l^2 u(1-u) - 2u^2 l^+ l^-]^{-\epsilon}\right\} \tag{A.14}$$

Note that $l^- = -k^-$; $k^- \leq 0$, such that $\text{sign}(l^-) = 1$.

We consider first the integral in the UV region where $\epsilon < 0, l^2 \neq 0$.
For $l^2 \neq 0$, the $u-$integral is finite and thus η can be dropped in $1/(ul^+ + i\eta)$, leading to

$$\begin{aligned} J_{2,\mathrm{uv}}^{A,ML}(l) &= -\frac{i\pi^{\frac{m}{2}}}{l^+}\Gamma(\epsilon)(-l^2)^{-\epsilon}\int_0^1 du\, u^{-1-\epsilon}\Big\{(1-u)^{-\epsilon} - [1-u(1-\chi_l)]^{-\epsilon}\Big\} \\ \chi_l &= \frac{2l^+l^-}{l^2} = \frac{2ln\, ln^*}{nn^*\, l^2} \end{aligned}$$

As long as we assume $l^2 \neq 0$, we can expand in ϵ and we obtain

$$\begin{aligned} J_{2,\mathrm{uv}}^{A,ML}(l) &= -\frac{i\pi^{\frac{m}{2}}}{l^+}(-l^2)^{-\epsilon}\,\epsilon\cdot\Gamma(\epsilon)\Big\{-\int_0^1 du\,\frac{\ln(1-u)}{u} + \int_0^1 du\,\frac{\ln[1-u(1-\chi_l)]}{u}\Big\} \\ &= -\frac{i\pi^{\frac{m}{2}}}{l^+}(-l^2)^{-\epsilon}\Gamma(1+\epsilon)\{Li_2(1) - Li_2(1-\chi_l)\} \end{aligned} \tag{A.15}$$

which is an UV finite expression.
For $l^2 = 0$, the integral (A.14) is only meaningful if $\epsilon < 0$. But since the integral is UV finite, expression (A.14) can be analytically continued to negative ϵ without doing any subtraction. For negative ϵ, l^2 can be set to zero in (A.14), leading to the following expression for $J_2^{A,ML}(l)$ in the infrared region:

$$J_{2,\mathrm{ir}}^{A,ML}(l) = i\pi^{\frac{m}{2}}\,\Gamma(\epsilon)\int_0^1 du\,\frac{1}{ul^+ + i\eta}\,[-2u^2\,l^+l^-]^{-\epsilon} \tag{A.16}$$

If $l^2 = (p-k)^2 = 0$ holds, one has the relation

$$2l^+l^- = -2l^+k^- = -2(1-x)p^+k^- = -(1-x)k^2 = (1-x)|k^2| \tag{A.17}$$

leading to

$$J_{2,\mathrm{ir}}^{A,ML}(l) = i\pi^{\frac{m}{2}}\,\Gamma(\epsilon)\,[-(1-x)|k^2|]^{-\epsilon}\int_0^1 du\,u^{-2\epsilon}\frac{1}{ul^+ + i\eta} \tag{A.18}$$

Note that there is an overall factor $(-1)^{-\epsilon}$ in (A.18) which will be of importance in connection with the imaginary part method explained in detail in Appendix C. Since in this Appendix we treat only those virtual integrals which appear together with the phase space constraint $\delta(l^2)$, we need only the real part of $(-1)^{-\epsilon}$ here:

$$(-1)^{-\epsilon} = 1 - \epsilon^2\frac{\pi^2}{2} + \mathcal{O}(\epsilon^4) + \Im m\,.$$

Now we have to choose whether we regulate the spurious infrared pole $u \to 0$ in (A.18) with the PVI– or with the $\epsilon-$regularization method.

$\epsilon-$regularization method

If we use the $\epsilon-$regularization method, we simply drop η in $1/(ul^+ + i\eta)$, using the dimensional ϵ to regulate also the spurious pole $u \to 0$. Then we obtain

$$J^{A,ML}_{2,\mathrm{ir}}(l) = i\pi^{\frac{m}{2}}\,\Gamma(\epsilon)\,[-(1-x)|k^2|]^{-\epsilon}\frac{1}{l^+}\left(-\frac{1}{2\epsilon}\right)\,. \tag{A.19}$$

Therefore, using the general definition

$$\begin{aligned} J^{A}_{2,\mathrm{ir}}(l) &= -\frac{Q^k_\epsilon}{l^+}\,C^{\mathrm{ir}}_0 \\ Q^k_\epsilon &= i\pi^{\frac{m}{2}}\Gamma(1+\epsilon)|k^2|^{-\epsilon} \end{aligned}$$

we obtain with ML prescription and $\epsilon-$regularization

$$C^{ML,\mathrm{ir}}_{0,\epsilon} = \frac{1}{2\epsilon^2} - \frac{1}{2\epsilon}\ln(1-x) + \frac{1}{4}\ln^2(1-x) - \frac{\pi^2}{4} \tag{A.20}$$

PVI regularization method

The PVI regularization method suggests to do the replacement

$$\frac{1}{ul^+ + i\eta} \to \frac{ul^+}{(ul^+)^2 + \delta^2} \tag{A.21}$$

This allows to distinguish the spurious poles from the "usual" ones, since the spurious poles will now appear in terms of I_0 and I_1 defined in Eqs. (3.61) and (3.62), while the usual soft and collinear poles will still appear as poles in ϵ. Hence doing the replacement (A.21), we obtain

$$C^{ML,\mathrm{ir}}_{0,\mathrm{PVI}} = -\frac{1}{\epsilon}[I_0 + \ln(1-x)] + 2I_1 - I_0\ln(1-x) \tag{A.22}$$

A.3 Results for virtual integrals in terms of form factors

In our calculation we need two-point integrals and three-point integrals, which, depending on their number of Lorentz indices, can be classified as scalar, vector or rank two tensor integrals. Higher rank tensor integrals have been reduced within the programs to the ones given below by using Passarino-Veltman reduction [63].
The ubiquitous factor Q^r_ϵ which can be extracted from each integral is defined as

$$Q^r_\epsilon = i\pi^{\frac{m}{2}}\Gamma(1+\epsilon)(-r^2)^{-\epsilon}\,.$$

A.3.1 Feynman part integrals

$$
\begin{aligned}
J_2^F(r) &= Q_\epsilon^r T_0 \quad ; \quad T_0 = \frac{1}{\epsilon_{\rm uv}} + 2 \\
J_2^{F\mu}(r) &= -Q_\epsilon^r T_1 r^\mu \quad ; \quad T_1 = \frac{1}{2} T_0 \\
J_2^{F\mu\nu}(r) &= Q_\epsilon^r \left(T_2 r_\mu r_\nu + T_3 r^2 g_{\mu\nu}\right) \\
T_2 &= \frac{1}{3\epsilon_{\rm uv}} + \frac{13}{18} \quad ; \quad T_3 = -\frac{1}{12\epsilon_{\rm uv}} - \frac{2}{9}
\end{aligned}
$$

$$
\begin{aligned}
J_3^F(k,p) &= -Q_\epsilon^k (-k^2)^{-1} R_0 \\
J_3^{F\mu}(k,p) &= Q_\epsilon^k (-k^2)^{-1} (R_1 p^\mu + R_2 k^\mu) \\
J_3^{F\mu\nu}(k,p) &= -Q_\epsilon^k (-k^2)^{-1} (R_3 p^\mu p^\nu + R_4 k^\mu k^\nu + R_5 \{kp\}^{\mu\nu} + k^2 R_6 g^{\mu\nu}) \\
\{kp\}^{\mu\nu} &= k^\mu p^\nu + k^\nu p^\mu \, .
\end{aligned}
$$

The following table gives the parameters R_i for the special kinematics $p^2 = 0$ and $(p-k)^2 = 0$ which is the kinematics for all one-loop insertions into the virtual diagrams if we do not consider the contributions at $x = 1$, which arise when the cut gluon line in the virtual diagrams has axial ghost kinematics. Those integrals which are needed to calculate real diagrams via the imaginary part of the full two-loop diagrams also require $(p-k)^2 \neq 0$; they will be treated separately in Appendix C.

R_0	R_1	R_2	R_3	R_4	R_5	R_6
$\frac{1}{\epsilon^2} - \frac{\pi^2}{6}$	$\frac{1}{\epsilon^2} + \frac{2}{\epsilon} + 4 - \frac{\pi^2}{6}$	$-\frac{1}{\epsilon} - 2$	$R_1 + \frac{1}{\epsilon} + 3$	$-\frac{1}{2\epsilon} - 1$	$-\frac{1}{2\epsilon} - \frac{3}{2}$	$\frac{1}{4\epsilon_{\rm uv}} + \frac{3}{4}$

A.3.2 Axial part integrals

The axial part two-point integrals $J_2^A(r)$ and $J_{2\mu}^A(r)$ will first be given in both schemes for an arbitrary off-shell external momentum r. Then we will list the result for all axial integrals needed in our calculation, using the special kinematics given there. As explained in Section A.2, we have to distinguish in the two-point integrals between on-shell and off-shell external momenta. For an arbitrary off-shell external momentum r, we have:

$$
\begin{aligned}
J_2^A(r) &= -\frac{Q_\epsilon^r}{rn} P_0(r) \\
J_{2\mu}^A(r) &= \frac{Q_\epsilon^r}{rn} \left\{P_1(r)\, r_\mu + P_2(r)\, n_\mu^* + P_3(r)\, n_\mu\right\} .
\end{aligned}
$$

The results for the form factors P_0, P_1, P_2 and P_3 depend on the regularization of the axial denominator $1/qn$.

Form factors for the ML scheme

If we use ML prescription we get

$$P_0^{ML}(r) = Li_2(1) - Li_2(1-\chi_r) \tag{A.23}$$

$$P_1^{ML}(r) = -\frac{\chi_r \ln \chi_r}{1-\chi_r} \tag{A.24}$$

$$P_2^{ML}(r) = \frac{rn}{nn^*}\left(\frac{1}{\epsilon_{uv}} + 2 + \frac{\chi_r \ln \chi_r}{1-\chi_r}\right) \tag{A.25}$$

$$P_3^{ML}(r) = \frac{rn^*}{nn^*}\left(-1 + \frac{\ln \chi_r}{1-\chi_r} + \frac{1}{\chi_r}[Li_2(1) - Li_2(1-\chi_r)]\right) \tag{A.26}$$

$$\chi_r = \frac{2\,rn\,rn^*}{nn^*\,r^2} \tag{A.27}$$

Form factors for the PV scheme

Using PV prescription we obtain

$$P_0^{PV}(r) = \frac{1}{\epsilon_{uv}}[I_0 + \ln(r^+)] - I_1 + I_0 \ln(r^+) + \frac{1}{2}\ln^2(r^+) + Li_2(1) \tag{A.28}$$

$$P_1^{PV}(r) = \frac{1}{\epsilon_{uv}} + 2 \tag{A.29}$$

$$P_2^{PV}(r) = 0 \tag{A.30}$$

$$P_3^{PV}(r) = \frac{r^2}{2\,rn}\left\{\frac{1}{\epsilon_{uv}}[I_0 + \ln(r^+) - 2] - I_1 + I_0 \ln(r^+) + \frac{1}{2}\ln^2(r^+) - 4 + Li_2(1)\right\} \tag{A.31}$$

We used the definitions (3.61) and (3.62) for I_0 and I_1 as well as $r^+ = rn/pn$. Note that n^* is not present in the PV case.

Two-point and three-point integrals for special momenta k and p

The special kinematics used in the calculation of the virtual diagrams for $x < 1$ *after* UV renormalization is given by

$$\begin{aligned} p &= n^* \;\; ; \;\; (n^*)^2 = 0 \\ l^2 = (p-k)^2 &= 0 \;\; \Rightarrow \;\; pk = \frac{k^2}{2} \;\; ; \;\; k_\perp^2 = -k^2(1-x) \;\; ; \;\; k^2 < 0 \\ k^+ &= x \;\; ; \;\; p^+ = 1 \\ \chi_k &= \frac{2\,kn\,kn^*}{nn^*\,k^2} = x \end{aligned} \tag{A.32}$$

Before having subtracted the UV poles, we obviously have to keep p^2 and l^2 off-shell.

Two-point integrals

The space-like momentum k^2 in our calculation is always different from zero, therefore we can read off the form factors for $J_2^A(k)$ and $J_{2\mu}^A(k)$ directly from relations (A.23) to (A.31). The integrals $J_2^A(p)$ and $J_{2\mu}^A(p)$ only contribute to the UV counterterm, so p^2 has to be off-shell in this case and $\chi_p = 2\,p^+p^-/p^2 = 1 \quad \text{for } p^2 \neq 0,\ \vec{p}_\perp = 0$. In the infrared region, where $\epsilon < 0$ and $p^2 = 0$, the integrals $J_2^A(p)$ and $J_{2\mu}^A(p)$ vanish due to the overall factor $(-p^2)^{-\epsilon}$.

The form of the integrals $J_2^{A,ML}(l)$ and $J_{2\mu}^{A,ML}(l)$ in the UV region ($l^2 \neq 0, \epsilon > 0$) is different from the one in the IR region where $l^2 = 0, \epsilon < 0$, as has been explained in Section A.2. Therefore we distinguish form factors $C_i^{\rm uv}$ and $C_i^{\rm ir}$ in this case. In addition, we have to decide how to regulate the spurious infrared poles present in $J_2^{A,ML}(l)$. PVI regularization leads to a result containing I_0 and I_1 whereas $\epsilon-$regularization leads to a $1/\epsilon^2$ pole in $J_2^{A,ML}(l)$. The form factors obtained with the two regularization methods of the spurious infrared poles are denoted by $C_{0,\rm PVI}^{ML,\rm ir}$ and $C_{0,\epsilon}^{ML,\rm ir}$ respectively.

Two-point integrals in parameter form:

$$
\begin{aligned}
J_2^A(k) &= -\frac{Q_\epsilon^k}{kn}\,P_0 \\
J_{2\mu}^A(k) &= \frac{Q_\epsilon^k}{kn}\,\{P_1\,k_\mu + P_2\,n_\mu^* + P_3\,n_\mu\} \\
J_2^A(p) &= -\frac{Q_\epsilon^p}{pn}\,B_0 \\
J_{2\mu}^A(p) &= \frac{Q_\epsilon^p}{pn}\,\{B_1\,p_\mu + B_2\,n_\mu^* + B_3\,n_\mu\} \\
J_2^A(l) &= -\frac{R_\epsilon}{ln}\,C_0 \\
J_{2\mu}^A(l) &= \frac{R_\epsilon}{ln}\,(C_1\,l_\mu + C_2\,n_\mu^* + C_3\,n_\mu) \\
I_2^A(k,p) &= -\frac{R_\epsilon}{pn}\,K_0 \\
I_2^A(-k,l) &= -\frac{R_\epsilon}{pn}\,D_0
\end{aligned}
\tag{A.33}
$$

Note that in the PV scheme, the parameters $C_i^{PV,\rm ir}$ $(i = 0,\ldots,3)$, $K_0^{PV,\rm ir}$ and $D_0^{PV,\rm ir}$ are not needed since they have an overall factor $(-l^2)^{-\epsilon}$ or $(-p^2)^{-\epsilon}$. In the ML scheme, the situation is different: Due to the presence of n^*, $(-l^2)^{-\epsilon}$ is not the only invariant scale, so the integral in the IR region can be nonvanishing, e.g. proportional to $(2ln\,ln^*/nn^*)^{-\epsilon} \sim [-(1-x)k^2]^{-\epsilon}$, as can be seen from the example in Section A.2. That is why we extract only the overall factor

$$R_\epsilon = i\pi^{\frac{m}{2}}\Gamma(1+\epsilon)$$

in integrals depending *on* l, whereas the factor $(-l^2)^{-\epsilon}$ or $(-k^2)^{-\epsilon}$ is shown in this case explicitly together with the corresponding form factor.

Form factors for two-point integrals in the ML scheme

$$
\begin{aligned}
P_0^{ML} &= Li_2(1) - Li_2(1-x) \\
P_1^{ML} &= -\frac{x \ln x}{1-x} \\
P_2^{ML} &= x \left\{ \frac{1}{\epsilon} + 2 + \frac{x \ln x}{1-x} \right\} \\
P_3^{ML} &= \frac{k^2}{2pn} \left\{ -1 + \frac{\ln x}{1-x} + \frac{1}{x} \left[Li_2(1) - Li_2(1-x) \right] \right\} \\
B_0^{ML} &= Li_2(1) \quad ; \quad B_1^{ML} = 1 \quad ; \quad B_2^{ML} = \frac{1}{\epsilon_{\rm uv}} + 1 \\
B_3^{ML} &= \frac{p^2}{2pn} \{ -2 + Li_2(1) \} \\
C_0^{ML,{\rm uv}} &= (-l^2)^{-\epsilon} \left(Li_2(1) - Li_2(1-\chi_l) \right) \quad ; \quad \chi_l = \frac{2lnln^*}{nn^* l^2} \\
C_1^{ML,{\rm uv}} &= (-l^2)^{-\epsilon} \left(-\frac{\chi_l \ln \chi_l}{1-\chi_l} \right) \\
C_2^{ML,{\rm uv}} &= (-l^2)^{-\epsilon} \frac{ln}{n^* n} \left(\frac{1}{\epsilon_{\rm uv}} + 2 + \frac{\chi_l \ln \chi_l}{1-\chi_l} \right) \\
C_3^{ML,{\rm uv}} &= (-l^2)^{-\epsilon} \frac{ln^*}{nn^*} \left(-1 + \frac{\ln \chi_l}{1-\chi_l} + \frac{\ln \chi_l \ln (1-\chi_l)}{\chi_l} + \frac{Li_2(\chi_l)}{\chi_l} \right) \\
D_0^{ML,{\rm uv}} &= \text{finite} \\
C_{0,{\rm PVI}}^{ML,{\rm ir}} &= (-k^2)^{-\epsilon} \left(-\frac{1}{\epsilon} \left[\ln (1-x) + I_0 \right] + 2I_1 - I_0 \ln (1-x) \right) \\
C_{0,\epsilon}^{ML,{\rm ir}} &= (-k^2)^{-\epsilon} \left(\frac{1}{2\epsilon^2} - \frac{1}{2\epsilon} \ln (1-x) + \frac{1}{4} \ln^2 (1-x) - \frac{\pi^2}{4} \right) \\
C_1^{ML,{\rm ir}} &= (-k^2)^{-\epsilon} \left(-\frac{1}{\epsilon} - 2 + \ln (1-x) \right) \\
C_2^{ML,{\rm ir}} &= (-k^2)^{-\epsilon} (1-x) \left(\frac{1}{\epsilon} + 2 - \ln (1-x) \right) \\
C_3^{ML,{\rm ir}} &= (-k^2)^{-\epsilon} \frac{1}{2} \frac{k^2}{pn}
\end{aligned}
$$

$$K_0^{ML,\mathrm{ir}} = (-k^2)^{-\epsilon}\frac{1}{1-x}\left(\frac{\ln x}{\epsilon} - Li_2(1-x) - \frac{1}{2}\ln^2 x\right)$$
$$D_0^{ML,\mathrm{ir}} = (-k^2)^{-\epsilon}\left(\frac{1}{\epsilon}[\ln x - \ln(1-x)] - \frac{1}{2}\ln^2 x + \frac{1}{2}\ln^2(1-x) - \frac{\pi^2}{2}\right)$$

Form factors for two-point integrals in the PV scheme

$$P_0^{PV} = \frac{[I_0 + \ln x]}{\epsilon} - I_1 + I_0 \ln x + \frac{1}{2}\ln^2 x + Li_2(1)$$
$$P_1^{PV} = \frac{1}{\epsilon} + 2$$
$$P_2^{PV} = 0$$
$$P_3^{PV} = \frac{k^2}{2kn}\left\{\frac{[I_0 + \ln x - 2]}{\epsilon} - I_1 + I_0 \ln x + \frac{1}{2}\ln^2 x - 4 + Li_2(1)\right\}$$
$$B_0^{PV} = \frac{I_0}{\epsilon_{\mathrm{uv}}} - I_1 + Li_2(1) \quad ; \quad B_1^{PV} = \frac{1}{\epsilon_{\mathrm{uv}}} + 2 \quad ; \quad B_2^{PV} = 0$$
$$B_3^{PV} = \frac{p^2}{2pn}\left\{\frac{[I_0 - 2]}{\epsilon_{\mathrm{uv}}} - I_1 - 4 + Li_2(1)\right\}$$
$$C_0^{PV,\mathrm{uv}} = (-l^2)^{-\epsilon}\left(\frac{[I_0 + \ln(1-x)]}{\epsilon_{\mathrm{uv}}} - I_1 + I_0 \ln(1-x) + \frac{1}{2}\ln^2(1-x) + Li_2(1)\right)$$
$$C_1^{PV,\mathrm{uv}} = (-l^2)^{-\epsilon}\left(\frac{1}{\epsilon_{\mathrm{uv}}} + 2\right)$$
$$C_2^{PV,\mathrm{uv}} = 0$$
$$C_3^{PV,\mathrm{uv}} = (-l^2)^{-\epsilon}\frac{l^2}{2ln}\left\{\frac{[I_0 + \ln(1-x) - 2]}{\epsilon_{\mathrm{uv}}} - I_1 + I_0 \ln(1-x) + \frac{1}{2}\ln^2(1-x) - 4 + Li_2(1)\right\}$$
$$D_0^{PV,\mathrm{uv}} = (-p^2)^{-\epsilon}\Big(\frac{1}{\epsilon_{\mathrm{uv}}}[\ln(1-x) - \ln x] + \frac{1}{2}\ln^2 x - \frac{1}{2}\ln^2(1-x) + Li_2(1) - 2Li_2(1-x) - \ln(1-x)\ln x\Big)$$

Three-point integrals

The three-point integrals needed for the virtual part are given by $J_3^A(p,k)$, $J_{3\mu}^A(p,k)$ and $J_3^A(-k,l)$. They are calculated only in the IR region since they are UV finite. The integral $J_3^A(-k,l)$, like $J_2^A(l)$, in the ML scheme contains spurious infrared poles which can be regulated either by PVI– or by $\epsilon-$regularization, therefore we distinguish between the form factors $U_{0,\mathrm{PVI}}^{ML}$ and $U_{0,\epsilon}^{ML}$.

$$
\begin{aligned}
J_3^A(p,k) &= \frac{Q_\epsilon^k}{pn}|k^2|^{-1}\,S_0 \\
J_{3\mu}^A(k,p) &= -\frac{Q_\epsilon^k}{pn}|k^2|^{-1}(S_1 p_\mu + S_2 k_\mu + S_3 n_\mu + S_4 n_\mu^*) \\
J_3^A(-k,l) &= \frac{Q_\epsilon^k}{ln}|k^2|^{-1}\,U_0
\end{aligned}
$$

Form factors in the ML scheme

$$
\begin{aligned}
S_0^{ML} &= \frac{1}{\epsilon^2}+\frac{1}{\epsilon}\ln x - 2Li_2(1) - 2Li_2(1-x) - \frac{1}{2}\ln^2 x \\
S_1^{ML} &= \frac{1}{\epsilon^2}+\frac{1}{\epsilon}-\frac{1}{\epsilon}\frac{x\ln x}{1-x} - \frac{x\ln x}{1-x} - Li_2(1) + \frac{2x}{1-x}Li_2(1-x) + \frac{1}{2}\frac{x}{1-x}\ln^2 x \\
S_2^{ML} &= \frac{1}{\epsilon}\frac{\ln x}{1-x} - \frac{2}{1-x}Li_2(1-x) - \frac{1}{2}\frac{\ln^2 x}{1-x} \\
S_3^{ML} &= -\frac{1}{2}\frac{k^2}{kn}\left(Li_2(1) - \frac{Li_2(1-x)}{1-x}\right) \\
S_4^{ML} &= -\frac{1}{\epsilon}+\frac{x\ln x}{1-x} \\
U_{0,\mathrm{PVI}}^{ML} &= \frac{1}{\epsilon^2}+\frac{1}{\epsilon}[-I_0 + \ln x - 2\ln(1-x)] + 2I_1 - I_0\ln(1-x) + \text{finite} \\
U_{0,\epsilon}^{ML} &= \frac{3}{2\epsilon^2}+\frac{1}{\epsilon}[\ln x - \frac{3}{2}\ln(1-x)] + Li_2(1-x) - \frac{13}{2}Li_2(1) \\
&\quad -\frac{1}{2}\ln^2 x + \frac{3}{4}\ln^2(1-x)
\end{aligned}
$$

Form factors in the PV scheme

$$
\begin{aligned}
S_0^{PV} &= \frac{1}{\epsilon^2}-\frac{1}{\epsilon}[I_0 - \ln x] + I_1 - I_0\ln x - 2Li_2(1) - 2Li_2(1-x) - \frac{1}{2}\ln^2 x \\
S_1^{PV} &= \frac{1}{\epsilon^2}-\frac{1}{\epsilon}\frac{x\ln x}{1-x} + \frac{x}{1-x}Li_2(1-x) - Li_2(1) \\
S_2^{PV} &= \frac{1}{\epsilon}\frac{\ln x}{1-x} - \frac{Li_2(1-x)}{1-x} \\
S_3^{PV} &= -\frac{1}{2}\frac{k^2}{kn}\left(\frac{I_0}{\epsilon}+\frac{1}{\epsilon}\frac{\ln x}{1-x} - I_1 + \frac{I_0\ln x}{1-x} - Li_2(1) - \frac{xLi_2(1-x)}{1-x} + \frac{1}{2}\ln^2 x\right) \\
S_4^{PV} &= 0 \\
U_0^{PV} &= \frac{1}{\epsilon^2}+\frac{1}{\epsilon}[-I_0 + \ln x - 2\ln(1-x)] + I_1 - I_0\ln x \\
&\quad +2Li_2(1-x) - \frac{1}{2}\ln^2 x + \ln^2(1-x) - 6Li_2(1)
\end{aligned}
$$

A.4 Two–loop integrals

For the calculation of the $C_F T_f$ part of the two-loop quark selfenergy we need some integrals with an extra non-integer power of $(-r^2)$ in the integrand, where r is the loop momentum. Making use of the identities

$$\begin{aligned}\frac{1}{a^\alpha b} &= \alpha \int_0^1 dx \frac{x^{\alpha-1}}{[ax+b(1-x)]^{\alpha+1}}\,, \\ \frac{1}{a^\alpha bc} &= \alpha(\alpha+1)\int_0^1 dx \int_0^{1-x} dy \frac{x^{\alpha-1}}{[ax+by+c(1-x-y)]^{\alpha+2}}\,, \end{aligned} \tag{A.34}$$

one obtains rather easily:

$$\int \frac{d^m r}{(2\pi)^m} \frac{(-r^2)^{-\epsilon}}{(p-r)^2} = \frac{i}{16\pi^2}(4\pi)^\epsilon \left(-p^2\right)^{1-2\epsilon} \frac{\epsilon\Gamma(2\epsilon)}{\Gamma(1+\epsilon)} \frac{\Gamma(1-\epsilon)\Gamma(1-2\epsilon)}{\Gamma(3-3\epsilon)} \tag{A.35}$$

$$\int \frac{d^m r}{(2\pi)^m} \frac{(-r^2)^{-\epsilon}}{r^2(p-r)^2} = \frac{i}{16\pi^2}(4\pi)^\epsilon \left(-p^2\right)^{-2\epsilon} \frac{\Gamma(2\epsilon)}{\Gamma(1+\epsilon)} \frac{\Gamma(1-\epsilon)\Gamma(1-2\epsilon)}{\Gamma(2-3\epsilon)}$$

$$\int \frac{d^m r}{(2\pi)^m} \frac{(-r^2)^{-\epsilon}}{r^2(p-r)^2[nr]_{\rm ML}} = \left(-p^2\right)^{-\epsilon} \left(1+\epsilon^2\zeta(2)\right) \int \frac{d^m r}{(2\pi)^m} \frac{1}{r^2(p-r)^2[nr]_{\rm ML}} \tag{A.36}$$

where the integral on the right-hand side of (A.36) has been determined in Appendix A.3. Note that the integral in (A.35) vanishes if the factor $(-r^2)^{-\epsilon}$ is not present.
Finally, with PV prescription one obtains for the integral in (A.36):

$$\int \frac{d^m r}{(2\pi)^m} \frac{(-r^2)^{-\epsilon}}{r^2(p-r)^2[nr]_{\rm PV}} = \frac{i}{16\pi^2}(4\pi)^\epsilon \left(-p^2\right)^{-2\epsilon} \frac{1}{2\epsilon\, pn} \left[I_0 + \epsilon\zeta(2) - 2\epsilon I_1\right] + \mathcal{O}(\epsilon)\,, \tag{A.37}$$

while

$$\int \frac{d^m r}{(2\pi)^m} \frac{1}{r^2(p-r)^2[nr]_{\rm PV}} = \frac{i}{16\pi^2}(4\pi)^\epsilon \left(-p^2\right)^{-\epsilon} \frac{1}{\epsilon\, pn} \left[I_0 + \epsilon\zeta(2) - \epsilon I_1\right] + \mathcal{O}(\epsilon)\,. \tag{A.38}$$

Appendix B

Phase spaces

The momenta are parametrized as

$$
\begin{aligned}
p &= (P, \vec{0}, P) \quad (P > 0) \quad ; \quad n = (\frac{pn}{2P}, \vec{0}, -\frac{pn}{2P}) \\
k &= (xP + \frac{k^2 + k_\perp^2}{4xP}, \vec{k}_\perp, xP - \frac{k^2 + k_\perp^2}{4xP}) \\
l_1 &= (z_1 P + \frac{t_1^2}{4z_1 P}, \vec{t}_1, z_1 P - \frac{t_1^2}{4z_1 P}) \quad \text{if } l_1^2 = 0\,;\; z_1 \neq 0 \\
l_2 &= (z_2 P + \frac{t_2^2}{4z_2 P}, \vec{t}_2, z_2 P - \frac{t_2^2}{4z_2 P}) \quad \text{if } l_2^2 = 0\,;\; z_2 \neq 0 \\
x &= \frac{kn}{pn}\,;\; z_1 = \frac{l_1 n}{pn}\,;\; z_2 = \frac{l_2 n}{pn}
\end{aligned}
$$

In light-cone parametrization, the momenta are written as $r = (r_+, r_-, \vec{r}_\perp)$, where

$$
\begin{aligned}
r_\pm &= \frac{1}{\sqrt{2}}(r_0 \pm r_3) \quad \text{and thus} \\
r^2 &= 2 r_+ r_- - r_\perp^2
\end{aligned}
$$

It is convenient to set $pn = p_+ = 1$.

The Feynman rule for a cut gluon line is given by

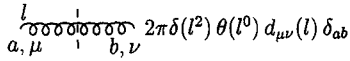

$$2\pi\delta(l^2)\,\theta(l^0)\,d_{\mu\nu}(l)\,\delta_{ab}$$

whereas for a cut axial ghost line we have

$$2\pi\delta(ln)\,\theta(l^0)\,D^{\rm gh}_{\mu\nu}(l)\,\delta_{ab}\,;\; D^{\rm gh}_{\mu\nu}(l) = -(l_\mu n_\nu + l_\nu n_\mu)/l_\perp^2$$

So for the cut lines one has to distinguish between "physical" gluon lines and axial ghost lines. The case that all cut lines of a given diagram are ghost lines only gives a contribution at $x = 1$.

B.1 Phase space integral for virtual contributions

The phase space integral needed for the virtual diagrams, where only one physical gluon line is cut, is given by

$$\begin{aligned} PS^{virt} &= 2\pi\, z \int \frac{d^m k}{(2\pi)^m}\,\delta(x-z)\,\delta((p-k)^2) \quad \text{where} \qquad \text{(B.1)} \\ (p-k)^2 &= -\frac{k_\perp^2}{x} - \frac{(1-x)}{x}k^2 \Longrightarrow \delta((p-k)^2) = x\,\delta(k_\perp^2 + (1-x)k^2) \end{aligned}$$

Since the integrand has no angular dependence, the angular integral is trivial here, so

$$\int d^m k = K_{m-2}\int dk^2\,\frac{dx}{2x}\,d|\vec{k}_\perp|\,|\vec{k}_\perp|^{m-3} = K_{m-2}\int dk^2\,\frac{dx}{2x}\,\frac{1}{2}\,dk_\perp^2\,\left(k_\perp^2\right)^{\frac{m-4}{2}}$$

$K_{m-2} = 2\,\pi^{\frac{m-2}{2}}/\Gamma(\frac{m-2}{2})$ is the surface of a $(m-2)$ dimensional hypersphere. Thus in $m = 4 - 2\epsilon$ dimensions, the phase space for the virtual diagrams is given by

$$\begin{aligned} PS^{virt} &= 2\pi\, z \int \frac{d^m k}{(2\pi)^m}\,\delta(x-z)\,\delta((p-k)^2) \\ &= \frac{2\pi}{(2\pi)^{4-2\epsilon}}\,\frac{1}{4}\,K_{2-2\epsilon}\int dk^2\,dk_\perp^2\,\left(k_\perp^2\right)^{-\epsilon}\,x\,\delta(k_\perp^2 + (1-x)k^2) \\ &= \frac{1}{16\pi^2}\,\frac{(4\pi)^\epsilon}{\Gamma(1-\epsilon)}\int_0^{Q^2} d|k^2|\,|k^2|^{-\epsilon}\,x\,(1-x)^{-\epsilon} \end{aligned}$$

The upper limit of the $d|k^2|$ integral ($k^2 < 0$) is denoted by a large momentum scale Q^2 whose actual value is irrelevant since only the pole part of the k^2-integration is needed.

B.2 Phase space integrals for real contributions

The real contributions are the ones where two internal lines are cut. If the cut lines are gluon lines, we will distinguish between "usual" real diagrams where both gluon lines are physical on-shell gluons and "ghost diagrams" where one cut line, say l_2, is an axial ghost line. The case that both cut gluon lines are ghost lines only gives a contribution at $x = 1$. The following table summarizes the different kinematics:

l_2 being a physical gluon	l_2 being an axial ghost
$l_2^2 = 0$	$l_2^2 = -t_2^2$
$l_2^+ = z_2 p^+$	$l_2^+ = 0$
$l_2^- = t_2^2/(2z_2 p^+)$	$2p^+ l_2^- =: \xi$
$l_1^+ = (1-x-z_2)\,p^+$	$l_1^+ = (1-x)\,p^+$
$pl_2 = t_2^2/(2z_2)$	$pl_2 = \frac{1}{2}\xi$
$l_1 l_2 = \frac{z_1}{2z_2}\,t_2^2 + \frac{z_2}{2z_1}\,t_1^2 - \vec{t}_1\vec{t}_2$	$l_1 l_2 = \frac{1}{2}\xi z_1 - \vec{t}_1\vec{t}_2$

B.2.1 Phase space for physical real part

Using the parametrization of momenta given above, the two-body phase space for l_1 and l_2 being on-shell physical momenta is given by

$$\begin{aligned} d\Phi(l_1,l_2) &= \frac{4\pi^2}{(2\pi)^m}\int dl_1^+ dl_2^+ dl_1^- dl_2^-\, d^{(m-2)}\vec{t}_1 d^{(m-2)}\vec{t}_2\,\delta(p^+ - k^+ - l_1^+ - l_2^+) \\ &\quad \cdot\delta^{(m-2)}(\vec{k}_\perp + \vec{t}_1 + \vec{t}_2)\,\delta(k^- + l_1^- + l_2^-)\,\delta(l_1^2)\,\delta(l_2^2) \end{aligned}$$

Now we use $\delta(l_1^2) = \frac{1}{2l_1^+}\,\delta(l_1^- - \frac{\vec{t}_1^{\,2}}{2l_1^+})$ and the analogous relation for l_2,

then

$$\begin{aligned} d\Phi(l_1,l_2) &= \frac{4\pi^2}{(2\pi)^m}\int \frac{dl_1^+}{2l_1^+}\frac{dl_2^+}{2l_2^+}\,d\vec{t}_1 d\vec{t}_2\,\delta(p^+ - k^+ - l_1^+ - l_2^+) \\ &\quad \cdot\delta\,(\vec{k}_\perp + \vec{t}_1 + \vec{t}_2)\,\delta(k_- + \frac{\vec{t}_1^{\,2}}{2l_1^+} + \frac{\vec{t}_2^{\,2}}{2l_2^+}) \\ &= \frac{2\pi^2}{(2\pi)^m}\int \frac{dz_1}{z_1}\frac{dz_2}{z_2}\,d\vec{t}_1 d\vec{t}_2\,\delta(1-x-z_1-z_2) \\ &\quad \cdot\delta\,(\vec{k}_\perp + \vec{t}_1 + \vec{t}_2)\,\delta(\frac{k^2}{x} + \frac{\vec{k}_\perp^{\,2}}{x} + \frac{\vec{t}_1^{\,2}}{z_1} + \frac{\vec{t}_2^{\,2}}{z_2}) \end{aligned}$$

Including also the $\vec{k}_\perp$–part from the $d^m k$–integration into the phase space leads to

$$PS^{\text{phys}} = \int d\vec{k}_\perp\, d\Phi(l_1,l_2) = \frac{2\pi^2}{(2\pi)^m}\int \frac{dz_1}{z_1}\frac{dz_2}{z_2}\,\delta(1-x-z_1-z_2)$$

$$\cdot \int d\vec{t}_1 d\vec{t}_2\, \delta\left(\frac{k^2}{x} + \frac{(\vec{t}_1+\vec{t}_2)^2}{x} + \frac{\vec{t}_1^2}{z_1} + \frac{\vec{t}_2^2}{z_2}\right) \tag{B.2}$$

Now new momenta $\vec{h}_1$ and $\vec{h}_2$ will be introduced such that the $\delta-$function becomes diagonal in h_1 and h_2 and the angular dependence of the denominators gets as simple as possible. The angular integration will be carried out in the following way: In all diagrams where no axial ghost is present, $\vec{h}_1$ and $\vec{h}_2$ can be chosen such that one denominator factor is only proportional to h_1^2 or h_2^2 and the other denominator factor is proportional to $(\vec{h}_1+\vec{h}_2)^2$ or has no angular dependence at all. Then the arguments of the matrix element $M(k^2, h_1^2, h_2^2, \vec{h}_1\vec{h}_2, x, z_1, z_2, \epsilon)$ will be changed to $M(k^2, h_1^2, \lambda, \theta, x, z_1, z_2, \epsilon)$ where λ is defined by the ratio

$$\lambda^2 = h_1^2/h_2^2$$

and θ is the angle between $\vec{h}_1$ and $\vec{h}_2$.
The transformation of integration variables is given by

$$\int d\vec{t}_1\, d\vec{t}_2 \longrightarrow \int d\vec{h}_1\, d\vec{h}_2\, |DJ|$$

where the $d\vec{h}_i$ integrals can, for $m = 4-2\epsilon$, be written as

$$\int d\vec{h}_1\, d\vec{h}_2 \;=\; \frac{\pi^{2-2\epsilon}}{\Gamma^2(1-\epsilon)} \int dh_1^2 (h_1^2)^{-\epsilon} dh_2^2 (h_2^2)^{-\epsilon} \cdot \frac{\Gamma(1-\epsilon)}{\sqrt{\pi}\Gamma(\frac{1}{2}-\epsilon)} \int_0^\pi d\theta (\sin\theta)^{-2\epsilon}$$

So in terms of the new variables, the phase space PS^{phys} is given by

$$\begin{aligned} PS^{\text{phys}} \;=\; & \frac{2\pi^{4-2\epsilon}}{(2\pi)^m} \frac{1}{\Gamma^2(1-\epsilon)} \int \frac{dz_1}{z_1}\frac{dz_2}{z_2}\, \delta(1-x-z_1-z_2)\, |DJ| \\ & \cdot \int dh_1^2 (h_1^2)^{-\epsilon} dh_2^2 (h_2^2)^{-\epsilon}\, \delta(f^{(a)}(k^2, h_1^2, h_2^2, x, z_1, z_2)) \\ & \cdot \frac{\Gamma(1-\epsilon)}{\sqrt{\pi}\Gamma(\frac{1}{2}-\epsilon)} \int_0^\pi d\theta (\sin\theta)^{-2\epsilon} \end{aligned} \tag{B.3}$$

The functions $f^{(a)}(k^2, h_1^2, h_2^2, x, z_1, z_2)$ depend on the topologies (a), since for different denominators the new variables h_i are defined differently. They are given in Table B.1.

	topologies (b) and (h)	topology (d)	topology (f)
denominators	(b): $(p-l_1)^2 = -t_1^2/z_1$ $(p-l_2)^2 = -t_2^2/z_2$ (h):$(p-l_2)^4 = t_2^4/z_2^2$	$(p-l_1)^2 = -t_1^2/z_1$ $(l_1+l_2)^2 = \frac{z_1}{z_2}\,t_2^2 + \frac{z_2}{z_1}\,t_1^2 - 2\vec{t}_1\vec{t}_2$	$(l_1+l_2)^4 = \left(\frac{z_1}{z_2}\,t_2^2 + \frac{z_2}{z_1}\,t_1^2 - 2\vec{t}_1\vec{t}_2\right)^2$
new variables	$\vec{t}_1 = \vec{h}_1$ $\vec{t}_2 = -z_2/(1-z_1)\,(\vec{h}_1+\vec{h}_2)$	$\vec{t}_1 = z_1\sqrt{(1-z_1)}\,\vec{h}_1$ $\vec{t}_2 = -z_2/\sqrt{(1-z_1)}\,(\vec{h}_2 + z_1\vec{h}_1)$	$\vec{t}_1 = \sqrt{z_1 z_2}/(1-x)\,\vec{h}_1 + \vec{h}_2$ $\vec{t}_2 = -\sqrt{z_1 z_2}/(1-x)\,\vec{h}_1 + z_2/z_1\,\vec{h}_2$
new denominators	$(p-l_1)^2 = -h_1^2/z_1$ $(p-l_2)^2 = -\frac{z_2}{(1-z_1)^2}\,(\vec{h}_1+\vec{h}_2)^2$	$(p-l_1)^2 = -z_1(1-z_1)\,h_1^2$ $(l_1+l_2)^2 = \frac{z_1 z_2}{(1-z_1)}\,(\vec{h}_1+\vec{h}_2)^2$	$(l_1+l_2)^4 = h_1^4$
Jacobian	$\lvert DJ\rvert = (\frac{z_2}{1-z_1})^{m-2}$	$\lvert DJ\rvert = (z_1 z_2)^{m-2}$	$\lvert DJ\rvert = \left(\frac{z_2}{z_1}\right)^{\frac{m-2}{2}}$
δ−function	$f^{(b)} = \frac{k^2}{x} + \frac{1}{z_1(1-z_1)}\,h_1^2 + \frac{z_2}{x(1-z_1)}\,h_2^2$	$f^{(c)} = \frac{k^2}{x} + \frac{z_2}{x}\,h_2^2 + z_1\,h_1^2$	$f^{(f)} = \frac{k^2}{x} + \frac{1}{1-x}\,h_1^2 + \frac{1-x}{x z_1^2}\,h_2^2$
integration limits	$h^2_{1,\text{split}} = \lvert k^2\rvert \cdot z_1/(1-z_2)$	$h^2_{1,\text{split}} = \lvert k^2\rvert/((1-x)(1-z_1))$	
	$h^2_{1,\text{max}} = \lvert k^2\rvert \cdot z_1(1-z_1)/x$	$h^2_{1,max} = \lvert k^2\rvert/(x z_1)$	$h^2_{1,\text{max}} = \lvert k^2\rvert \cdot (1-x)/x$

Table B.1: Variable transformations for different topologies

Angular integration

The angular dependence of the numerator of the matrix elements is of the structure

$$M(\cos\theta) = A + B \cdot \cos\theta + C \cdot \cos^2\theta$$

The denominators of the matrix elements contain an angular dependence (if at all) only in the term

$$(\vec{h}_1 + \vec{h}_2)^2 = h_2^2(1 + \lambda^2 + 2\lambda\cos\theta)$$

so the angular integrals to perform are

$$I_A = \frac{\Gamma(1-\epsilon)}{\sqrt{\pi}\Gamma(\frac{1}{2}-\epsilon)} \int_0^\pi d\theta\,(\sin\theta)^{-2\epsilon} = 1 \tag{B.4}$$

$$I_B = \frac{\Gamma(1-\epsilon)}{\sqrt{\pi}\Gamma(\frac{1}{2}-\epsilon)} \int_0^\pi d\theta\,(\sin\theta)^{-2\epsilon}\cos\theta = 0 \tag{B.5}$$

$$I_C = \frac{\Gamma(1-\epsilon)}{\sqrt{\pi}\Gamma(\frac{1}{2}-\epsilon)} \int_0^\pi d\theta\,\frac{(\sin\theta)^{-2\epsilon}}{1+\lambda^2+2\lambda\cos\theta} \tag{B.6}$$

$$I_D = \frac{\Gamma(1-\epsilon)}{\sqrt{\pi}\Gamma(\frac{1}{2}-\epsilon)} \int_0^\pi d\theta\,(\sin\theta)^{-2\epsilon}\cos^2\theta = \frac{1}{2}\cdot\frac{1}{1-\epsilon}$$

I_C leads to a hypergeometric function depending on λ^2 and ϵ:

$$I_C = \begin{cases} F(1, 1+\epsilon; 1-\epsilon, \lambda^2) & \text{for } \lambda^2 < 1 \\ \frac{1}{\lambda^2} F(1, 1+\epsilon; 1-\epsilon, \frac{1}{\lambda^2}) & \text{for } \lambda^2 > 1 \end{cases} \tag{B.7}$$

So if there is an angular dependence in the denominator, the integration range for the transverse momenta has to be split into a region where $\lambda^2 < 1$ and into one where $\lambda^2 > 1$.

Combining the results for the angular integrals we finally obtain for the matrix element after angular integration

$$\begin{aligned} M(h_1^2, \lambda, x, z_1, z_2) &= \frac{\Gamma(1-\epsilon)}{\sqrt{\pi}\Gamma(\frac{1}{2}-\epsilon)} \int_0^\pi d\theta \frac{(\sin\theta)^{-2\epsilon}\,(A + B\,\cos\theta + C\,\cos^2\theta)}{(1+\lambda^2+2\lambda\cos\theta)} \\ &=: I_C \cdot U_1 + U_2 \end{aligned} \tag{B.8}$$

$$\begin{aligned} U_1 &= A - B\frac{1+\lambda^2}{2\lambda} + C\frac{(1+\lambda^2)^2}{4\lambda^2} \\ U_2 &= \frac{B}{2\lambda} - C\frac{(1+\lambda^2)}{4\lambda^2} \end{aligned}$$

Transverse momentum integration

After having integrated out h_2^2 using the δ–functions given in Table B.1, the integration over h_1^2 can be transformed into an integral from zero to one, in the case of topology $(\mathrm{d})^{\mathrm{tr.}}_{\mathrm{real}}$ for example by defining

$$\begin{aligned} h_1^2 &= \frac{|k^2|}{xz_1} \cdot u \\ \text{Then} \quad \lambda^2 &= \frac{h_1^2}{h_2^2} = \frac{au}{1-u} \quad ; \quad a = \frac{z_2}{xz_1} \end{aligned}$$

and

$$\begin{aligned} PS^{\mathrm{phys},(d)_{\mathrm{r}}} &= \frac{2\pi^{4-2\epsilon}}{(2\pi)^m} \frac{(|k^2|)^{1-2\epsilon}}{\Gamma^2(1-\epsilon)} \int dz_1\, dz_2\, \delta(1-x-z_1-z_2)\, z_1^{-2\epsilon} \\ &\cdot \Big\{ a^{-\epsilon} \int_0^{\frac{1}{1+a}} du\, u^{-\epsilon} (1-u)^{-\epsilon} + a^{-\epsilon} \int_{\frac{1}{1+a}}^1 du\, u^{-\epsilon} (1-u)^{-\epsilon} \Big\} \end{aligned}$$

After insertion of the matrix element
$M(u,x,z_1,z_2) = I_C(a,u) \cdot U_1(u,x,z_1,z_2) + U_2(u,x,z_1,z_2)$ and the substitution

$$\begin{aligned} v &= \frac{au}{1-u} \quad \text{for } u < \frac{1}{1+a} \\ v &= \frac{1-u}{au} \quad \text{for } u > \frac{1}{1+a} \end{aligned}$$

we arrive (besides trivial integrals) at integrals of the type

$$\begin{aligned} J_0 &= \int_0^1 dv\, v^{-1-\epsilon} (1+\frac{v}{a})^{2\epsilon} \cdot F(1,1+\epsilon;1-\epsilon,v) \\ &+ \int_0^1 dv\, v^{-\epsilon} (v+\frac{1}{a})^{2\epsilon} \cdot F(1,1+\epsilon;1-\epsilon,v) \\ J_1 &= a^{-1} \int_0^1 dv\, v^{-\epsilon} (1+\frac{v}{a})^{-1+2\epsilon} \cdot F(1,1+\epsilon;1-\epsilon,v) \\ &+ a^{-1} \int_0^1 dv\, v^{-\epsilon} (v+\frac{1}{a})^{-1+2\epsilon} \cdot F(1,1+\epsilon;1-\epsilon,v) \\ J_2 &= a^{-2} \int_0^1 dv\, v^{1-\epsilon} (1+\frac{v}{a})^{-2+2\epsilon} \cdot F(1,1+\epsilon;1-\epsilon,v) \\ &+ a^{-2} \int_0^1 dv\, v^{-\epsilon} (v+\frac{1}{a})^{-2+2\epsilon} \cdot F(1,1+\epsilon;1-\epsilon,v) \end{aligned}$$

Using

$$F(1,1+\epsilon;1-\epsilon;v) = (1-v)^{-1-2\epsilon} F(-\epsilon,-2\epsilon,1-\epsilon;v) = (1-v)^{-1-2\epsilon} \{1+2\epsilon^2\, Li_2(v) + \mathcal{O}(\epsilon^3)\}$$

we obtain the results

$$J_0 = -\frac{2}{\epsilon}\frac{\Gamma^2(1-\epsilon)}{\Gamma(1-2\epsilon)}\left(1+\epsilon\,\ln\frac{1+a}{a}+\epsilon^2\,\frac{\pi^2}{6}+O(\epsilon^2\,z_1)\right) \tag{B.9}$$

$$J_1 = -\frac{1}{\epsilon}\frac{1}{(1+a)}+\frac{\ln a}{(1+a)}+O(\epsilon\,z_1) \tag{B.10}$$

$$J_2 = -\frac{1}{\epsilon}\frac{1}{(1+a)^2}+\frac{\ln a}{(1+a)^2}+\frac{a-1}{(1+a)^2}+O(\epsilon\,z_1) \tag{B.11}$$

The remaining integrals over z_1 are straightforward, containing in the PV scheme and in the ML scheme with PVI regularization terms like $z_1^{1-\epsilon}/(z_1^2+\delta^2)$ which lead to the spurious poles I_0 and I_1 defined in Eqs. (3.61) and (3.62).

B.2.2 Phase space for axial ghost contributions

We fix our notation such that l_1 is always the usual gluon momentum, and l_2 is the axial ghost momentum. The phase space $PS^{\rm gh}$ then is governed by the condition $l_2^+=0$:

$$\begin{aligned} PS^{\rm gh} &= \frac{4\pi^2}{(2\pi)^m}\int dl_1^+dl_2^+dl_1^-dl_2^-\,d\vec{t}_1d\vec{t}_2\,d\vec{k}_\perp\,\delta(p^+-k^+-l_1^+-l_2^+) \\ &\quad\cdot\delta(\vec{k}_\perp+\vec{t}_1+\vec{t}_2)\,\delta(k^-+l_1^-+l_2^-)\,\delta(l_2^+)\,\delta(l_1^2)\,\theta(l_2^0) \end{aligned}$$

Now we use $\delta(l_1^2) = \frac{1}{2l_1^+}\delta(l_1^- - \frac{\vec{t}_1^{\,2}}{2l_1^+})$ to eliminate l_1^- and substitute l_2^- by

$$\xi = 2p^+l_2^- \Rightarrow dl_2^- = \frac{d\xi}{2p^+}$$

Note that $\xi \geq 0$ because of the theta function $\theta(l_2^0)$: $\theta(l_2^0)=\theta(l_2^+ + l_2^-)=\theta(l_2^-)$ for $l_2^+=0$. Hence

$$\begin{aligned} PS^{\rm gh} &= \frac{2\pi^2}{(2\pi)^m}\int\frac{dz_1}{z_1}dz_2\delta(z_2)\delta(1-x-z_1-z_2)\int d\vec{k}_\perp\,d\vec{t}_1d\vec{t}_2\,\delta\,(\vec{k}_\perp+\vec{t}_1+\vec{t}_2) \\ &\quad \int_0 d\xi\,\delta(\frac{k^2}{x}+\frac{\vec{k}_\perp^{\,2}}{x}+\xi+\frac{\vec{t}_1^{\,2}}{z_1}) \\ &= \frac{2\pi^2}{(2\pi)^m}\frac{1}{1-x}\int d\vec{k}_\perp\,d\vec{t}_1d\vec{t}_2\,\delta\,(\vec{k}_\perp+\vec{t}_1+\vec{t}_2) \\ &\quad \int_0 d\xi\,\delta(\frac{k^2}{x}+\frac{\vec{k}_\perp^{\,2}}{x}+\xi+\frac{\vec{t}_1^{\,2}}{z_1}) \end{aligned} \tag{B.12}$$

The condition $\theta(l_1^0)=\theta(1-x+\frac{\vec{t}_1^{\,2}}{2(1-x)})$ is trivially fulfilled.

Now there are two different ways to proceed, depending on whether the spurious poles are regulated with δ or with ϵ. If all poles are regulated with ϵ, parametrization 1, which shifts the angular dependence into t_2^2, is the most convenient one, since then the $\delta-$function containing ξ is naturally diagonal. On the other hand, the spurious poles correspond to the limit $t_2^2 \to 0$, so if we choose to regulate the spurious poles with δ, we should avoid an angular dependence in addition to the $\delta-$dependence in t_2^2 by using parametrization 2.

Parametrization 1

In parametrization 1, we define the angle θ and the parameter β by

$$\vec{k}_\perp \vec{t}_1 = k_\perp t_1 \cos\theta \quad ; \quad \beta^2 = \frac{k_\perp^2}{t_1^2}\,, \tag{B.13}$$

leading to

$$t_2^2 = (\vec{t}_1 + \vec{k}_\perp)^2 = t_1^2(1 + \beta^2 + 2\beta\cos\theta) \tag{B.14}$$

Hence we obtain

$$\begin{aligned} PS^{\rm gh} &= F_\epsilon \int \frac{dz_1}{z_1}\delta(1-x-z_1) \int dt_1^2 (t_1^2)^{-\epsilon} dk_\perp^2 (k_\perp^2)^{-\epsilon} \cdot \\ &\quad \int_0 d\xi\, \delta\Big(\frac{k^2}{x} + \frac{\vec{k}_\perp^2}{x} + \xi + \frac{\vec{t}_1^2}{z_1}\Big) \cdot \frac{\Gamma(1-\epsilon)}{\sqrt{\pi}\Gamma(\frac{1}{2}-\epsilon)} \int_0^\pi d\theta (\sin\theta)^{-2\epsilon} \qquad \text{(B.15)} \\ F_\epsilon &= \frac{2\pi^{4-2\epsilon}}{(2\pi)^m} \frac{1}{\Gamma^2(1-\epsilon)} \end{aligned}$$

Now we substitute

$$k_\perp^2 = |k^2| \cdot u \quad ; \quad t_1^2 = |k^2| \frac{(1-x)}{x}(1-u)\cdot y$$

then

$$\beta^2 = \frac{k_\perp^2}{t_1^2} = \frac{xu}{(1-x)(1-u)y} = \frac{bu}{(1-u)} \tag{B.16}$$

$$b = \frac{x}{(1-x)y} \tag{B.17}$$

This is leading to

$$\begin{aligned} PS^{\rm gh} &= F_\epsilon\, |k^2|^{2-2\epsilon} x^{-1+\epsilon} (1-x)^{-\epsilon} \int_0^1 du\, u^{-\epsilon}(1-u)^{1-\epsilon} \int_0^1 dy\, y^{-\epsilon} \cdot \\ &\quad \int_0 d\xi\, \delta\Big(\frac{k^2}{x}(1-u)(1-y) + \xi\Big) \cdot \frac{\Gamma(1-\epsilon)}{\sqrt{\pi}\Gamma(\frac{1}{2}-\epsilon)} \int_0^\pi d\theta (\sin\theta)^{-2\epsilon} \qquad \text{(B.18)} \end{aligned}$$

Finally the integral over θ can, by substituting $w = \frac{1}{2}(1+\cos\theta)$, be written as

$$\begin{aligned} PS^{\rm gh} &= F_\epsilon\,|k^2|^{2-2\epsilon}\,x^{-1+\epsilon}(1-x)^{-\epsilon}\int_0^1 du\,u^{-\epsilon}(1-u)^{1-\epsilon}\int_0^1 dy\,y^{-\epsilon}\cdot \\ &\quad \frac{1}{B(\frac{1}{2}-\epsilon,\frac{1}{2}-\epsilon)}\int_0^1 dw\,[w(1-w)]^{-\frac{1}{2}-\epsilon} \end{aligned} \tag{B.19}$$

The momenta occurring in the matrix elements in this parametrization are of the form

$$\begin{aligned} (l_1+l_2)^2 &= \frac{|k^2|}{x}\,(1-x-u) \\ (p-l_1)^2 &= -\frac{t_1^2}{1-x} = -\frac{|k^2|}{x}\,(1-u)\cdot y \\ t_1^2 &= |k^2|\frac{(1-x)}{x}\,(1-u)\cdot y \\ t_2^2 &= (\vec{t}_1+\vec{k}_\perp)^2 = t_1^2(1+\beta^2+2\beta\cos\theta) \\ &= |k^2|\frac{(1-x)}{x}\,(1-u)\,y\,(1-\beta)^2\,[1-zw]\;;\; z=\frac{-4\beta}{(1-\beta)^2} \\ (p-l_2)^2 &= -[\xi+t_2^2] = -\frac{|k^2|}{x}\,(1-u)\,[1-y+(1-x)\,y(1+\beta^2+2\beta\cos\theta)] \\ &= -\frac{|k^2|}{x}\,(1-u)\,[1-y+(1-x)\,y(1-\beta)^2\,[1-zw]\,] \end{aligned} \tag{B.20, B.21}$$

Parametrization 2

A parametrization where $\vec{t}_2^{\,2}$ contains no angular dependence and the $\delta-$function in (B.12) is diagonal shifts the angular dependence into $\vec{t}_1^{\,2}$ and $\vec{k}_\perp^{\,2}$. Substituting

$$\begin{aligned} \vec{t}_2 &= \vec{h}_2 \quad ; \quad \vec{t}_1 = x\,\vec{h}_1 - (1-x)\,\vec{h}_2 \\ \vec{k}_\perp &= -x\,(\vec{h}_1+\vec{h}_2) \end{aligned}$$

leads to

$$\begin{aligned} PS^{\rm gh} &= F_\epsilon\,(1-x)^{-1}x^{2-2\epsilon}\int dh_1^2(h_1^2)^{-\epsilon}dh_2^2(h_2^2)^{-\epsilon}\cdot \\ &\quad \int_0 d\xi\,\delta(\frac{k^2}{x}+\xi+\frac{x\vec{h}_1^{\,2}}{1-x}+\vec{h}_2^{\,2})\cdot\frac{\Gamma(1-\epsilon)}{\sqrt{\pi}\Gamma(\frac{1}{2}-\epsilon)}\int_0^\pi d\theta(\sin\theta)^{-2\epsilon} \end{aligned}$$

Now we substitute

$$h_1^2 = \frac{|k^2|}{x^2}\,(1-x)\cdot u \quad ; \quad h_2^2 = \frac{|k^2|}{x}\,(1-u)\cdot y \quad ; \quad w = \frac{1}{2}(1+\cos\theta) \tag{B.22}$$

to obtain again expression (B.19) for the phase space $PS^{\rm gh}$.

The momenta occurring in the denominators of the matrix elements are in this parametrization given by

$$t_2^2 = \frac{|k^2|}{x}(1-u)\cdot y \tag{B.23}$$

$$t_1^2 = |k^2|\frac{(1-x)^2}{x}(1-u)\,y\,(1+\lambda^2-2\lambda\cos\theta)$$

$$(p-l_2)^2 = -[\xi+t_2^2] = -\frac{|k^2|}{x}(1-u)$$

$$(p-l_1)^2 = -\frac{t_1^2}{1-x} = -\frac{|k^2|}{x}(1-x)(1-u)\,y\,(1+\lambda^2-2\lambda\cos\theta) \tag{B.24}$$

$$(l_1+l_2)^2 = \frac{|k^2|}{x}[1-x-xy(1-u)(1+\beta^2+2\beta\cos\theta)] \tag{B.25}$$

$$\beta^2 = \frac{bu}{1-u} \quad ; \quad b=\frac{(1-x)}{xy} \quad ; \quad \lambda=\frac{x}{1-x}\beta \tag{B.26}$$

The $\delta-$regulator for the spurious poles then regulates the spurious pole at $t_2^2 \to 0$ as follows:

$$\frac{1}{t_2^2} \to \frac{t_2^2}{(t_2^2)^2+\delta^2(2p^+l_2^-)^2}$$

$$2p^+l_2^- = \xi = \frac{|k^2|}{x}(1-u)(1-y)$$

$$t_2^2 = \frac{|k^2|}{x}(1-u)\cdot y$$

$$\text{Hence} \quad t_2^{-2} \to \left[\frac{|k^2|}{x}(1-u)\right]^{-1}\cdot\frac{y}{y^2+\delta^2(1-y)^2} \tag{B.27}$$

$$= \left[\frac{|k^2|}{x}(1-u)\right]^{-1}\cdot\frac{y}{y^2+\delta^2} \tag{B.28}$$

where $\delta^2(1-y)^2$ has been set equal to δ^2 since only the limit $y=0$ has to be regulated by δ, so the difference between (B.27) and (B.28) will be of order δ.

Appendix C

Imaginary parts of two-loop integrals

In this Appendix, we will show explicitly how to obtain the imaginary part of a nontrivial loop integral done with ML prescription. As an example we will choose the two-point integral $J_2^{A,ML}(l)$ where we did already the integration over the loop momentum, ending up at expression (A.14). The next integration we have to do is the one over $d^m k$, given by Eq. (B.1), but *without* the $\delta-$function $\delta((p-k)^2) = \delta(l^2)$ since we want to evaluate the full two-loop diagram *without* any cut and only then take the discontinuity. How the different discontinuities are related to the cuts of a certain diagram has been explained in Section 3.5.1. Here we show how to extract the imaginary part of a given two-loop integral, the latter consisting of a one-loop integral as defined in Appendix A, but with $l^2 \neq 0$, and the following integration over l^2. The tranverse momentum integration over $k_\perp^2$ contained in $\int d^m k$ is related to the l^2 integration by

$$\begin{aligned} l^2 = (p-k)^2 &= -2p^+k^- + k^2 = -\frac{1}{x}(k^2 + k_\perp^2) + k^2 = \frac{1}{x}(|k^2|\tilde{x} - k_\perp^2) \\ \tilde{x} &= 1 - x \end{aligned}$$

Now we substitute

$$k_\perp^2 = |k^2|\tilde{x}\,\kappa \text{ to obtain } l^2 = |k^2|\frac{\tilde{x}}{x}(1-\kappa) \tag{C.1}$$

Furthermore, we will use

$$2l^+l^- = l^2 + l_\perp^2 = l^2 + k_\perp^2 = |k^2|\frac{\tilde{x}}{x}(1 - \kappa\,\tilde{x})$$

Thus we have, combining the phase space for the $d^m k$ integration with the virtual integral $\frac{1}{(2\pi)^m} J_2^{A,ML}(l)$ given in (A.14):

$$z\int \frac{d^m k}{(2\pi)^{2m}}\,\delta(x-z)\,J_2^{A,ML}(l)$$

$$
\begin{aligned}
&= \frac{1}{32\pi^3}\frac{(4\pi)^\epsilon}{\Gamma(1-\epsilon)}\int_0^{Q^2} d|k^2| \int dk_\perp^2 (k_\perp^2)^{-\epsilon}\frac{1}{(2\pi)^m} J_2^{A,ML}(l) \\
&= -\frac{i}{2\pi}\frac{(4\pi)^{2\epsilon}}{(16\pi^2)^2}\frac{\Gamma(1+\epsilon)}{\Gamma(1-\epsilon)}\frac{1}{\epsilon}\int_0^{Q^2} d|k^2||k^2|^{1-\epsilon}\tilde{x}^{1-\epsilon}\int_0^{\kappa_{\max}} d\kappa\,\kappa^{-\epsilon} \\
&\quad \int_0^1 du \frac{1}{ul^+ + i\eta}\left\{[-|k^2|\frac{\tilde{x}}{x}(1-\kappa)(1-u)]^{-\epsilon} - [-|k^2|\frac{\tilde{x}}{x}u(1-\kappa+\kappa x u)]^{-\epsilon}\right\} \\
&=: \frac{i}{2\pi}\frac{(4\pi)^{2\epsilon}}{(16\pi^2)^2}\frac{\Gamma(1+\epsilon)}{\Gamma(1-\epsilon)}\tilde{x}^{1-\epsilon}\int_0^{Q^2} d|k^2||k^2|^{1-2\epsilon}\cdot I_\kappa^{J_2^{A,ML}}
\end{aligned}
$$

$$
\begin{aligned}
I_\kappa^{J_2^{A,ML}} &= -\left(\frac{\tilde{x}}{x}\right)^{-\epsilon}\frac{1}{\epsilon}\int_0^{\kappa_{\max}} d\kappa\,\kappa^{-\epsilon}\int_0^1 du\,\frac{1}{ul^+ + i\eta}\Big\{[(\kappa-1)(1-u)]^{-\epsilon} - \\
&\quad [\kappa - 1 - \kappa x u]^{-\epsilon}\Big\} \\
&=: I_{\kappa I} - I_{\kappa II}
\end{aligned}
$$

$$
\begin{aligned}
I_{\kappa I} &= -\left(\frac{\tilde{x}}{x}\right)^{-\epsilon}\frac{1}{\epsilon}\int_0^{\kappa_{\max}} d\kappa\,\kappa^{-\epsilon}\int_0^1 du\,\frac{1}{ul^+ + i\eta}[-(1-\kappa)(1-u)]^{-\epsilon} \\
I_{\kappa II} &= -\left(\frac{\tilde{x}}{x}\right)^{-\epsilon}\frac{1}{\epsilon}\int_0^{\kappa_{\max}} d\kappa\,\kappa^{-\epsilon}\int_0^1 du\,\frac{1}{ul^+ + i\eta}[\kappa - 1 - \kappa x u]^{-\epsilon}
\end{aligned}
$$

Now we have to extract the imaginary parts of $I_\kappa^{J_2^{A,ML}}$. We see that $I_{\kappa I}$ develops an imaginary part for $\kappa < 1$, leading to

$$
I_{\kappa I} = -\frac{1}{\epsilon}(-1)^{-\epsilon}\left(\frac{\tilde{x}}{x}\right)^{-\epsilon}\int_0^1 d\kappa\,\kappa^{-\epsilon}(1-\kappa)^{-\epsilon}\int_0^1 du\,\frac{u^{-\epsilon}}{ul^+ + i\eta}(1-u)^{-\epsilon} \tag{C.2}
$$

whereas $I_{\kappa II}$ has an imaginary part for $u > \frac{\kappa-1}{\kappa x}$. From the condition $0 \le u \le 1$ we therefore deduce $\kappa_{\max} = 1/\tilde{x}$ in the case of $I_{\kappa II}$, leading to

$$
I_{\kappa II} = -\frac{1}{\epsilon}(-1)^{-\epsilon}\left(\frac{\tilde{x}}{x}\right)^{-\epsilon}\int_0^{1/\tilde{x}} d\kappa\,\kappa^{-\epsilon}(\kappa-1)^{-\epsilon}\int_{\frac{\kappa-1}{\kappa x}}^1 du\,\frac{u^{-\epsilon}}{ul^+ + i\eta}[1 - \frac{\kappa x u}{\kappa - 1}]^{-\epsilon} \tag{C.3}
$$

Using now[1]

$$
(-1)^{-\epsilon} = \epsilon\, i\pi(1 - \epsilon^2\frac{\pi^2}{6}) + \text{real} + \mathcal{O}(\epsilon^5)
$$

and extracting the coefficients of $i\pi$ we obtain the imaginary parts of the integrals $I_{\kappa I}$ and $I_{\kappa II}$ after having carried out the parameter integrations over u and κ.
Note that in the same way as for the one-loop integrals treated in Appendix A, we

[1]The sign of the $\epsilon\, i\pi$ term actually is determined by the $i\eta$ term accompanying the term $l^2 + i\eta$; see Eq. (3.121).

still have the choice to use PVI or $\epsilon-$regularization for the spurious infrared poles, as has been explained in Sections 3.3 and A.2:

$$\begin{aligned} \text{PVI}: \quad & \frac{u^{-\epsilon}}{ul^+ + i\eta} \to u^{-\epsilon}\frac{ul^+}{(ul^+)^2+\delta^2} \\ \epsilon-\text{reg.}: \quad & \frac{u^{-\epsilon}}{ul^+ + i\eta} \to \frac{1}{l^+}u^{-1-\epsilon} \end{aligned}$$

The imaginary parts of the integrals given in Table C.1 are the values obtained by using $\epsilon-$regularization.
The full matrix element of the diagrams calculated with this "imaginary part method" contains additional factors $(1-\kappa)^{-1}$ from the $1/(l^2+i\eta)$ denominator of the gluon propagator $D^{ab}_{\mu\nu}(l)$. Additional factors $(1-\kappa)$ from the numerator also appear. We therefore need three types of integrals:

$$\int_0^{\kappa_{\max}} d\kappa\, \kappa^{-\epsilon}(1-\kappa)^{-1}\, J(\kappa)\,, \quad \int_0^{\kappa_{\max}} d\kappa\, \kappa^{-\epsilon}\, J(\kappa) \quad \text{and} \quad \int_0^{\kappa_{\max}} d\kappa\, \kappa^{-\epsilon}(1-\kappa)\, J(\kappa)$$

where $J(\kappa)$ stands for any one-loop integral needed during the calculation and having an imaginary part. The definitions of the one-loop integrals are given in Appendix A. The vector and higher rank tensor integrals have been reduced to scalar ones by Passarino-Veltman reduction [63]. There is only one parameter of a vector integral containing an imaginary part which cannot be fully expressed by scalar ones due to the presence of n^*, which is the parameter $C_2(\kappa)$ of the integral $J^{A,ML}_{2\mu}(l)$ (see Eq. (A.33)). Since we do not need the imaginary part of the full vector integral, we only give the result for this parameter in Table C.1.

	$\int_0^{\kappa_{\max}} d\kappa\, \kappa^{-\epsilon}(1-\kappa)^{-1}$	$\int_0^{\kappa_{\max}} d\kappa\, \kappa^{-\epsilon}$	$\int_0^{\kappa_{\max}} d\kappa\, \kappa^{-\epsilon}(1-\kappa)$
$J_2^F(l)$	$-\frac{1}{\epsilon} - 2 + \ln\tilde{x} - \ln x$	1	$\frac{1}{2}$
$J_3^F(p,k)$	$\frac{1}{k^2}\left[\frac{1}{\epsilon^2} - \frac{\ln\tilde{x}}{\epsilon} + \frac{1}{2}\ln^2\tilde{x} + 2Li_2(\tilde{x}) - \frac{\pi^2}{2}\right]$	$\frac{x}{k^2\tilde{x}}\left[\frac{\ln x}{\epsilon} + \frac{1}{2}\ln^2 x - \ln x\ln\tilde{x} - 2Li_2(\tilde{x})\right]$	$\frac{x}{k^2\tilde{x}^2}\left[-\frac{\tilde{x}+x\ln x}{\epsilon} - 2\tilde{x} - \tilde{x}\ln x - \frac{x}{2}\ln^2 x + \ln\tilde{x}(\tilde{x}+x\ln x) + 2x\,Li_2(\tilde{x})\right]$
$J_2^{A,ML}(l)$	$-\frac{1}{\tilde{x}}\left[\frac{1}{2\epsilon^2} - \frac{\ln\tilde{x}}{2\epsilon} + \frac{1}{4}\ln^2\tilde{x} - \ln x\ln\tilde{x} - Li_2(\tilde{x}) - \frac{\pi^2}{4}\right]$	$-\frac{\ln\tilde{x}}{\tilde{x}}$	$\frac{1}{2\tilde{x}}\left[\ln\tilde{x} + \frac{x}{\tilde{x}}\right]$
$C_2(\kappa)$	$-\ln x - \frac{\tilde{x}}{x}\ln\tilde{x}$	$-\frac{\ln\tilde{x}}{x}$	not needed
$I_2^{A,ML}(k,p)$	$-\frac{1}{\tilde{x}}\left[\frac{\ln x}{\epsilon} + \frac{1}{2}\ln^2 x - \ln x\ln\tilde{x} - 2Li_2(\tilde{x})\right]$	$\frac{1}{\tilde{x}}\ln x$	$\frac{1}{2\tilde{x}}\ln x$
$I_2^{A,ML}(-k,l)$	$\frac{\ln x - \ln\tilde{x}}{\epsilon} + \frac{1}{2}\ln^2 x + \frac{1}{2}\ln^2\tilde{x} + 2Li_2(\tilde{x}) - \frac{\pi^2}{6}$	$-\frac{1}{\tilde{x}}\left[\frac{1}{\epsilon} + 2 + \ln x\right]$	not needed
$I_2^{A,ML}(-p,-l)$	not needed	$-\frac{1}{\tilde{x}}$	not needed
$J_3^{A,ML}(k,p)$	$-\frac{1}{k^2}\left[\frac{1}{\epsilon^2} + \frac{2\ln x - \ln\tilde{x}}{\epsilon} + \frac{1}{2}\ln^2\tilde{x} - 4Li_2(\tilde{x}) - 2\ln x\ln\tilde{x} - 3\frac{\pi^2}{6}\right]$	$-\frac{1}{k^2}\left[-\frac{1}{\epsilon} + \ln\tilde{x} + \frac{2x}{\tilde{x}}\ln x\right]$	$-\frac{1}{k^2}\left[-\frac{1}{2\epsilon} + \frac{1}{2}\ln\tilde{x} - \frac{x^2}{\tilde{x}^2}\ln x - \frac{1}{2}\frac{1+x}{\tilde{x}}\right]$
$J_3^{A,ML}(-k,l)$	$-\frac{1}{k^2\tilde{x}}\left[\frac{3}{2\epsilon^2} - \frac{3}{2\epsilon}\ln\tilde{x} + \frac{3}{4}\ln^2\tilde{x} - 2\ln x\ln\tilde{x} - 2Li_2(\tilde{x}) - \frac{3\pi^2}{4}\right]$	$-\frac{1}{k^2\tilde{x}}\left[-\frac{\ln\tilde{x}}{\epsilon} + \frac{1}{2}\ln^2\tilde{x} + Li_2(\tilde{x}) - \frac{\pi^2}{6}\right]$	$-\frac{1}{k^2\tilde{x}}\left[-\frac{\ln\tilde{x}}{\epsilon} - \frac{x}{\epsilon\tilde{x}} - 2\ln\tilde{x} + \frac{1}{2}\ln^2\tilde{x} - \frac{x}{\tilde{x}}(\ln x + 2) + Li_2(\tilde{x}) - \frac{\pi^2}{6}\right]$
$J_3^{A,ML}(-p,-l)$	not needed	$-\frac{x}{k^2\tilde{x}}\left[\frac{\ln x - \ln\tilde{x}}{\epsilon} - 2\ln x\ln\tilde{x} + \frac{1}{2}\ln^2\tilde{x} + \frac{1}{2}\ln^2 x - 2Li_2(\tilde{x}) - \frac{\pi^2}{6}\right]$	$-\frac{x}{k^2\tilde{x}}\left[-\frac{1}{\epsilon} - 2 + 2\ln\tilde{x} + \frac{x}{\tilde{x}} - \frac{1-3x}{\tilde{x}}\ln x\right]$

Table C.1: Imaginary parts after κ integration. The entries are the imaginary parts of the integrals listed in the left column after integration over κ as indicated in the first row. All entries except the one for $C_2(\kappa)$ have an overall factor $i\pi^{\frac{m}{2}}\Gamma(1+\epsilon)|k^2|^{-\epsilon}$.

Bibliography

[1] H. Fritzsch, M. Gell-Mann, H. Leutwyler, *Phys. Lett.* **B47** (1973) 365.

[2] S. Weinberg, *Phys. Rev. Lett.* **31** (1973) 494.

[3] D. J. Gross, F. Wilczek, *Phys. Rev. Lett.* **30** (1973) 1343; *Phys. Rev.* **D8** (1973) 3633.

[4] H. D. Politzer, *Phys. Rev.* **30** (1973) 1346.

[5] R. P. Feynman, *Phys. Rev. Lett.* **23** (1969) 1415;
J. D. Bjorken, E. A. Paschos, *Phys. Rev.* **185** (1969) 1975.

[6] K. G. Wilson, *Phys. Rev.* **179** (1969) 1499.

[7] W. Zimmermann, *Lectures on Elementary Particles and Quantum Field Theory*, eds. S. Deser *et al.*, MIT Press, 1971.

[8] W. Zimmermann, *Ann. Phys.* **77** (1973) 570.

[9] C. G. Callan, *Phys. Rev.* **D2** (1970) 1541.

[10] K. Symanzik, *Comm. Math. Phys.* **18** (1970) 227.

[11] D. J. Gross, F. Wilczek, *Phys. Rev.* **D9** (1974) 980.

[12] H. Georgi, H. D. Politzer, *Phys. Rev.* **D9** (1974) 416.

[13] G. Altarelli, G. Parisi, *Nucl. Phys.* **B126** (1977) 298.

[14] V. N. Gribov, L. N. Lipatov, *Sov. J. Nucl. Phys.***15** (1972) 438;
L. N. Lipatov, *Sov. J. Nucl. Phys.***20** (1975) 95;
Yu. L. Dokshitzer, *Sov. Phys. JETP***46** (1977) 641.

[15] For reviews, see e.g. Yu. L. Dokshitzer, D. I. Dyakonov and S. I. Troyan, *Phys. Rep.* **58** (1980) 270;
G. Altarelli, *Phys. Rep.* **81** (1982) 1.

[16] R. K. Ellis, W. J. Stirling and B. R. Webber, *QCD and Collider Physics*, Cambridge, University Press (1996).

[17] R. Doria, J. Frenkel, J. C. Taylor, *Nucl. Phys.* **B168** (1980) 93.

[18] T. Kinoshita, *J. Math. Phys.* 3 (1962) 650;
T. D. Lee, M. Nauenberg, *Phys. Rev.* **133** (1964) 1549.

[19] J. C. Collins and D. E. Soper, *Ann. Rev. Nucl. Part. Sci.* **37** (1987) 383.

[20] J. C. Collins, D. E. Soper, G. Sterman, in *Perturbative Quantum Chromodynamics*, ed. A. H. Mueller, World Scientific, Singapore 1989.

[21] S. G. Gorishnii, A. L. Kataev and S. A. Larin, *Phys. Lett.* **B259** (1991) 144;
M. A. Samuel and L. R. Surguladze *Phys. Rev. Lett.* **66** (1991) 560.

[22] E. B. Zijlstra and W. L. van Neerven, *Nucl. Phys.* **B383** (1992) 525;
ibid Phys. Lett. **B297** (1992) 377;
Nucl. Phys. **B417** (1994) 61; E: *Nucl. Phys.* **B426** (1994) 245.

[23] R. Hamberg, W. L. van Neerven and T. Matsuura, *Nucl. Phys.* **B359** (1991) 343;
W. L. van Neerven and E. B. Zijlstra, *Nucl. Phys.* **B382** (1992) 11.

[24] S. A. Larin, T. van Ritbergen, J. A. M. Vermaseren, *Nucl. Phys.* **B427** (1994) 41;
S. A. Larin, P. Nogueira, T. van Ritbergen, J. A. M. Vermaseren, *Nucl. Phys.* **B492** (1997) 338.

[25] T. van Ritbergen, J. A. M. Vermaseren, S. A. Larin, *Phys. Lett.* **B400** (1997) 379.

[26] A. L. Kataev, A. V. Kotikov, G. Parente, A. V. Sidorov, *Phys. Lett.* **B388** (1996) 179.

[27] E. G. Floratos, D. A. Ross and C. T. Sachrajda, *Nucl. Phys.* **B129** (1977) 66;
E: *Nucl. Phys.* **B139** (1978) 545; *Nucl. Phys.* **B152** (1979) 493;
A. Gonzalez-Arroyo, C. Lopez and F. J. Yndurain, *Nucl. Phys.* **B153** (1979) 161;
A. Gonzales-Arroyo and C. Lopez, *Nucl. Phys.* **B166** (1980) 429;
E. G. Floratos, R. Lacaze and C. Kounnas, *Nucl. Phys.* **B192** (1981) 417.

[28] R. K. Ellis, H. Georgi, M. Machacek, H. D. Politzer and G. G. Ross, *Nucl. Phys.* **B152** (1979) 285.

[29] G. Curci, W. Furmanski and R .Petronzio, *Nucl. Phys.* **B175** (1980) 27.

[30] W. Furmanski and R. Petronzio, *Phys. Lett.* **B97** (1980) 437.

[31] R. Mertig and W. L. van Neerven, *Z. Phys.* **C70** (1996) 637.

[32] W. Vogelsang, *Nucl. Phys.* **B475** (1996) 47;
W. Vogelsang, *Phys. Rev.* **D54** (1996) 2023.

[33] R. Hamberg, W. van Neerven, *Nucl. Phys.* **B379** (1992) 143.

[34] J. C. Collins and R. J. Scalise, *Phys. Rev.* **D50** (1994) 4117.

[35] Y. Matiounine, J. Smith, W. L. van Neerven, hep-ph/9801224.

[36] S. Mandelstam, *Nucl. Phys.* **B213** (1983) 149.

[37] G. Leibbrandt, *Phys. Rev.* **D29** (1984) 1699.

[38] A. Bassetto, M. Dalbosco, I. Lazzizzera and R.Soldati, *Phys. Rev.* **D31** (1985) 2012.

[39] G. McCartor, D.G. Robertson, *Z. Phys.* **C62** (1994) 349.

[40] A. Bassetto, *Phys. Rev.* **D47** (1993) 727;
A. Bassetto, *Nucl. Phys. Proc. Suppl.* **51C** (1996) 281.

[41] A. Bassetto, G. Nardelli, R. Soldati, *Yang-Mills theories in algebraic noncovariant gauges*, World Scientific, Singapore 1991.

[42] G. Leibbrandt, *Noncovariant gauges: Quantization of Yang-Mills and Chern-Simons theory in axial type gauges*, World Scientific, Singapore 1994.

[43] J. C. Collins and D. E. Soper, *Nucl. Phys.* **B194** (1982) 445.

[44] R. K. Ellis, W. Furmanski, R. Petronzio, *Nucl. Phys.* **B207** (1982) 1;
R. K. Ellis, W. Furmanski, R. Petronzio, *Nucl. Phys.* **B212** (1983) 29.

[45] R. K. Ellis and W. Vogelsang, hep-ph/9602356.

[46] H. D. Politzer, *Nucl. Phys.* **B129** (1977) 301;
D. Amati, R. Petronzio,G. Veneziano, *Nucl. Phys.* **B140** (1978) 54, *Nucl. Phys.* **B146** (1978) 29;
S. Libby, G. Sterman, *Phys. Rev.* **D18** (1978) 3252, *ibid* 4737 (1978);
C. T. Sachrajda, *Phys. Lett.* **B73** (1978) 185;
A.V. Efremov, A.V. Radyushkin, *Theor. Math. Phys.* **44** (1980) 327; *ibid* 664 (1981).

[47] G. Leibbrandt, S. Nyeo, *Phys. Lett.* **140B** (1984) 417.

[48] M. Dalbosco, *Phys. Lett.* **180B** (1986) 121.

[49] M. Dalbosco, *Phys. Lett.* **163B** (1985) 181.

[50] G. Leibbrandt, *Rev. Mod. Phys.* **59** (1987) 1067.

[51] D. M. Capper, D. R. T. Jones, A. T. Suzuki, *Z. Phys.* **C29** (1985) 585.

[52] R. T. Herrod, S. Wada, *Phys. Lett.* **96B** (1980) 195.

[53] G. Leibbrandt, J. Williams, *Nucl. Phys.* **B440** (1995) 573.

[54] J. Williams, Ph.D. thesis, University of Guelph (1998).

[55] A. Bassetto, M. Dalbosco and R. Soldati, *Phys. Rev.* **D36** (1987) 3138.

[56] N. N. Bogoliubov, O. S. Parasiuk, *Acta Math.***97** (1957) 227;
K. Hepp, *Comm. Math. Phys.***2** (1966) 301;
W. Zimmermann, *Comm. Math. Phys.***15** (1969) 208.

[57] T. Muta, *Foundations of Quantum Chromodynamics*, World Scientific, 1987.

[58] G. Sterman, *QCD and beyond, Proceedings of the Theoretical Advanced Study Institute, Boulder 1995*, Ed. D. E. Soper, World Scientific 1996.

[59] M. Oegren, *Classical and Quantum Gravity*, **No. 3** (1986) 581.

[60] D. M. Capper, J. J. Dulwich and M. J. Litvak, *Nucl. Phys.* **B241** (1984) 463.

[61] J. A. M. Vermaseren, FORM Version 2.0; Tutorial and Reference Manual published by Computer Algebra Nederland, Amsterdam 1991.

[62] S. Wolfram, Mathematica Version 2.2, Addison-Wesley Publishing Company, 1991.

[63] G. Passarino, M. Veltman, *Nucl. Phys.* **B160** (1979) 151.

[64] S. Catani, *Z. Phys.* **C75** (1997) 665.

[65] G. Heinrich, Z. Kunszt, hep-ph/9708334, accepted for publication in *Nucl. Phys.* **B**.

[66] A. Bassetto, G. Heinrich, Z. Kunszt, W. Vogelsang, hep-ph/9805283, accepted for publication in *Phys. Rev.* **D**.

Curriculum Vitae

Personal data

Name : Heinrich, Gudrun
Born : January 15, 1968 in Radolfzell am Bodensee
Nationality : German

Education

1974-78 : Primary school in Steisslingen;
1978-87 : Hegau-Gymnasium in Singen;
1987-93 : Undergraduate studies at the Albert-Ludwigs-Universität in Freiburg im Breisgau;
1993 : Diplom in physics;
1994-98 : Graduate studies at the Institute for Theoretical Physics of ETH Zürich under the supervision of Prof. Zoltan Kunszt.

Scientific Experience

1992/93 : Diplom work on dynamical symmetry breaking and radiative corrections in models without elementary scalar fields under the advisorship of Prof. J.J. van der Bij;
1994-98 : Research devoted to perturbative quantum chromodynamics, especially on anomalous dimensions in next-to-leading order and the light-cone gauge;
June 1995 : Participation in the Theoretical Advanced Study Institute in Boulder, Colorado.

Publications

-G. Heinrich, Z. Kunszt, hep-ph/9708334, accepted for publication in Nucl. Phys. **B**
Two-loop anomalous dimension in light-cone gauge with Mandelstam-Leibbrandt prescription.

-A. Bassetto, G. Heinrich, Z. Kunszt, W. Vogelsang, hep-ph/9805283, accepted for publication in Phys. Rev. **D**
The light-cone gauge and the calculation of the two-loop splitting functions.

Acknowledgements

First of all I would like to thank my advisor Zoltan Kunszt. He always has good ideas in abundance, and I could profit a lot from his experience. Whenever I was on the way to get lost in details, he put an infatiguable effort in broadening my perspectives. I also appreciated very much the freedom he gave me in choosing my own way to tackle a problem by giving me advices, but not insisting on them. In many occasions I could enjoy the feeling that he is really trusting me, thus providing me an independence which I appreciated a lot.

To my coreferent Christoph Schmid I would like to thank for his interest in my work and the constructive suggestions concerning my thesis.

I am also very much indebted to Werner Vogelsang for his collaboration during the last months of this work. The discussions with him and the joint work contributed a lot to this period being a very delightful and productive one.
In addition, I am very grateful to Antonio Bassetto, whose competence considerably enriched our collaboration.

There are many members or former members of our institute whose presence I enjoyed a lot, in particular the one of Adrian Signer, Nilanjana Datta, Ivo Sachs, Peter Widerin, Stefano Frixione, Dominik Schwarz, David Hasler and our system administrator Elmar Heeb.

Special thanks I due to Daniel Schenker, who motivated me not only in work but also in exploring the climbs of the Swiss Jura.

Furthermore, I appreciated a lot the contact to the experimental particle physics group, especially to Hubert Niggli, Monika Wagener and Stefano Passaggio. I also enjoyed the interaction with people from the Paul Scherrer Institut, in particular with Markus Roth and Dirk Graudenz.

Finally, I would like to thank the secretaries Annet Schultze, Martina Lopez and Christine Schütterle who are definitely more than secretaries, they are something like the "good spirits" of the institute.